

UNCLASSIFIED

AD NUMBER: AD0814069

LIMITATION CHANGES

TO:

Approved for public release; distribution is unlimited.

FROM:

Distribution authorized to US Government Agencies only;
Export Controlled; 1 May 1967. Other requests shall be referred to Air Force
Materials Laboratory, Wright-Patterson AFB, OH 45433.

AUTHORITY

USAFSC ltr dtd 26 May 1972

AFML-TR-67-70

ADVANCED EXPLOSIVE FORMING PROCESSES

(HEREF)

K. R. Agricola
J. T. Snyder
J. B. Patton, et al
MARTIN MARIETTA CORPORATION



AD814069

TECHNICAL REPORT AFML-TR-67-70
MAY 1967

This document is subject to special export controls and each transmittal to foreign governments or foreign nationals may be made only with prior approval of the Manufacturing Technology Division (MATF), Air Force Materials Laboratory, Wright-Patterson AFB, Ohio 45433.

ADVANCED FABRICATION TECHNIQUES BRANCH
MANUFACTURING TECHNOLOGY DIVISION
AIR FORCE MATERIALS LABORATORY
WRIGHT-PATTERSON AIR FORCE BASE, OHIO



AFML-TR-67-70

ADVANCED EXPLOSIVE FORMING PROCESSES

(HERF)

K. R. Agricola
J. T. Snyder
J. B. Patton, et al
MARTIN MARIETTA CORPORATION

TECHNICAL REPORT AFML-TR-67-70
MAY 1967

This document is subject to special export controls and each transmittal to foreign governments or foreign nationals may be made only with prior approval of the Manufacturing Technology Division (MATF), Air Force Materials Laboratory, Wright-Patterson AFB, Ohio 45433.

ADVANCED FABRICATION TECHNIQUES BRANCH
MANUFACTURING TECHNOLOGY DIVISION
AIR FORCE MATERIALS LABORATORY
WRIGHT-PATTERSON AIR FORCE BASE, OHIO

Approved: Gaylen A. Thurston
Dr. G. A. Thurston, Manager
High Energy Rate Processes

FOREWORD

This Final Technical Report Covers all work performed under Contract AF 33(615)-3167 from June 1965 to February 1967. The manuscript was released by the authors in April 1967 for publication as an AFML Technical Report.

This contract with Martin Marietta Corporation, Denver Division, Denver, Colorado was initiated under Manufacturing Methods Project 8-358, "Advanced Explosive Forming Processes (HERF)". It was accomplished under the technical direction of Captain Gordon F. Hollobaugh, Advanced Fabrication Techniques Branch (MATF), Manufacturing Technology Division, Air Force Materials Laboratory, Wright-Patterson Air Force Base, Ohio.

Sincere appreciation is given to all those who contributed to the success of this program. Special thanks go to D. Wilson and K. Stillman for their assistance in the preparation of the manuscript.

This project has been accomplished as a part of the Air Force Manufacturing Methods Program, the primary objective of which is to develop, on a timely basis, manufacturing processes, techniques and equipment for use in economical production of USAF materials and components. This program encompasses the following technical areas:

Rolled Sheet, Forgings, Extrusions, Castings, Fiber and Powder Metallurgy, Component Fabrication, Joining, Forming, Material Removal, Fuels, Lubricants, Ceramics, Graphites, Nonmetallic Structural Materials, Solid State Devices, Passive Devices, Thermionic Devices.

Your comments are solicited on the potential utilization of the information contained herein as applied to your present or future production programs. Suggestions concerning additional Manufacturing Methods Development required on this or other subjects will be appreciated.

This technical report has been reviewed and is approved.

Melvin E. Fields

MELVIN E. FIELDS
Colonel, USAF
Chief, Manufacturing Technology Division
AF Materials Laboratory

ABSTRACT

Several high-strength steels, namely HP 9-4-25, D6AC, 12% nickel and 18% nickel maraging steels, and a high-strength aluminum alloy 7039, were investigated with respect to explosive forming and subsequent effects of forming on mechanical behavior. In addition, criteria necessary for full-scale die design were developed.

The stress-corrosion behavior of each alloy was evaluated using a standard 3% NaCl alternate immersion test. Samples stressed to 80% of the 0.2% offset tensile yield strength were exposed for periods up to 200 hours both before and after explosive deformation. Three of the alloys, HP 9-4-25, 12Ni-5Cr-3Mo, and vacuum-melted 18% nickel maraging steel, were found to be only slightly affected by stress corrosion. Explosive deformation did not alter the resistance of the alloys. The D6AC steel and air-melted 18% nickel maraging steel had fair resistance to stress-corrosion, while the 7039-T6 aluminum was unsuitable for structural use in a corrosive environment.

Using plane strain, center notch, fracture-toughness specimens, none of the alloys were found to be affected by explosive deformation. High toughness was exhibited by all the alloys both before and after explosive forming, with the greatest toughness shown by HP 9-4-25 and D6AC steels.

Both HP 9-4-25 and D6AC steels were highly formable in the annealed condition. The other alloys were formable, but to a lesser degree. Formability limit curves were developed for each alloy using a blank diameter-to-die opening diameter ratio of 1.58. Explosive charge requirements to achieve specified draw depths were also established with pressed TNT explosive charges. The greatest charge requirement was for the air-melted 18% nickel maraging steel, although all of the steels took roughly the same explosive charge for a given draw depth. None of the steels could be formed to a hemispherical shape in one forming operation; however, hemispheres could be formed from all the alloys in two or more operations. The 7039-O aluminum was formed to full contour in one operation.

Verification of scaling was demonstrated by forming the steels on both six-inch- and 24-inch-diameter dies. Conditions established on the small die were used on the larger die, and

empirical results agreed with predictions to within 3 1/2% for the HP 9-4-25 and D6AC steels. Variations from predictions for the other two steels were up to 14.5%. Deviations could be explained by differences in blank thickness and yield strength between the two different sized models. The 7039-0 aluminum results were predictable to within 3 to 4% at part sizes to 120 inches, thus the usefulness of scaling has been demonstrated.

Computer predictions did not agree well with experiment when metal draw depth or blank pull-in were unknown. When blank pull-in was known, the computer program could rather accurately predict radial strains and draw depth. Program accuracy was greater for the shallower draw depths and, in general, overprediction resulted because accurate data for explosive energy transfer and energy release are not available.

Criteria developed on six-inch- and 24-inch-diameter shell dies showed the practicality of the concept. Clamping stiffness was found to be the most critical design parameter.

Explosive charges up to two pounds on the 24-inch-diameter die could be used on the initial forming shot without serious die damage. This corresponds to 550 pounds on a 156-inch diameter die. Sizing shots up to one-half pound could be used without effect on the die. Greater charges caused plastic deformation of the die shell and shearing of attachment bolts.

TABLE OF CONTENTS

<u>Section</u>	<u>Page</u>
I. INTRODUCTION	1
II. EXPERIMENTAL PROCEDURE	4
1. MATERIALS	4
2. STRESS-CORROSION AND MECHANICAL TESTING	9
a. Stress-Corrosion	9
b. Tensile Testing	14
c. Fracture Toughness	14
3. THEORETICAL ANALYSES	15
4. CHARGE PREPARATION AND FORMING	19
a. Explosive Charge Preparation	19
b. Explosive Forming	23
III. RESULTS AND DISCUSSION	33
1. MECHANICAL TESTING	33
a. Basic Mechanical Strength	33
b. Stress Corrosion Behavior	35
c. Fracture Toughness Behavior	44
2. THEORETICAL ANALYSIS	71
3. EXPLOSIVE FORMING	79
a. 7039 Aluminum	79
(1) Formability Limits	81
(2) Explosive Charge Estimation	86
(3) Verification of Subscale Forming Data	86
b. HP 9-4-25 Steel	93
(1) Formability Limits	93
(2) Explosive Charge Estimation	97
(3) Verification of Subscale Forming Experiments	101

TABLE OF CONTENTS - continued

<u>Section</u>	<u>Page</u>
c. D6AC Steel	103
(1) Formability Limits	103
(2) Estimation of Explosive Charge	103
(3) Verification of Subscale Forming Data	103
d. 12Ni-5Cr-3Mo Steel	108
(1) Formability Limits	108
(2) Estimation of Explosive Charge	111
(3) Scaling Verification Experiments	111
e. 18% Nickel Maraging Steel	114
(1) Formability Limits	114
(2) Estimation of Explosive Charge	117
(3) Scaling Verification Experiments	117
IV. CRITERIA FOR DIE DESIGN	123
1. CLAMPING STIFFNESS	126
2. EVALUATION OF DIE LOADS	133
V. CONCLUSIONS AND RECOMMENDATIONS	143
VI. REFERENCES	148

FORM 1473

ILLUSTRATIONS

<u>Figure</u>	<u>Title</u>	<u>Page</u>
1	Formula for Deflection of Stress-Corrosion Specimens	10
2	Stress-Corrosion Specimen Fixture Ready for Test	11
3	Calibration Arrangement for Stress-Corrosion Test Specimens	11
4	Measured and Calculated Strain Versus Deflection	12
5	Alternate Immersion Test Apparatus	13
6	Die for Fracture Toughness Specimen Preparation	16
7	Explosively Formed 7039-O Aluminum Plate Prior to Removal from the Die	17
8	Formed Fracture Toughness Material From 7039-O Aluminum Plate Showing Flat Portion with Photo-Gridded Strain Markings	18
9	View of 50-Ton Explosive Press for Charge Preparation	20
10	View of Small Pressing Cell Showing 12-Ton Press and Die Sets Used for Charge Pressing	21
11	Casting Die Used to Produce the Twenty-five Pound Full-Scale Explosive Charges	22
12	Pressed TNT Charge with Electric Blasting Cap for Six-Inch Die Experiments	24
13	Typical Pressed and Cast Charges for One-Fifth Scale and Full-Scale Forming Experiments	25
14	Six-Inch Diameter Explosive Forming Dies and Universal Die Base for Support of Six-Inch Diameter Forming Dies	26
15	Arrangement for Clamp and Ring Stiffness Experiments on a 6-Inch-Diameter Die	27
16	Lightweight 12% Nickel Maraging Steel Shell Die Fabricated from 6-Inch Formed Hemispherical Dome	28

<u>Figure</u>	<u>Title</u>	<u>Page</u>
17	24-Inch Hemispherical Die Used in Forming	29
18	Phase III Die Used for Forming the High-Strength Steels	30
19	Free-Forming Die for Full-Scale Experiments (120-Inch Diameter)	31
20	Effect of Explosive Deformation on the Corrosion Susceptibility under Stress for Several High Strength Alloys (200 hours exposure)	40
21	Effect of Explosive Deformation on the Corrosion Susceptibility under Stress for Several High Strength Steel Alloys (200 hours exposure)	41
22	Effect of Explosive Deformation on the Corrosion Susceptibility under Stress of 7039-T62 Aluminum Sheet (200 hours exposure)	42
23	Three-Point Flexural Loading Fatigue Fixture with 3/4-Inch 18% Ni Maraging Steel Specimen Shown	47
24	1/4-Inch 18% Ni Maraging Steel Specimen Design	49
25	Specimen Design For High-Strength Steels	50
26	Typical Fracture Surface for the 1/4-Inch D6AC High-Strength Steel	52
27	Experimental vs Theoretical Strain and Contour Data, Specimen 1	74
28	Experimental vs Theoretical Strain and Contour Data, Specimen 2	75
29	Experimental vs Theoretical Strain and Contour Data, Specimen 3	76
30	Experimental vs Theoretical Strain and Contour Data, Specimen 4	77
31	Experimental vs Theoretical Strain and Contour Data, Specimen 5	78

<u>Figure</u>	<u>Title</u>	<u>Page</u>
32	7039-0 Aluminum Formability Limit Curve	82
33	7039-0 Aluminum Formability Limit Curve	83
34	Typical Tensile Fracture of 7039-0 Aluminum Caused by an Excessive Explosive Charge	84
35	A Typical Failure of 7039-0 Aluminum Caused by Use of Too Small a Blank	85
36	Deformed Specimens of 7039-0 Aluminum Sheet Used to Establish the Relation between Explosive Charge and Metal Draw Depth	87
37	Estimation of Charge as a Function of Metal Draw Depth for 7039-0 Aluminum Sheet	88
38	Scaling Verification Results for 7039-0 Aluminum Using 24-Inch- and 120-Inch-Diameter Dies	92
39	Lifting of 120-Inch-Diameter Free Forming Tool for Explosive Forming	94
40	Explosive Standoff Installation for Full-Scale Forming	95
41	Full Scale Explosive Forming Shot Using 25 Pounds of 50/50 Cast Pentolite	96
42	HP9-4-25 Steel Formability Limit Curve	98
43	Deformed Specimens of HP9-4-25 Steel Sheet Used to Establish the Relation Between Explosive Charge and Metal Draw Depth	99
44	Estimation of Charge as a Function of Metal Draw Depth for HP9-4-25 Steel Sheet	100
45	Formability Limits for D6AC Alloy Steel	104
46	Typical Formed Parts from Thin Gage D6AC Steel Sheet	105
47	Estimation of Charge as a Function of Metal Draw Depth for D6AC Steel Sheet	106
48	Formability Limits for 12Ni-5Cr-3Mo Maraging Steel	109

<u>Figure</u>	<u>Title</u>	<u>Page</u>
49	Steel Hemispheres Produced During the Program Using Multiple Forming Sequences	110
50	Estimation of Charge as a Function of Metal Draw Depth for 12 Ni-5Cr-3Mo Maraging Steel	112
51	Failure of Formed Vacuum Melted 18% Nickel Maraging Steel Along Surface Striations Caused by Rolling	115
52	Formability Limits for 18% Nickel Maraging Steel	116
53	Estimation of Charge as a Function of Metal Draw Depth for 18% Nickel Maraging Steel Sheet	118
54	Summary of Formability Limit Curves	121
55	Summary of Charge Estimation for High-Strength Alloys	122
56	Swing Die Concept (Sheet Metal Parts)	125
57	Interchangeable Die Cavity Concept Using Water for Die Support	125
58	Shell Die Concept for Explosive Forming of High-Strength Steels	127
59	24-Inch-Diameter Hemisphere Formed from 0.150-Inch Thick 7039-O Aluminum	128
60	Flange Wrinkling of Explosively Formed D6AC Steel Sheet Caused by Inadequate Clamping Force and Force Location	129
61	Schematic of Flange Wrinkling Problem	130
62	Phase III Die Used for Forming the High-Strength Steels	135
63	Die Design Details for 24-Inch Phase III Forming Tool	137
64	Die Growth Caused by One-Pound Sizing Shots	139
65	Possible Lightweight Die Design	147

TABLES

<u>Table</u>	<u>Title</u>	<u>Page</u>
I	Chemical Composition for Several High-Strength Alloys	5
II	Average Mechanical Properties for Several High-Strength Alloys	6
III	Heat Treatment Schedules Used to Obtain Full-Strength Properties for the Five High-Strength Alloys	8
IV	Effect of Heat Treatment on the Response of Thin Gauge 18% Nickel Maraging Steel	35
V	Mechanical Properties of Re-Heat Treated 12% Nickel Maraging Steel Sheet	36
VI	Baseline Data for Undeformed and Deformed Materials	37
VII	Stress Corrosion Results of Undeformed Steel Plate Materials (0.750-inch thick starting material)	43
VIII	Undeformed 7039-T62 Aluminum Alloy Tensile Properties 3/4-Inch Nominal Thickness (Room Temperature)	53
IX	Parent Tensile Properties for Undeformed 1/4-Inch Nominal Thickness 18% Ni Maraging Steel (Room Temperature)	53
X	Parent Tensile Properties for Undeformed 1/4-Inch Nominal Thickness 12% Ni Maraging Steel (-110°F)	54
XI	Parent Tensile Properties for Undeformed 1/4-Inch Nominal Thickness HP 9-4 Steel (-110°F)	54
XII	Parent Tensile Properties for Undeformed 1/4-Inch Nominal Thickness D6AC Steel (-110°F)	55

<u>Table</u>	<u>Title</u>	<u>Page</u>
XIII	Room-Temperature Fracture Toughness Properties for Parent Transverse 7039-T62 Aluminum Alloy	57
XIV	Room-Temperature Fracture Toughness Properties for Explosively Deformed Transverse 7039-T62 Aluminum Alloy	58
XV	Room-Temperature Fracture Toughness Properties for Parent Longitudinal 7039-T62 Aluminum Alloy	59
XVI	Room-Temperature Fracture Toughness Properties for Explosively Deformed Longitudinal 7039-T62 Aluminum Alloy	60
XVII	Fracture Toughness Data for 1/4-Inch 18% Ni Maraging Steel - Room Temperature	61
XVIII	Fracture Toughness Data for 1/4-Inch 18% Ni Maraging Steel - Room Temperature	62
XIX	Two-Way Analysis of Variance for 18% Ni Maraging Steel Fracture Toughness Value	63
XX	Fracture Toughness Data for 1/4-Inch D6AC Steel at -110°F	65
XXI	Fracture Toughness Data for 1/4-Inch D6AC Steel at -110°F	66
XXII	Fracture Toughness Data for 1/4-Inch HP 9-4 Steel at -110°F	67
XXIII	Fracture Toughness Data for 1/4-Inch HP 9-4 Steel at -110°F	68
XXIV	Fracture Toughness Data for 1/4-Inch 12% Ni Maraging Steel at -110°F	69
XXV	Fracture Toughness Data for 1/4-Inch 12% Ni Maraging Steel at -110°F	70

<u>Table</u>	<u>Title</u>	<u>Page</u>
XXVI	Fracture Toughness Data for 3/4-Inch 18% Ni Maraging Steel - Room Temperature	72
XXVII	Fracture Toughness Data for 3/4-Inch 18% Ni Maraging Steel - Room Temperature	73
XXVIII	Summary of Data Used in Theoretical Pre- diction of Response	80
XXIX	Scaling Verification Experiments on 7039-0 Aluminum	90
XXX	Scaling Verification Results for HP 9 Ni-4Co-.25C High-Strength Steel	102
XXXI	Scaling Verification Results for D6AC High-Strength Steel	107
XXXII	Scaling Verification Tests for 12Ni-5Cr- 3Mo Maraging Steel	113
XXXIII	Scaling Verification Tests for RSM 250 18% Ni Maraging Steel	119
XXXIV	Results of Stiffness Experiments to Evaluate Holddown Ring and Clamp Combinations	132
XXXV	Evaluation of Die Loads	133
XXXVI	Design Criteria for Full-Scale Explosive Forming Dies	141

LIST OF SYMBOLS

D	Diameter of die opening, inches
f	Clamping force, pounds
L	Explosive standoff distance, inches
W	Draw depth of formed part, inches
K	Spring constant, pounds per inch
e	Explosive charge, grains
B_0	Original blank diameter, inches
B_1	Blank diameter after forming operation, inches
t_0	Initial blank thickness, inch
E	Young's modulus of elasticity, psi
σ	Tensile yield stress, psi
σ_{cr}	Critical buckling stress, psi
ϵ_r	Radial strain, in/in
ϵ_c	Circumferential strain, in/in
K_{Ic}	Plane strain fracture toughness

SECTION I

INTRODUCTION

The fabrication of high-strength alloys used by the Air Force in the manufacture of solid rocket motors, pressure vessels, spacecraft, and tactical aircraft has revealed the need for manufacturing methods capable of producing deep drawn shapes economically and reliably. The high-strength steels, maraging steels, and high-strength aluminum alloys require high equipment capacity and, because of their strength and reduced ductility, create the need for elevated-temperature forming. The use of explosive energy has long been recognized as a means of augmenting large press capacity by permitting the formation of deep drawn shapes without the need for elevated temperature. The process also precludes the requirement for intermediate thermal treatments in many cases. Successful use of high-energy methods has been made in the fabrication of Titan II domes⁽¹⁾ and Saturn parts^(2,3). Several research and development contracts have been sponsored by Air Force^(4,8), NASA^(9,12), the Navy^(13,14) and the Army^(15,18) to develop criteria for the fabrication of large parts or difficult shapes using high-energy methods.

Although these programs produced much useful data, much of the work was conducted on a trial and error basis. This was expensive and it was found that there were so many variables that influence the explosive forming process that it was difficult to study the separate and combined effects of the important variables within the scope and funds of the programs. Therefore, although procedures were developed for the production of specific parts, it was difficult to repeat experiments with a high degree of reliability; and when one changed materials or conditions of forming, prediction of results became difficult.

In 1958 the Martin Marietta Corporation became interested in explosive forming and recognized the need to understand the influence of important forming parameters on the deformation of metal blanks. The first step in the research and development program was to develop scaling laws for the explosive forming process^(19,20). This permitted the trial and error process to be done quickly and inexpensively on a small scale by providing a reliable method of scaling the results to full size. During the development of scaling laws, the important variables governing the process were identified. Each of these variables was then systematically investi-

gated to reveal some of the basic mechanisms operative during explosive forming.

In 1965, the Manufacturing Technology Division of the Air Force Materials Laboratory at Wright Patterson Air Force Base, Ohio became keenly aware of the potential of high-energy methods for the fabrication of large components from high-strength alloys. The interest centered on the development of necessary data that could be applied to specific hardware associated with a portion of the Air Force space charter, i.e., solid-rocket motor production. The basic understanding of the variables governing the explosive forming process by Martin Marietta resulted in the award of contract AF33(615)-3167 to apply previous knowledge to the fabrication of high-strength alloys of interest to the Air Force.

The basic objectives of the contract were to develop formability limits for five different alloys; establish relationships between explosive charge and metal draw depth; conduct computer analyses to permit the prediction of charge, draw depth, and part strain; develop design criteria for full-scale forming dies; and evaluate the effects of explosive deformation on material properties. Most of the objectives were met. The following sections present the procedures used and the results of technical work during the past 19 months.

Four of the five alloys studied under the contract were steel: D6AC, HP 9-4-25, and 12% nickel, and 18% nickel maraging steel. The fifth material was 7039-0 aluminum.

It was found that the vacuum-melted HP 9-4-25 alloy exhibited the best formability of the alloys studied, while vacuum-melted 18% nickel maraging steel (250 grade) was the least formable. Only the 7039-0 aluminum could be explosively formed in one operation to a hemispherical shape.

Explosive forming was not found to have a significant influence on fracture toughness behavior for any of the alloys. With respect to stress corrosion resistance, the HP 9-4-25, 12Ni-5Cr-3Mo, and vacuum-melted 18% nickel maraging steels were virtually unaffected by alternate exposure to 3% NaCl for up to 200 hours. The air-melted 18% nickel maraging steel showed a significant reduction in mechanical properties, while the D6AC and 7039 aluminum were moderately affected.

An IBM 1620 computer program was used to permit the prediction of blank draw depth, blank pull-in, explosive requirements,

and metal strain distribution. The empirical relations in the literature for predicting impulse from given charge weights did not provide good agreement between theory and experiment for draw depth. However, when the desired draw depth is known, the program calculates the strains present in the formed part with good accuracy. Empirical results of metal draw depth as a function of explosive charge revealed a generally linear relationship using nondimensional parameters. The subsequent use of charges selected from the empirical relations gave very good results with respect to predicted draw depth for a given material.

Die criteria were developed using both 6-inch and 24-inch diameter dies. The critical design parameter was found to be clamping stiffness. Significant stiffness is mandatory to prevent flange wrinkling of the high-strength steels. The use of conventional-design massive clamping rings, etc., creates serious logistics problems for full-scale dies, therefore, lightweight construction is preferred. Channel clamping rings produce high stiffness but specific design features such as mode of attachment and frontal area appear to be important. Thin-shell die cavity and support structure have been found to be very satisfactory for steel forming. No dimensional changes nor problems have been encountered with either the die shell or support structures when initial charges up to two pounds and sizing charges up to one-half pound are used on a 24-inch-diameter model die. (These charges scale to 548 pounds and 140 pounds for a 156-inch full-scale die, respectively.) Dimensional changes in the 4340 normalized die shell do occur when sizing shots of one pound are used. This problem can be eliminated by using a higher heat-treat level for the alloy.

SECTION II

EXPERIMENTAL PROCEDURE

1. MATERIALS

The materials selected for study under this program are all of high interest to the Air Force for use in booster structures. Alloys D6AC and HP 9-4-25 are steels that derive their maximum properties from quenching and tempering. The 12% and 18% nickel maraging steels are age-hardenable compositions and can be strengthened to high strength levels by a simple thermal treatment at 900 to 950°F. Aluminum alloy 7039 is also an age-hardenable material that is weldable and possesses good strength and toughness. Its use is mainly being considered for liquid propellant tankage rather than solid rocket motors, which involve the high-strength steels. The chemical composition and mechanical properties for all the alloys are presented in Tables I and II respectively.

To develop formability limit curves for the alloys it was necessary to explosively form sheet thicknesses down to 0.020 inch. The quality of the thinner sheets, i.e., 0.020- and 0.032-inch material, was quite poor. However, these sheet gauges were the thinnest produced by the industry at the time and were respectable considering the stage of production. The quality was further complicated by the need to roll the alloys on hand mills due to the small quantity. Sheet tolerances and surface waviness could not be controlled as precisely as with thicker materials. Mechanical properties also varied from data published by the manufacturer. In spite of the material variations, forming experiments using the thin stock were conducted satisfactorily.

Material produced for Phase II and Phase III was much more consistent, and the properties were found to be typical for the respective alloys. Thicknesses from 0.150 to 0.750 inch were used in forming, stress corrosion, and fracture toughness studies.

Because all the alloys investigated were explosively deformed in their softest condition, i.e., annealed, it was necessary to heat treat the materials after forming to produce maximum strength properties. In addition, undeformed material required heat treatment to permit the evaluation of forming effects on mechanical behavior. The heat treatment cycles used for each alloy are listed in Table III. Because the thermal process cycle for 7039 aluminum is proprietary, heat treat data on the alloy have been omitted

TABLE I
Chemical Composition for Several High-Strength Alloys

Alloys	Elements present, weight. per cent														
	C	Mn	Si	Co	Ni	Mo	Al	Ti	Fe	Cr	Mg	Zn	Cu	Zr	V
7039 Al	-----	0.25	0.05	-----	0.02	-----	Bal.	0.01	0.15	0.20	2.32	4.10	0.02	-----	-----
18% Ni (MA)	0.026	0.08	0.09	7.45	17.95	4.85	0.08	0.48	Bal.	-----	-----	-----	-----	0.02	-----
12% Ni (MA)	0.028	0.05	0.09	-----	11.98	2.93	0.45	0.20	Bal.	4.83	-----	-----	-----	-----	-----
D6AC	0.48	0.60	0.20	-----	0.57	1.01	-----	-----	Bal.	1.04	-----	-----	-----	-----	0.09
HP 9-1-25	0.27	0.28	0.01	3.92	8.30	0.49	-----	-----	Bal.	0.41	-----	-----	-----	-----	0.07

TABLE II

Average Mechanical Properties for Several High-Strength Alloys

Material	Condition	Thickness inch	Ultimate Tensile Strength KSI	Tensile yield Strength (0.2% Offset) KSI	Per cent Elongation in two inches	Remarks
7039 Al	T 61	0.032	65.0	56.0	10.5	As received 2 hr @ 775°F
	Annealed	0.032	46.0	21.3	18.5	
	T 61	0.063	66.2	57.8	11.7	
	Annealed	0.063	46.0	22.8	20.5	
	T 61	0.090	61.5	51.8	12.2	
	Annealed	0.090	46.7	21.4	22.5	
	T 61	0.125	62.4	53.2	12.5	
	Annealed	0.125	46.8	21.5	22.0	
	T 61	0.750	58.5	48.5	14.4	
	Annealed	0.750	42.0	22.2	20.1	
D6AC	Annealed	0.020	119.0	104.0	10.0	As received
	H T	0.020	210.0	198.0	5.5	
	Annealed	0.032	118.0	100.0	12.0	
	H T	0.032	214.0	198.0	6.5	
	Annealed	0.040	123.0	102.0	13.0	
	H T	0.040	214.0	200.0	7.0	
	Annealed	0.050	128.0	115.0	11.5	
	H T	0.050	212.0	200.0	7.0	
	Annealed	0.063	129.0	113.0	12.5	
	H T	0.063	210.0	198.0	7.0	
	Annealed	0.125	127.5	110.0	15.0	
	H T	0.125	216.0	201.0	10.0	
	Annealed	0.750	129.0	101.0	20.0	
H T	0.750	219.0	200.0	11.0		
18% Ni (RSM 250)	Annealed	0.020	122.0	104.0	2.5	As received MA 3 hr @ 950°F MA 3 hr @ 900°F
	Maraged	0.020	244.0	235.0	2.0	
	Annealed	0.032	136.0	111.0	3.5	
	Maraged	0.032	245.0	238.0	2.0	

TABLE II Continued

Material	Condition	Thickness Inch	Ultimate Tensile Strength KSI	Tensile yield strength (0.2% offset) KSI	Per cent Elongation in two inches	Remarks	
18% Ni (RSM 250)	Annealed	0.040	134.0	121.0	3.0		
	Maraged	0.040	245.0	230.0	2.5		
	Annealed	0.050	132.0	101.0	4.7		
	Maraged	0.050	245.0	232.0	3.0		
	Annealed	0.063	145.0	128.0	4.0		
	Maraged	0.063	258.0	245.0	4.0		
	Annealed	0.063	132.0	103.0	5.0	Vacuum melted	
	Maraged	0.063	232.0	222.0	3.0	Vacuum melted	
	Annealed	0.125	138.0	110.0	8.5		
	Maraged	0.125	255.0	245.0	5.0		
	Annealed	0.750	143.0	100.0	16.0		
	Maraged	0.750	250.0	240.0	10.5		
HP 9-4-25	Annealed	0.032	150.0	112.0	14.0	As received	
	H T	0.032	187.0	182.0	5.5	(AUS @ 1550°F +	
	Annealed	0.050	150.2	120.0	15.5	Double temper + 2 hr	
	H T	0.050	191.0	178.0	9.5	@ 1000°F)	
	Annealed	0.063	144.0	122.0	16.8		
	H T	0.063	190.0	179.0	9.0		
	Annealed	0.125	151.5	118.5	16.5		
	H T	0.125	193.2	181.0	11.8		
	Annealed	0.750	150.0	90.0	21.0		
	H T	0.750	194.0	178.0	19.0		
	12% Ni	Annealed	0.045	173.0	152.5	9.5	Annealed properties
		H T	0.045	188.0	180.0	7.0	well above published
Annealed		0.055	179.0	157.5	8.0	values	
H T		0.055	187.0	178.0	6.5		
Annealed		0.065	179.0	157.0	7.0		
H T		0.065	189.0	179.0	6.0		
Annealed		0.140	175.0	157.0	11.0		
H T		0.140	185.0	175.0	9.0		
Annealed	0.750	144.0	95.0	17.0			
H T	0.750	197.5	196.0	13.5			

TABLE III

Heat Treatment Schedules Used to Obtain
Full-Strength Properties for the Five High-Strength Alloys

RSM 250 18% maraging steel

Solution anneal: 1650°F (1 hour/inch of thickness)
Rockwell C 32
Age: 900°F for 3 hours - air cool

12Ni-5Cr-3Mo maraging steel

Solution anneal: 1550°F (1 hour/inch of thickness)
Rockwell C 35
Age: 900°F for 3 hours - air cool

HP 9Ni-4Co-0.25C

Anneal 1150°F for 36 hours - Rockwell C 30
Austenitize 1550°F for 1 hour/inch of thickness - oil quench
Temper: Double temper 1000°F - 2 hours each

D6AC

Anneal 1275°F - Rockwell C 28
Austenitize 1625°F/inch of thickness
Quench in 400/425°F salt for 15 minutes
Temper: 400°F for one hour
Double temper 1040°F - 2 hours each

7039-T6 Aluminum

Anneal 775°F for 2 hours
Heat treating: Proprietary Kaiser heat treat schedule

from the table. Appropriate data can be obtained from the producer, Kaiser Aluminum Company. It should be mentioned that the influence of explosive deformation on the response to heat treatment for the age-hardenable alloys in the program, i.e., 12% and 18% nickel maraging steel and 7039 aluminum, is to modify the kinetics of the reaction. This generally requires the reduction of aging time at temperature, or a reduction in aging temperature with the same time, to obtain optimum properties. Because a study of heat treatment effects caused by explosive forming was beyond the scope of the present program, the strength values for the three age-hardenable alloys reported in this document do not necessarily represent optimum properties.

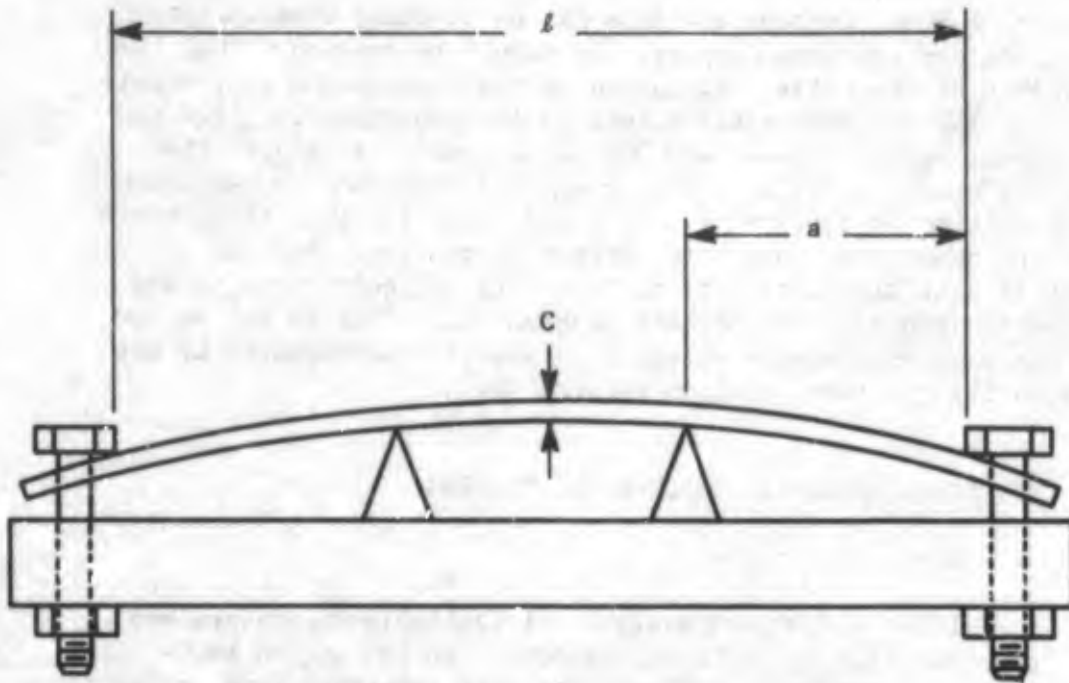
2. STRESS-CORROSION AND MECHANICAL TESTING

a. Stress Corrosion

After a thorough analysis of available literature and previous experience in stress-corrosion testing, a bent-beam type specimen configuration with two-point loading was selected for use during the program. Figure 1 is a schematic view of the specimen and presents the analytical method for determining fiber stress at a given sample deflection. A stress level of 80% of the tensile yield stress was used for all specimens during exposure of material to the corrosive media.

To facilitate the testing of stressed samples, a test fixture was constructed to permit the exposure of 12 samples simultaneously. Figure 2 shows the fixture with prestressed material in place. To ensure that the correct levels were used for given deflections of the specimens, several calibration runs were conducted using an SR-4-type strain indicator and paper strain gauges. Figure 3 shows the setup used to calibrate the loading fixture. Figure 4 shows the excellent agreement between calculated and measured values of strain as a function of sample end deflection.

An accurate and discriminatory method for sample exposure was necessary to evaluate the effects of explosive deformation. Alternate immersion in a 3% NaCl solution maintained at $72 \pm 2^\circ\text{F}$ was used through the program. The stressed samples were loaded on the immersion rack shown in Figure 5, and an air actuated cylinder connected to an electric timer permitted immersion of the rack when desired.



$$\Delta Y = \frac{(3l^2 - 4a^2) \sigma}{24EC}$$

σ = Stress

E = Modulus of Elasticity

C = $\frac{1}{2}$ Specimen Thickness

l = Fixture Constant (Length of Span)

a = End of Specimen to Point of Support

ΔY = Deflection

Figure 1 Formula for Deflection of Stress-Corrosion Specimens

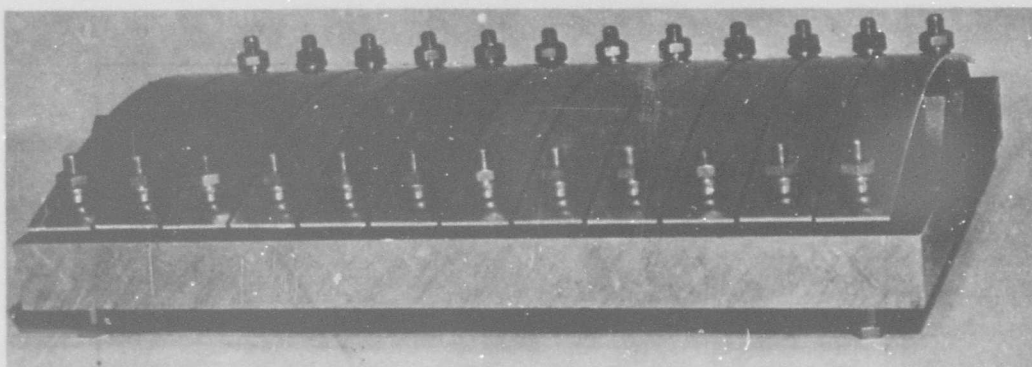


Figure 2 Stress-Corrosion Specimen Fixture Ready for Test

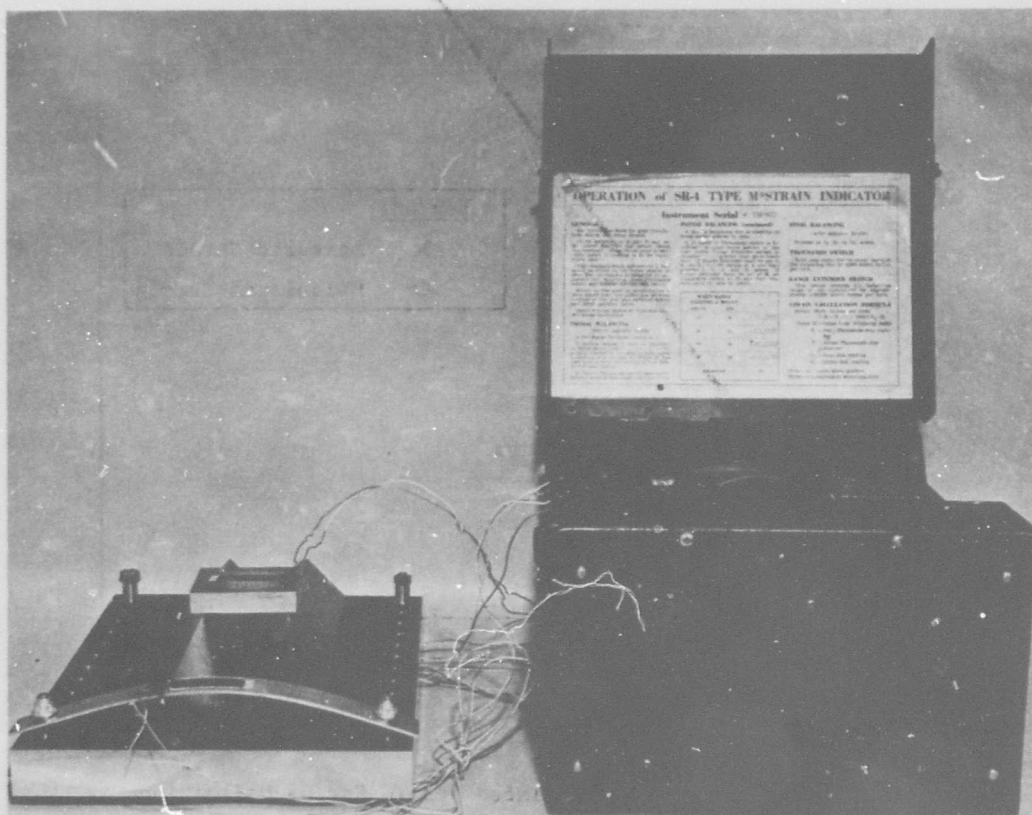


Figure 3 Calibration Arrangement for Stress-Corrosion Test Specimens

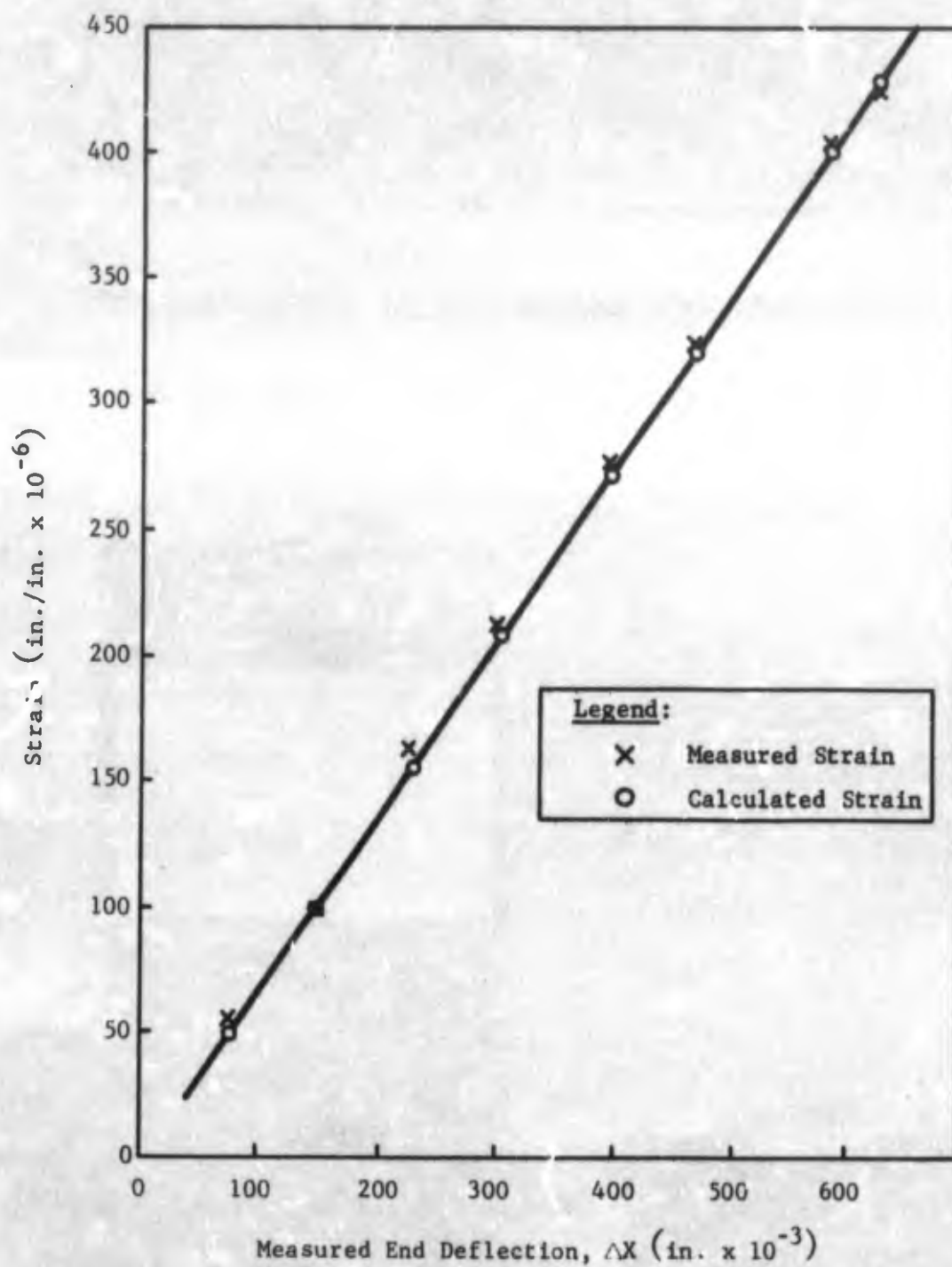


Figure 4 Measured and Calculated Strain Versus Deflection

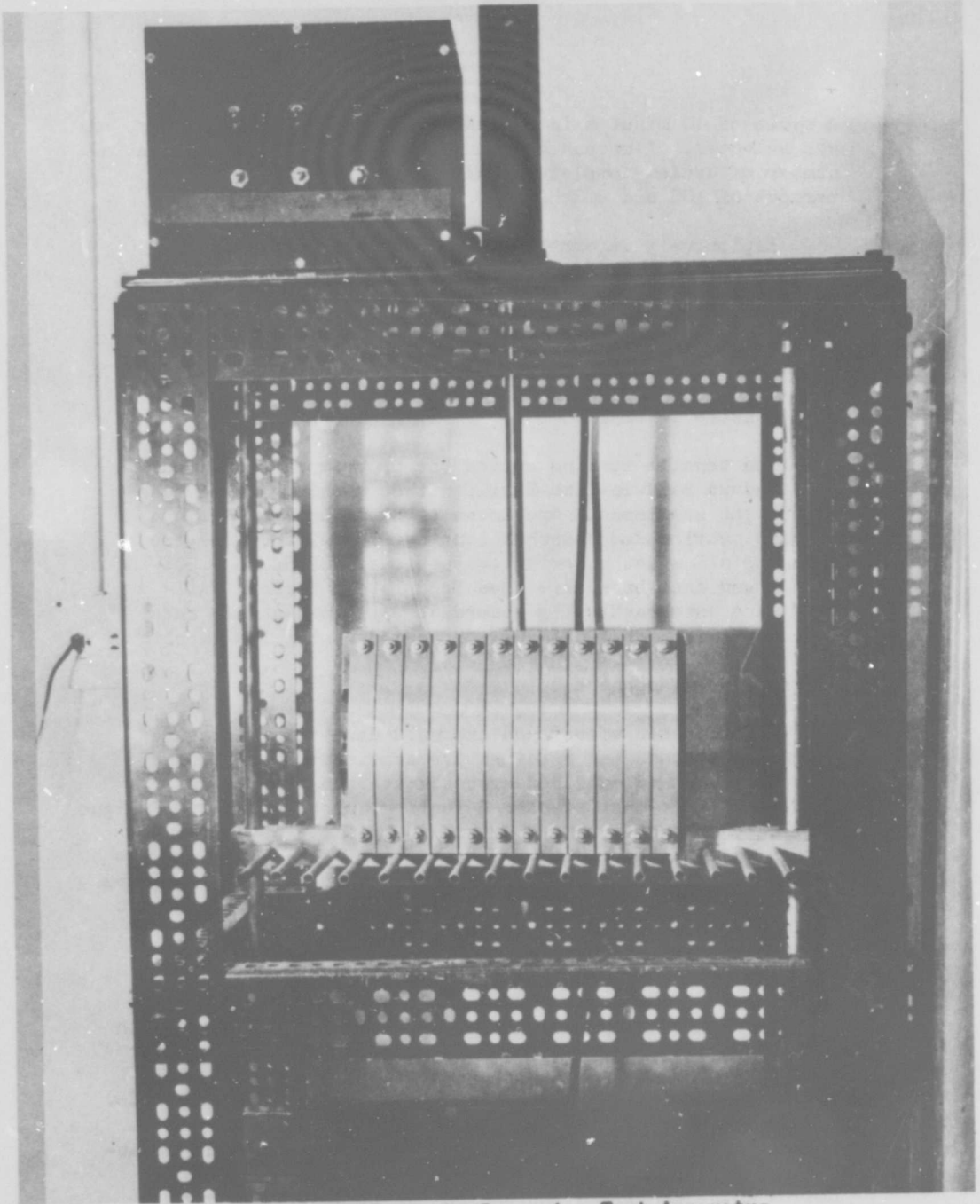


Figure 5 Alternate Immersion Test Apparatus

A cycle of 10 minutes in the bath and 50 minutes of drying was selected. A mechanical counter was used to record the number of cycles completed. All alloys were exposed for periods of 100 and 200 hours.

Explosively deformed material for stress-corrosion testing was prepared by forming the separate alloys in a shallow flat-bottomed die. Strains on the order of 4 to 6% were produced in the samples. A disc-shaped charge of TNT pressed under 7000 psi and centrally positioned over the blank was used to effect forming.

b. Tensile Testing

The tensile testing during the program was conducted on standard Baldwin-Lima-Hamilton test machines using "dog-bone" type specimens. Specimens eight inches long with a reduced section 2.250 inches long by 0.500 inch wide were used for all sheet material evaluations. Standard 0.505-inch round test bars were used for plate material. All data were autographically recorded. Specimen strain rates of 0.005 inch/inch/minute were produced during load application.

c. Fracture Toughness

Considerable effort was expended developing fracture toughness methods and specimen preparation. Evaluation of both arc-burn and machined precrack starter defects was conducted. Arc-burn starter defects required excessive fatigue cycling to promote crack growth, and multiple crack fronts sometimes resulted. However, the elliptical crack shape resulting from this method was usually excellent. The machined precrack yielded crack growth with fewer fatigue cycles, but crack shape was generally less desirable. A combination of the two methods was used for the program surface-crack specimens.

Width and thickness studies were conducted to establish dimensions sufficient to ensure plane-strain conditions for the comparative tests with each material and remain within the available test machine load capability of 150,000 pounds.

Plane-strain fracture toughness, K_{Ic} , values were established using the Irwin expression for plane-strain crack toughness, where:

$$K_{Ic}^2 = 1.21 \pi \sigma^2 \left(\frac{a}{Q}\right)$$

where:

$\frac{a}{Q}$ = normalized or "resolved" crack depth,

σ = gross applied stress,

a = flaw depth (fatigue advanced crack),

limitations accepted in the equation are:

$a \leq \frac{B}{2}$ (B = specimen thickness)

$\sigma_{\text{gross}} \leq \sigma_{\text{ys}}$ and $\sigma_{\text{gross}} \geq 0.09 \sigma_{\text{net}}$

Area of crack should be $< 10\%$ of specimen area
(for a semielliptic crack, the crack area should
be $\geq 0.064 BW$, where W = sample width)

Fracture toughness specimens for evaluation of explosive deformation effects were produced by deforming large blanks into a flat-bottomed steel die. The die is shown in Figure 6. A typical formed piece before removal of the part from the die is shown in Figure 7. To effectively evaluate the influence of variations in strain of samples taken from the deformed panels, a photo-grid was placed on the bottom of the blank. Samples extracted from the gridded panel could then be accurately categorized with respect to specific strain across the piece. Figure 8 shows a gridded and deformed panel of 7039-O aluminum before cutting for sample preparation.

The detailed fracture-toughness program description begins on page 44.

3. THEORETICAL ANALYSES

An IBM 1620 digital computer program was used to predict the dynamic response of flat blanks to an explosive charge. The program was developed as part of the analytical work under our ARPA contract to establish a Center for High-Energy Forming Processes.

When total impulse from a given charge calculated from empirical relations is used as input to the program, the predicted draw depth is higher than that resulting from experiment. However, when the impulse is lowered until the draw depth agrees

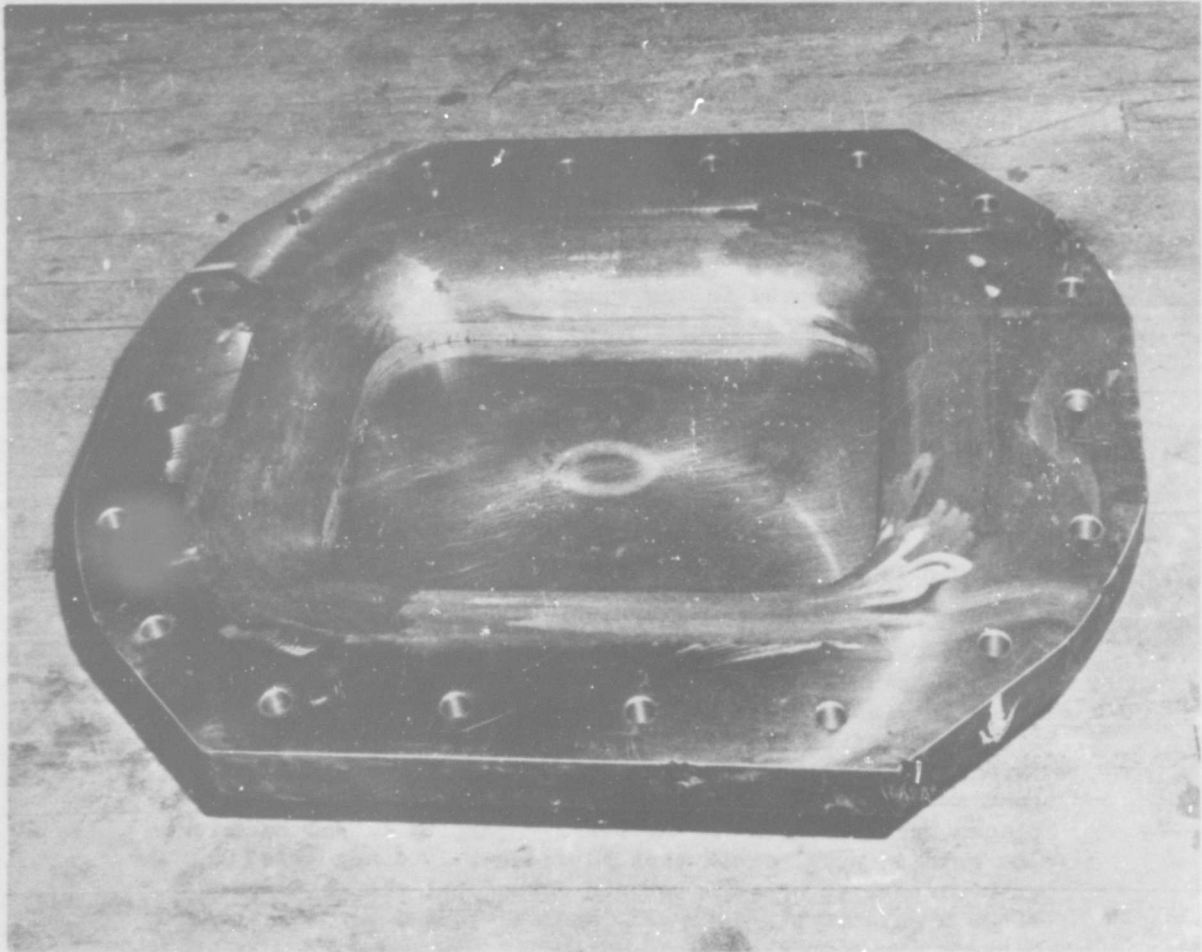


Figure 6 Die for Fracture Toughness Specimen Preparation

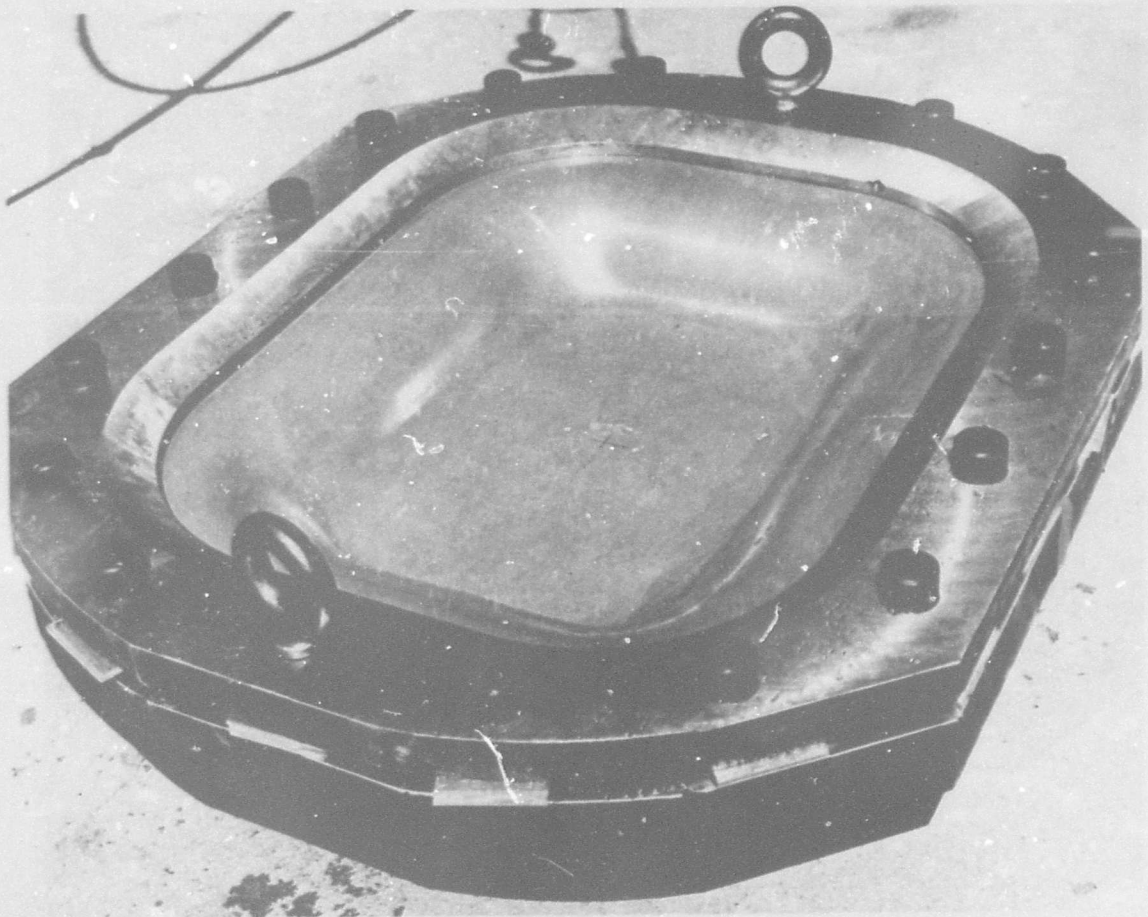


Figure 7 Explosively Formed 7039-0 Aluminum Plate Prior to Removal from the Die

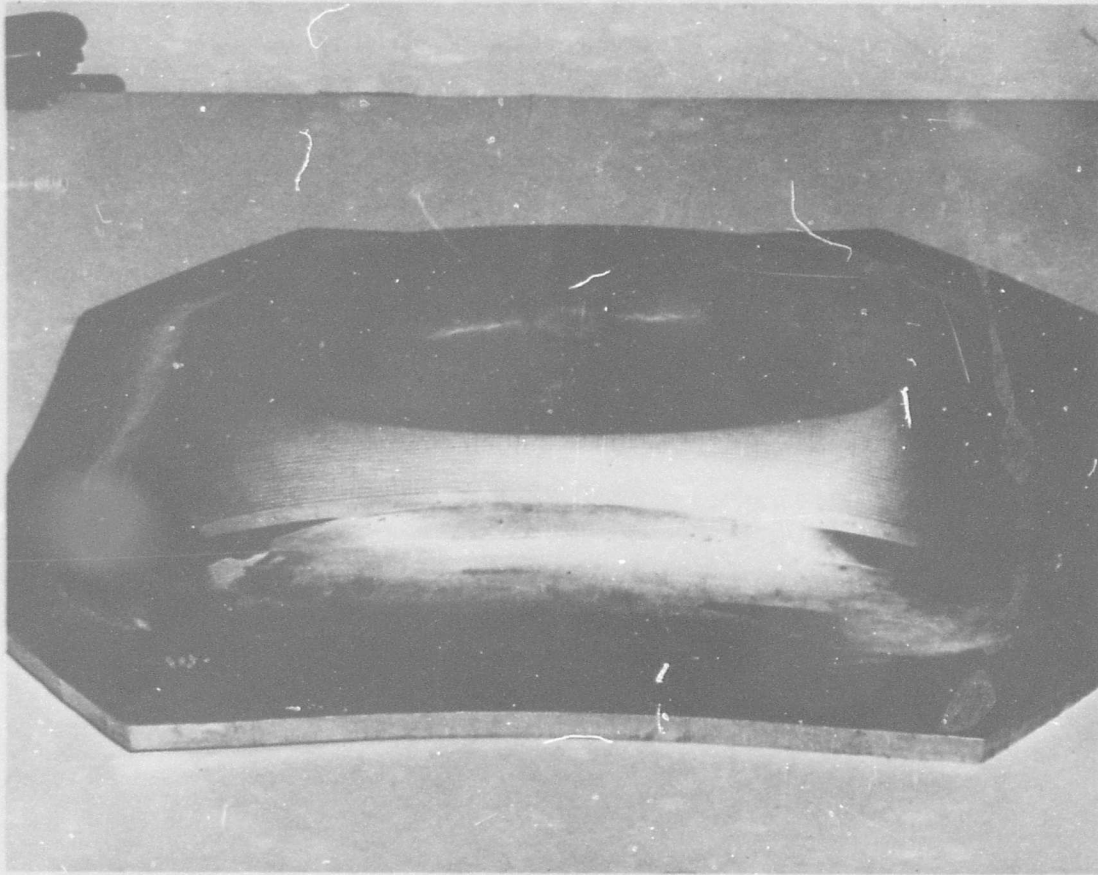


Figure 8 Formed Fracture Toughness Material from 7039-0 Aluminum Plate Showing Flat Portion with Photo Gridded Strain Markings

with the measured value, good agreement is found between theory and experiment for deflected shape and for radial and circumferential strains.

4. CHARGE PREPARATION AND FORMING

a. Explosive Charge Preparation

Trinitrotoluene (TNT) was used as the explosive throughout the program. Uniform and reproducible charges were produced by pressing granulated TNT using a 12- or 50-ton hydraulic press. Figure 9 is a view of the 50-ton press in our new Ordnance Laboratory. Note the television monitor for remote operation. The pressing dies used for subscale and full-scale charge preparation are shown in Figures 10 and 11, respectively.

The general procedure was as follows:

- 1) The pressing dies were cleaned with acetone to remove all foreign matter;
- 2) The desired granulated TNT was weighed on a powder balance;
- 3) The weighed TNT was poured into the cylindrical container above the die and the load plunger placed in the cylinder over the powder;
- 4) The die cavity was evacuated using a standard mechanical vacuum pump;
- 5) Pressure was applied to the die plunger to produce 7000 psi on the explosive;
- 6) Pressure was released and the die removed from the charge. At this stage the pressed charge was snugly wedged in the cylinder;
- 7) A press-out collar was placed in the cylinder and the cylinder placed on a heavy walled container that contained foam or soft paper;
- 8) Pressure was applied to the charge to force it out of the cylinder and into the container, and;
- 9) The charge was removed and taken to a storage magazine to await installation in the standoff device.

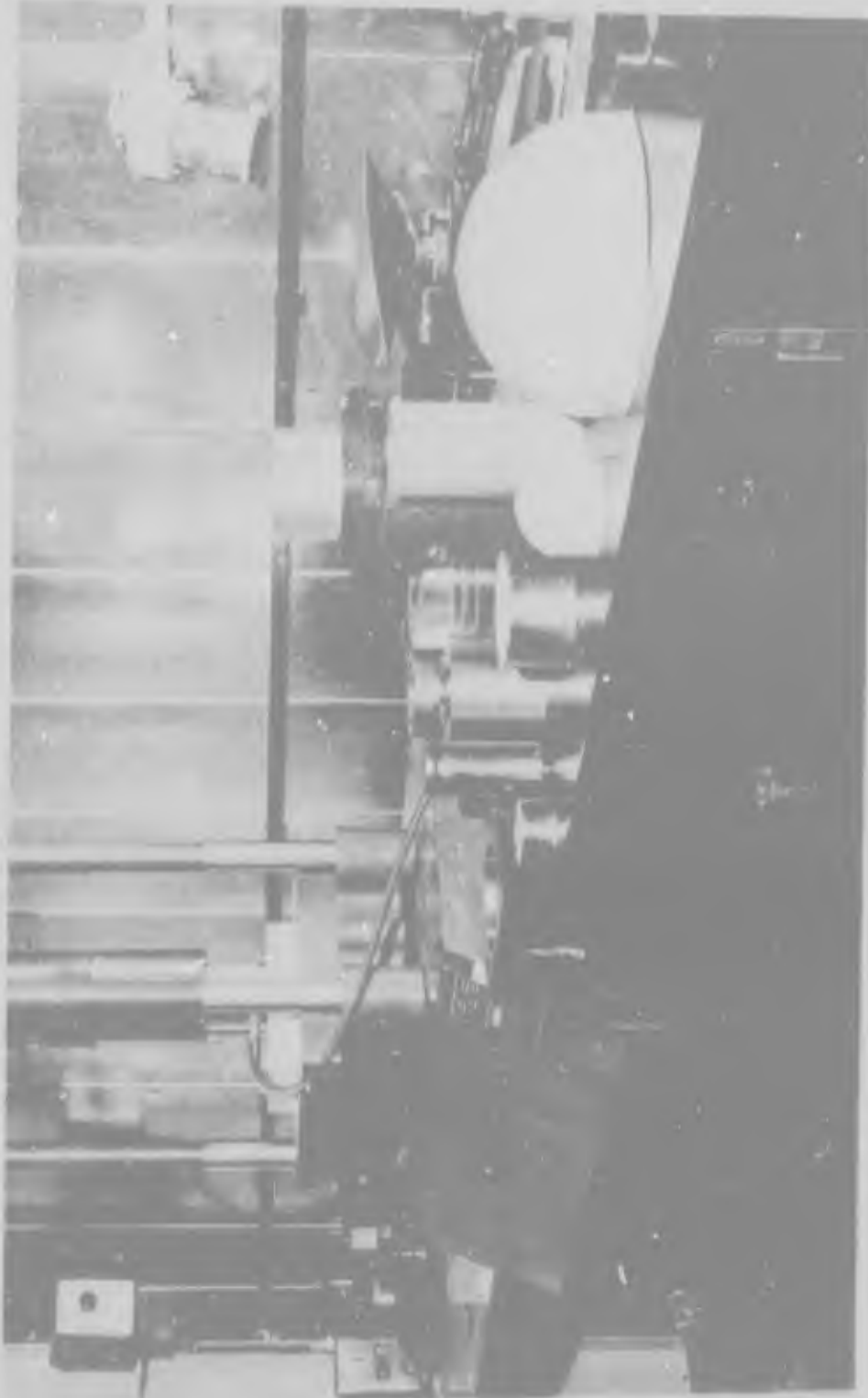


Figure 9. View of 50-Ton Explosive Press for Charge Preparation

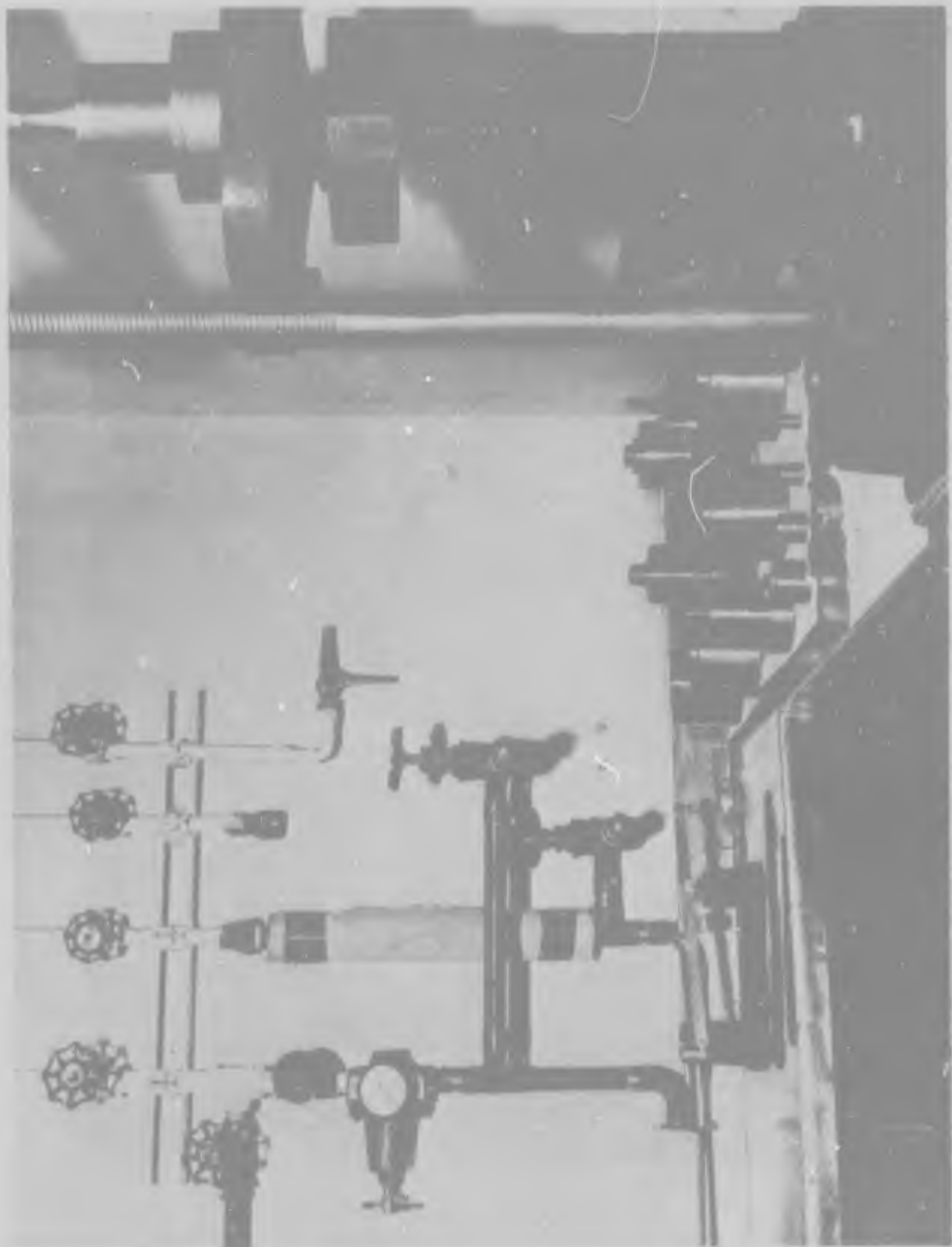


Figure 10. View of Small Pressing Cell Showing 12-Ton Press and Die Sets Used for Charge Pressing

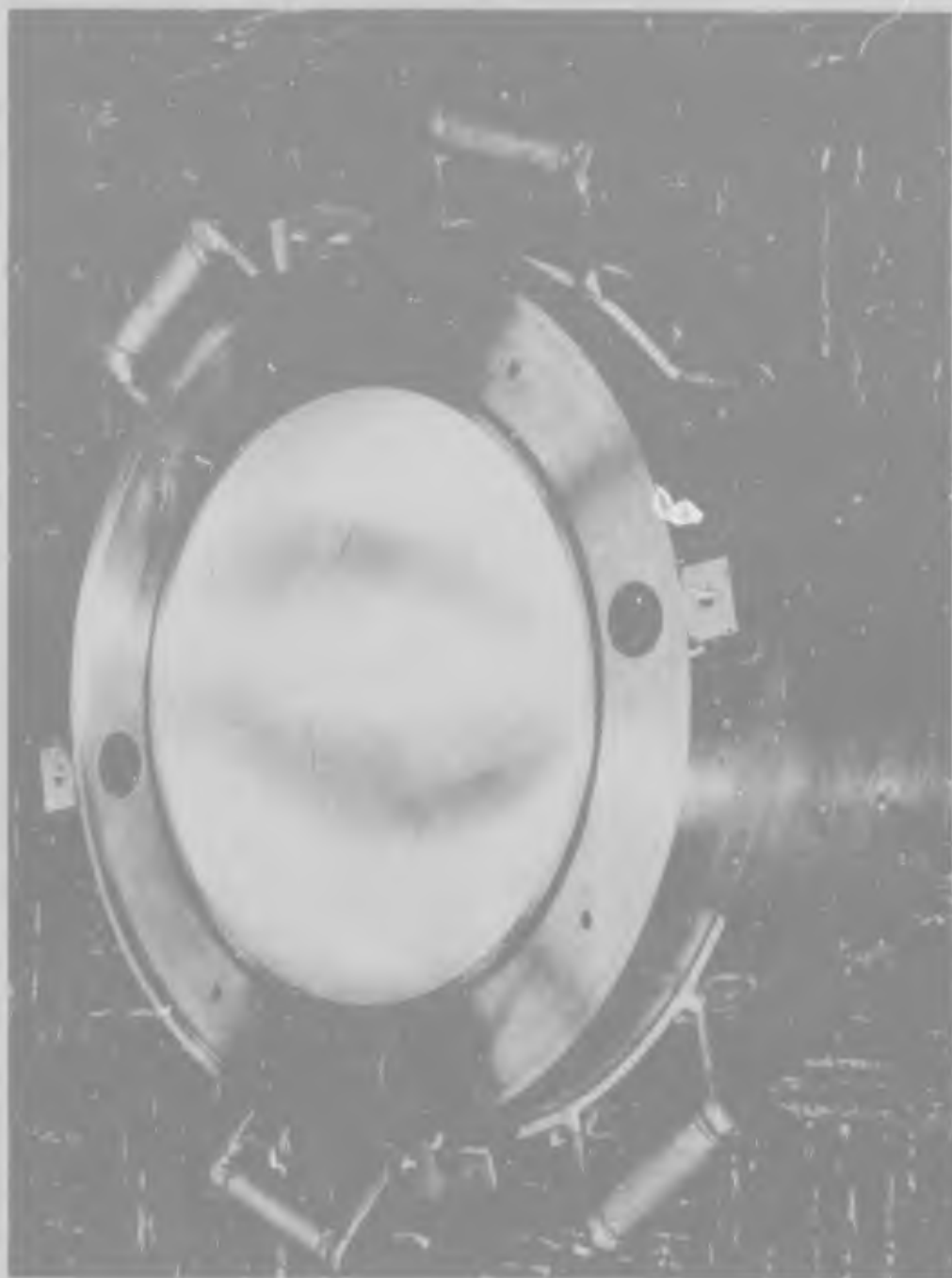


Figure 11 Casting Die Used to Produce the Twenty-five Pound Pull
Scale Explosive Charges

In all cases an RDX booster was simultaneously pressed into the center of the charge. The booster weight was in general about 3 to 10% of the charge weight depending on the size of the charge being used. Because TNT is a very insensitive explosive, the RDX booster ensures complete first-order detonations and maximum energy release. The booster weight was converted to equivalent weight of TNT to yield the total charge weight. A number 8 electric blasting cap (6.9 grains of contained pentaerythritol tetranitrate (PETN) was used to detonate the charge. Compensation for the cap explosive was made for all charges. Figure 12 shows a typical pressed charge and electric blasting-cap arrangement for subscale forming shots on the six-inch diameter dies. Figure 13 shows a pressed charge of TNT for 24-inch-diameter experiments and the cast pentolite charge used for full-scale tests.

5b. Explosive Forming

The forming work conducted throughout the program involved several different dies. The formability limit curves, charge-versus-draw-depth curves, stiffness experiments, and die criteria tests were all conducted on six-inch-diameter dies. The first two studies were completed on a series of dies ranging in draw depth from 0.6 inch to 3.5 inches. The dies were fabricated from 4340 alloy steel head-treated to a Rockwell C hardness of 38 to 42. Figure 14 shows the dies as delivered from the manufacturer. The deepest die of the series was also used to study the influence of die stiffness on metal formability. Figure 15 shows one of the arrangements used in the stiffness evaluations. One further use of six-inch subscale dies was for the development of die criteria. A shell die with cylindrical support section and gusset-strengthened draw ring was fabricated by using a previously formed 12% nickel maraging steel dome. Figure 16 illustrates the die and an aluminum hemisphere formed in the die.

To verify scaling from the six-inch dies to larger sizes, both 24-inch hemispherical die and a 120-inch free-forming tool were used. Figure 17 shows a Meehanite cast die used to form aluminum. A much stiffer die necessary for the wrinkle-free forming of steel parts was also used. Figure 18 indicates the method for adding significant stiffness to the clamping arrangement. Channel-type reinforcements were welded directly to the clamping ring for greater rigidity with minimum weight. One final tool used to verify scaling data on a full-scale die is shown in Figure 19. The die was a free-forming tool and

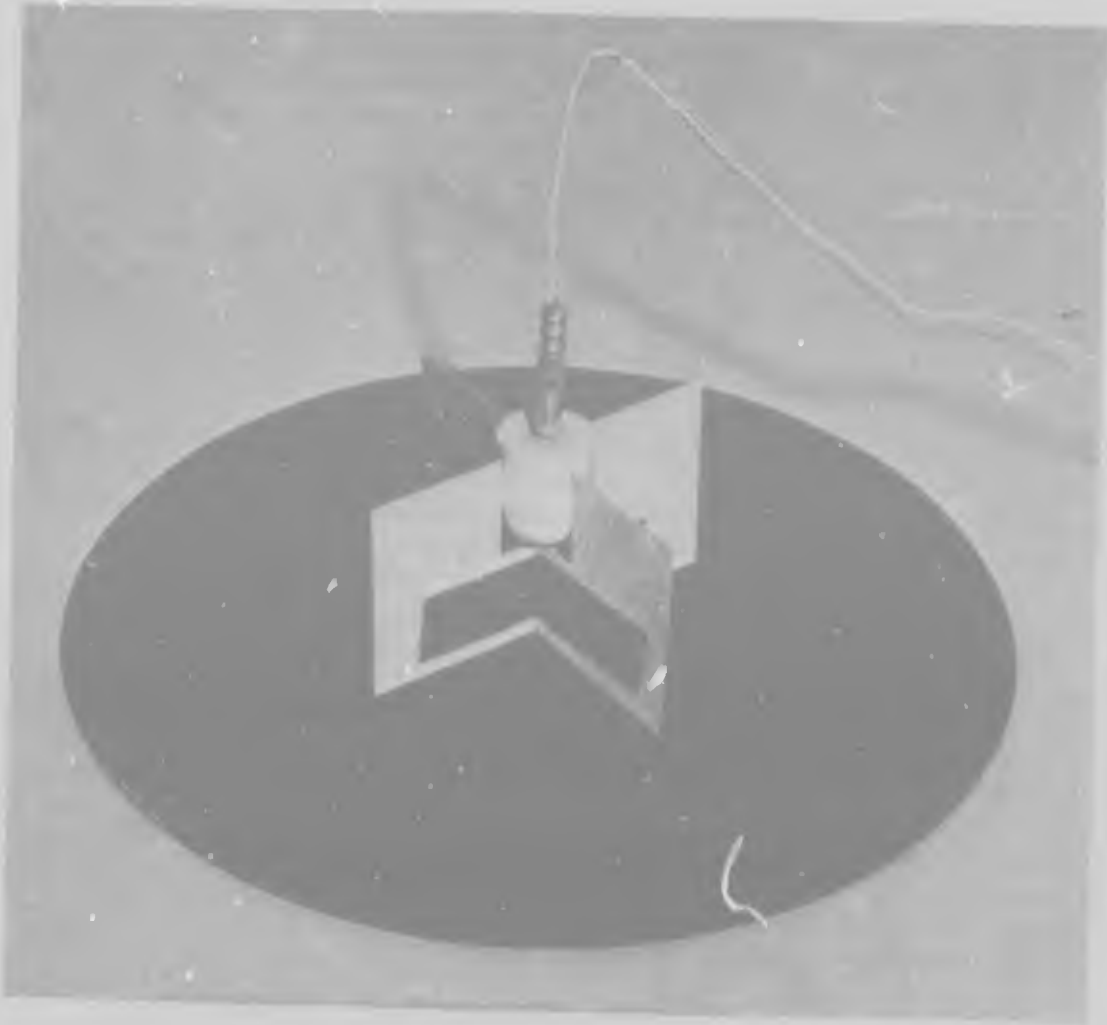


Figure 12 Pressed TNT Charge with Electric Blasting Cap for Six-Inch Die Experiments

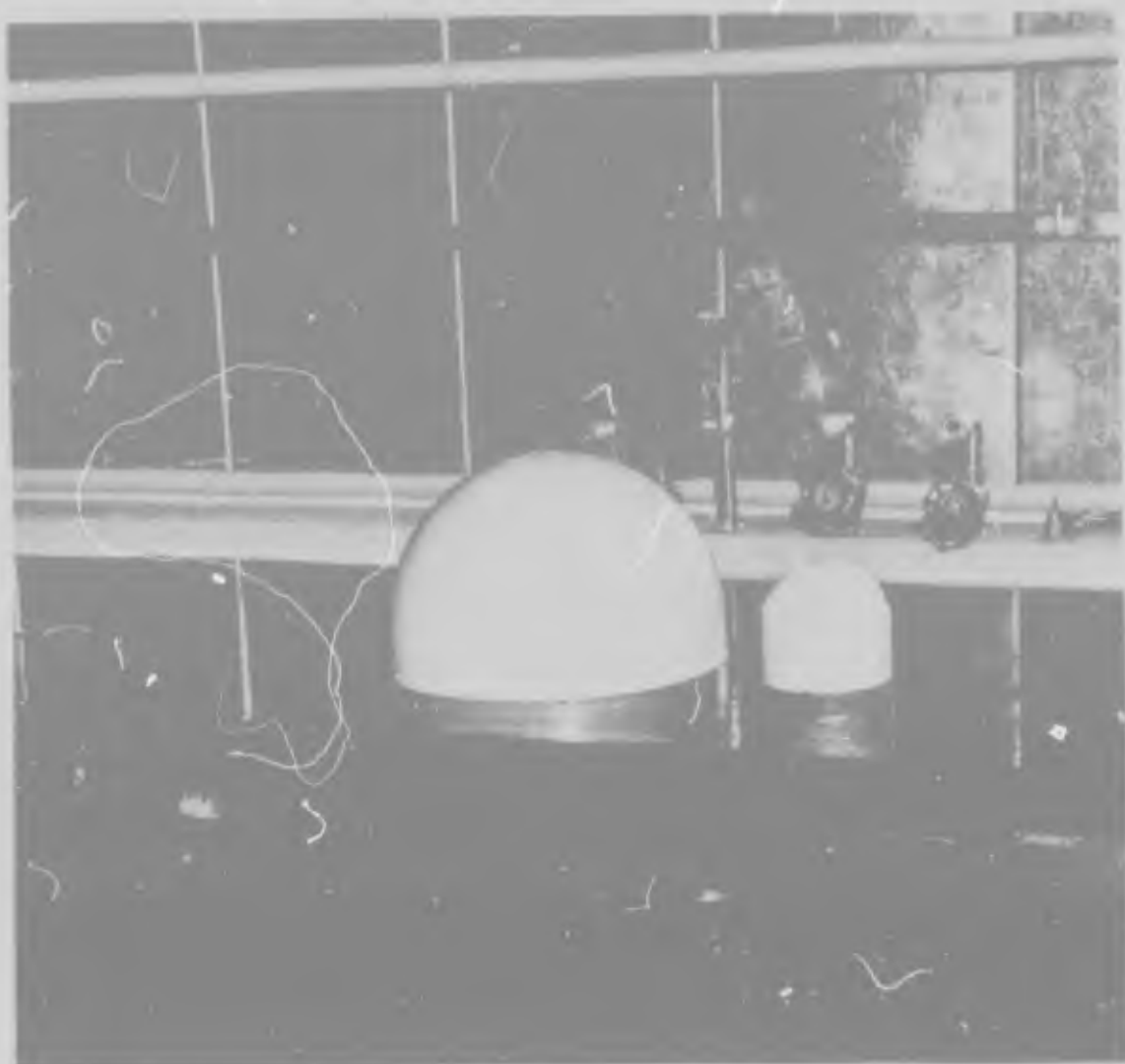


Figure 13. Typical Pressed and Cast Charges for One-Fifth Scale and Full-Scale Forming Experiments



Figure 14 Six-Inch Diameter Explosive Forming Dies and Universal Die for Support of Six-Inch Diameter Dies

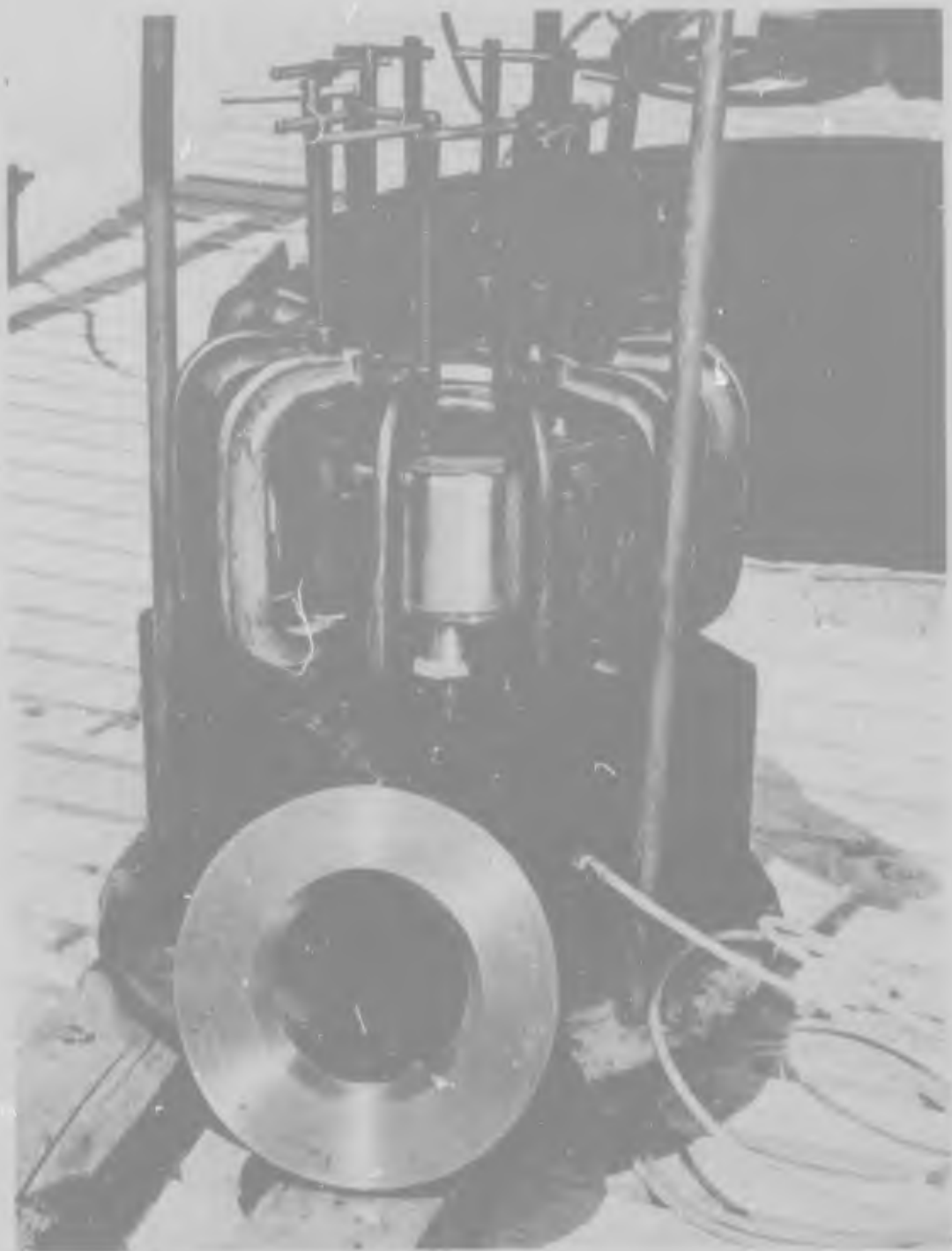


Figure 15 Arrangement for Clamp and Ring Stiffness Experiments on a Six-Inch Diameter Die



Figure 16 Lightweight 12% Nickel Maraging Steel Shell Die Fabricated from Six-Inch Formed Hemispherical Dome



Figure 17. 24-Inch Hemispherical Die Used in Forming



Figure 18. Phase III Die Used for Forming the High-Strength Steels



Figure 19. Free-forming Die for Full-Scale Experiments (120-Inch Diameter)

consisted mainly of a stiffened, cylindrical, steel container with a heavy draw ring welded to the upper periphery of the cylinder. A three-inch-thick clamping ring was used. Cast Meehanite C clamps with a capacity of 60,000 pounds each were used to clamp the hold-down ring and provide necessary restraint for the blank.

SECTION III

RESULTS AND DISCUSSION

1. MECHANICAL TESTING

Mechanical test results were obtained for three different properties: basic mechanical strength, stress-corrosion effects, and fracture toughness. The following sections present the results of mechanical evaluation.

a. Basic Mechanical Strength

All of the alloys were tested on receipt to determine whether typical properties existed for each of the different sheet and plate thicknesses. Table II, presented in the last section, summarizes the results. It should be noted that for 7039 aluminum, HP 9-4-25, and D6AC the properties are not significantly influenced by reductions in thickness. On the other hand, both of the maraging materials showed rather drastic changes in mechanical properties as the thickness decreased below about 0.063 inch. For the 18% nickel maraging steel, the tensile yield and ultimate strengths were typical for the alloy. The attendant percent elongation was very low, however, which created subsequent problems in deep drawing. Although the elongation for the 12% nickel alloy remained relatively constant with reduction in sheet thickness, the tensile yield strength was significantly higher than normal for all thicknesses below 0.140-inch.

Discussion of the discrepancies with Republic Steel Corporation resulted in the reprocessing of both the 12 and 18% nickel maraging steels. It was decided that a higher austenitizing temperature for the 18% nickel alloy might enhance the ductility. Material austenitized at 1650°F for one hour and water quenched yielded a material with greater elongation and lower yield strength. Upon subsequent maraging of the reheat-treated material at 900°F for three hours, an appreciable loss of ductility occurred. The alloy did not respond to maraging after the 1650°F austenitizing treatment. Table IV shows some typical results of the heat-treat study.

A study of the 12% nickel maraging steel revealed that

an improper heat treatment had been given the alloy at the source of manufacture. Material heat treated according to recommended procedures responded well and produced suitable stock for experimentation. Only in the thinnest gages was the elongation low. However, satisfactory results were produced with the reheat-treated material. Table V presents the results of tests conducted on reprocessed sheet.

To establish the influence of explosive deformation on the mechanical behavior of the several alloys in the program, standard tensile specimens were machined from flat sections of deformed material. Material for evaluation was deformed in the flat-bottomed die described earlier. Sample thicknesses studied were 0.063-inch and 0.125-inch. All of the tensile specimens were heat treated to recommended strength levels after forming and machining. Table VI presents average data from four specimens of each thickness taken from each of the five materials used in the program. In general, explosive deformation causes a reduction in tensile elongation of from 1 to 3.5%. The D6AC and 7039-T62 alloys were affected the most, while the 18% nickel maraging steel showed virtually no effect on elongation from explosive forming. In all but one case the tensile yield strength was reduced as a result of explosive forming. The same effect was observed for the ultimate strengths of 18% nickel maraging steel, HP 9-4-25, and 7039-T62 aluminum. The other two alloys improved in ultimate strength when explosively deformed.

With respect to explosive deformation effects one must realize that the enormous energy imposed on the alloys before thermal treatment can cause a significant modification in the heat-treat response. This effect has been observed in previous work conducted for the National Aeronautics and Space Administration⁽¹¹⁾. Because it was beyond the scope of the present contract to optimize the heat-treating schedule for each alloy, it is quite likely that adjustment in the recommended heat-treat temperatures and/or times will produce properties equal to or greater than those produced through standard heat-treating practice. The thermal response of each alloy after explosive forming should be evaluated before the incorporation of high-energy techniques in routine manufacturing methods. The indications from the cited previous work were that properties higher than those normally obtained could be expected from a modified thermal process.

TABLE IV

Effect of Heat Treatment on the Response of Thin Gauge 18% Nickel Maraging Steel			
Heat treatment schedule	Ultimate strength ksi	0.2% Offset yield strength ksi	% Elongation in 2 inches
As-received material	122.0	104.0	2.5
As-received material plus 3-Hour Marage at 950°F	244.0	235.0	2.0
1550°F Reaustenitize treatment plus 3 Hours at 950°F	263.0	255.0	1.5
1650°F Reaustenitize treatment	126.0	82.9	4.0
1650°F Reaustenitize treatment plus 3 Hours at 900°F	196.9	176.9	1.5

b. Stress-Corrosion Behavior

In the application of high-strength alloys to load bearing structures, the influence of exposure to corrosive environment on mechanical properties must be evaluated. Verbraak⁽²¹⁾ observed a decided detrimental effect of explosive deformation on the stress-corrosion resistance of austenitic stainless steel. There have been other reports of effects of high-energy forming on alloy performance under stress. Because the alloys in this program are very high strength and will be used in structures sustaining high tensile stresses, the resistance of each material to corrosive environment had to be established. Evaluation of material in a 3% NaCl solution under conditions of alternate immersion for periods up to 200 hours was completed on heat-treated and explosively formed plus heat-treated sheet. A stress level of 80% of the tensile yield strength was used. A study of stress-corrosion resistance of annealed plus explosively formed material was not felt to be important because the materials are used at maximum strength levels.

TABLE V

Mechanical Properties of Re-heat Treated
12% Nickel Maraging Steel Sheet

Sheet Thickness Inch	Ultimate strength ksi	0.2% Offset Yield strength ksi	Per cent elongation in two inches
.022 A	128.0	110.0	2.5
.022 MA	178.0	170.0	3.5
.032 A	133.5	101.4	4.0
.032 MA	187.0	179.0	5.0
.040 A	134.0	102.0	4.0
.040 MA	182.0	175.5	4.0
.050 A	136.5	100.0	6.0
.050 MA	185.0	178.3	5.0
.063 A	137.0	104.0	6.0
.063 MA	190.6	183.5	5.0
Typical properties			
.040 - .125 A	130 - 140	100 - 115	7 - 9
.040 - .125 MA	180 - 200	170 - 190	5 - 7
A - Solution annealed at 1550°F for 1 hour and air cooled.			
MA - Maraged at 900°F ± 10°F for 3 hours.			

TABLE VI

Baseline Data for Undeformed and Deformed Materials

Material	Thickness inch	As-received heat treated				Explosively formed heat treated		
		Ultimate tensile strength ksi	Tensile yield strength ksi	% Elongation in two inches	Ultimate strength ksi	Yield strength ksi	% Elongation in two inches	
HP 9-4-25	0.063	190.0	179.0	9.0	185.0	166.0	7.5	
HP 9-4-25	0.125	193.2	181.0	11.8	185.0	173.0	11.0	
D6AC	0.063	210.0	198.0	7.0	215.5	193.0	5.5	
D6AC	0.125	216.0	210.0	10.0	219.0	201.0	6.5	
12% N1 MA	0.063	190.6	183.5	5.0	192.5	178.5	5.0	
12% N1 MA	0.125	192.0	184.5	7.0	195.0	187.2	6.5	
18% N1 MA	0.063	258.0	245.0	4.0	253.0	232.0	3.0	
18% N1 MA	0.125	255.0	245.0	5.0	247.0	241.0	5.0	
7039-T6	0.063	66.2	57.8	11.7	61.7	51.8	9.3	
7039-T6	0.125	62.4	53.2	12.5	61.4	50.8	9.6	

An investigation of sheet thicknesses of each alloy prior to explosive deformation revealed that the resistance of undeformed material to corrosion under stress is good. Stress corrosion in the classical sense, i.e., intergranular attack with attendant crack propagation under stress was not observed for any of the alloys either before or after explosive deformation. General pitting type corrosion was present, however, in all stressed and exposed materials. The 12Ni-5Cr-3Mo alloy is unaffected by solution exposure under stress. The 18% nickel maraging steel and 7039-T62 aluminum alloys are significantly affected by the corrosive environment. Only a moderate reduction in properties was observed for the other alloys. The tensile elongation was adversely affected for all but the 12Ni-5Cr-3Mo alloy. Thus the order of resistance of the high-strength alloys to corrosion under stress prior to explosive deformation is as follows, in order of decreasing resistance: 12Ni-5Cr-3Mo, HP 9-4-25, D6AC, 7039-T62 aluminum, and 18% nickel maraging steel.

After explosive forming only the properties of the 7039-T62 aluminum alloy were significantly affected. Some increase in corrosion susceptibility was noted for the D6AC steel but the reduction in properties when compared to undeformed and exposed material was not severe. It should be noted that heavier gage material was, in general, more resistant to corrosion under stress than thin material. An important fact should be related regarding the apparent effects of explosive deformation on stress-corrosion resistance. Previous experience has shown a decided effect of explosive deformation on the response to heat treatment. Because shock deformation appreciably increases the number of dislocations in the structure and induces high energy in the crystal lattice, it is reasonable to expect a modification in the aging kinetics or tempering response of the alloy. Although the quench and temper materials showed a reduction in properties, the influence of explosive deformation was not great. However, for two of the alloys depending on precipitate strengthening from artificial aging (i.e., 7039-T62 and air-melted 18% nickel maraging steel) the effects of explosive forming were significant. Because the 12Ni-5Cr-3Mo alloy also depends on precipitate strengthening but exhibits virtually no change in strength, the data suggest that the aging mechanism for the alloy is different from that of the 18% nickel steel and 7039-T62 aluminum. Apparently the induced energy produced by explosive forming

did not affect the alloy's response to thermal treatment. In summary, the resistance to stress corrosion for the alloys after explosive deformation is as follows, in order of decreasing resistance: 12Ni-5Cr-3Mo, HP 9-4-25, D6AC, air-melted 18% nickel steel, and 7039-T62 aluminum. Thus explosive forming has a significant effect on the reduction in properties of 7039-T62 and air-melted 18% nickel steel. It was interesting to note that vacuum-melted 18% nickel maraging steel was almost completely resistant to stress-corrosion. The data clearly show the superiority of vacuum-melted versus air-melted material for resistance to stress corrosion. More study is necessary of heat-treatment response to ascertain whether the effect of high-energy deformation on stress-corrosion resistance is real or is caused by a radical change in aging kinetics. Summary data in bar graph form are presented in Figures 20-22.

Some difficulties were encountered in the evaluation of plate thicknesses of each alloy. Originally, consideration was given to the use of standard 0.505-inch round bar for a study of corrosion effects. The specimens would not have been satisfactory, however, because all of the corroded material would be removed during machining. Flat, "dog-bone" type specimens were machined. It was found that, because the ratio of exposed to unexposed material after machining was low, the effects of corrosion under stress were not noticeable. To get a better understanding of the influence of stress-corrosion exposures on the behavior of plate material, specimens were prepared from the exposed plate coupons to produce three tensile specimens: one from the compression surface of the coupon, one from the center of the coupon (unexposed), and one from the tension surface. The specimens so produced were approximately one-eighth-inch thick and of standard length and width. Results from "sheet" strips from plate showed the compression surface results agreed with those of the centrally located specimen; thus, all specimens from plate were prepared only from the tension and compression surfaces. Data obtained from plate after the 3% NaCl alternate immersion for 200 hours are listed in Table VII. In general, the results for plate material are similar to those obtained for sheet stock. Thus, plate does not appear to be any more susceptible to stress corrosion than sheet. In fact, for the 18% nickel steel and the HP 9-4-25 alloy, the data suggest greater resistance to stress corrosion.

ALLOY CONDITION				
Specimen	As Received	Explosively Formed	Heat Treated	200 Hour Exposure
A	X		X	
B	X		X	X
C	X	X	X	
D	X	X	X	X

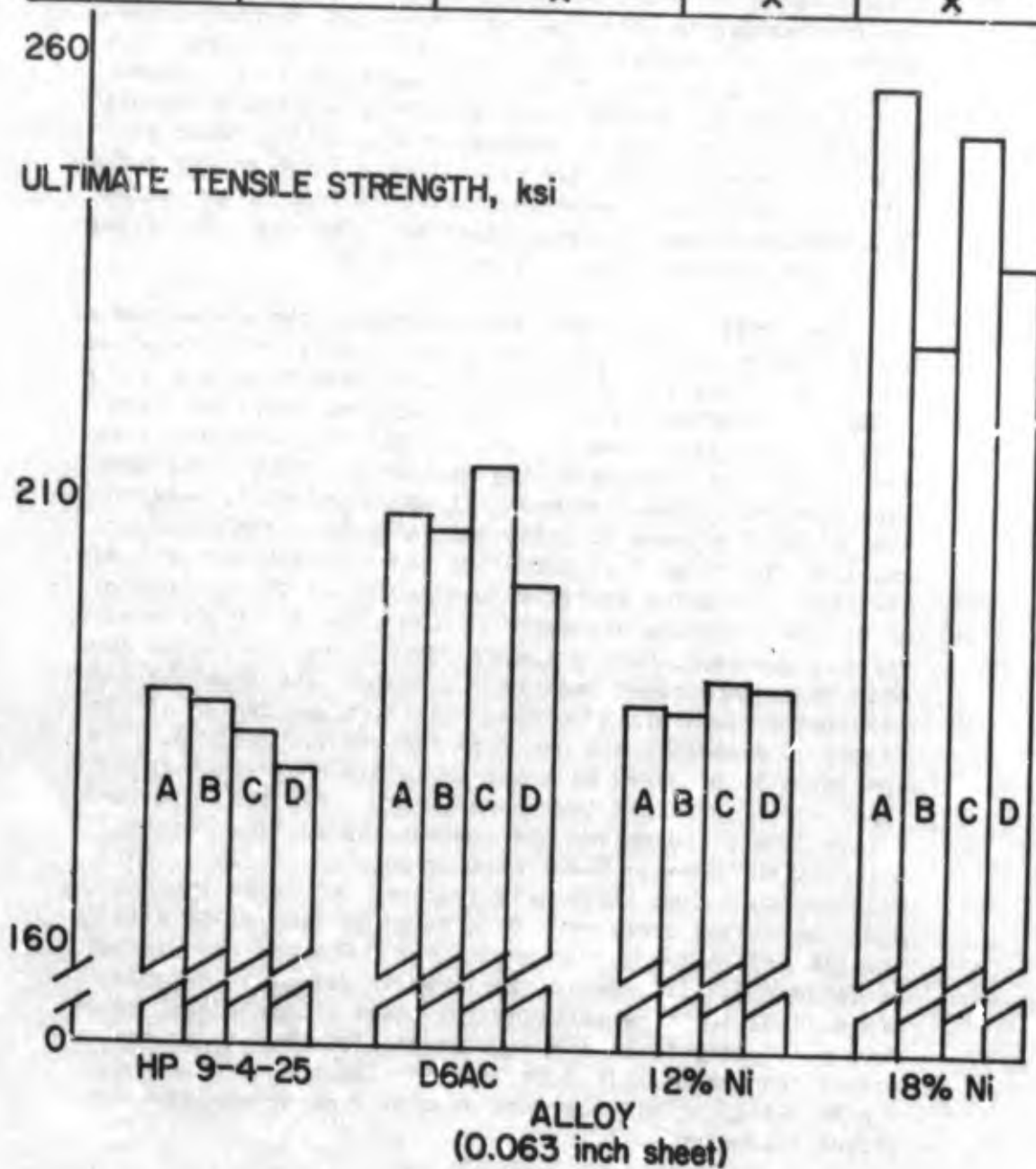


Figure 20. Effect of Explosive Deformation on the Corrosion Susceptibility under stress for Several High Strength Alloys (200 hours exposure)

ALLOY CONDITION				
Specimen	As Received	Explosively Formed	Heat Treated	200 Hour Exposure
A	X		X	
B	X		X	X
C	X	X	X	
D	X	X	X	X

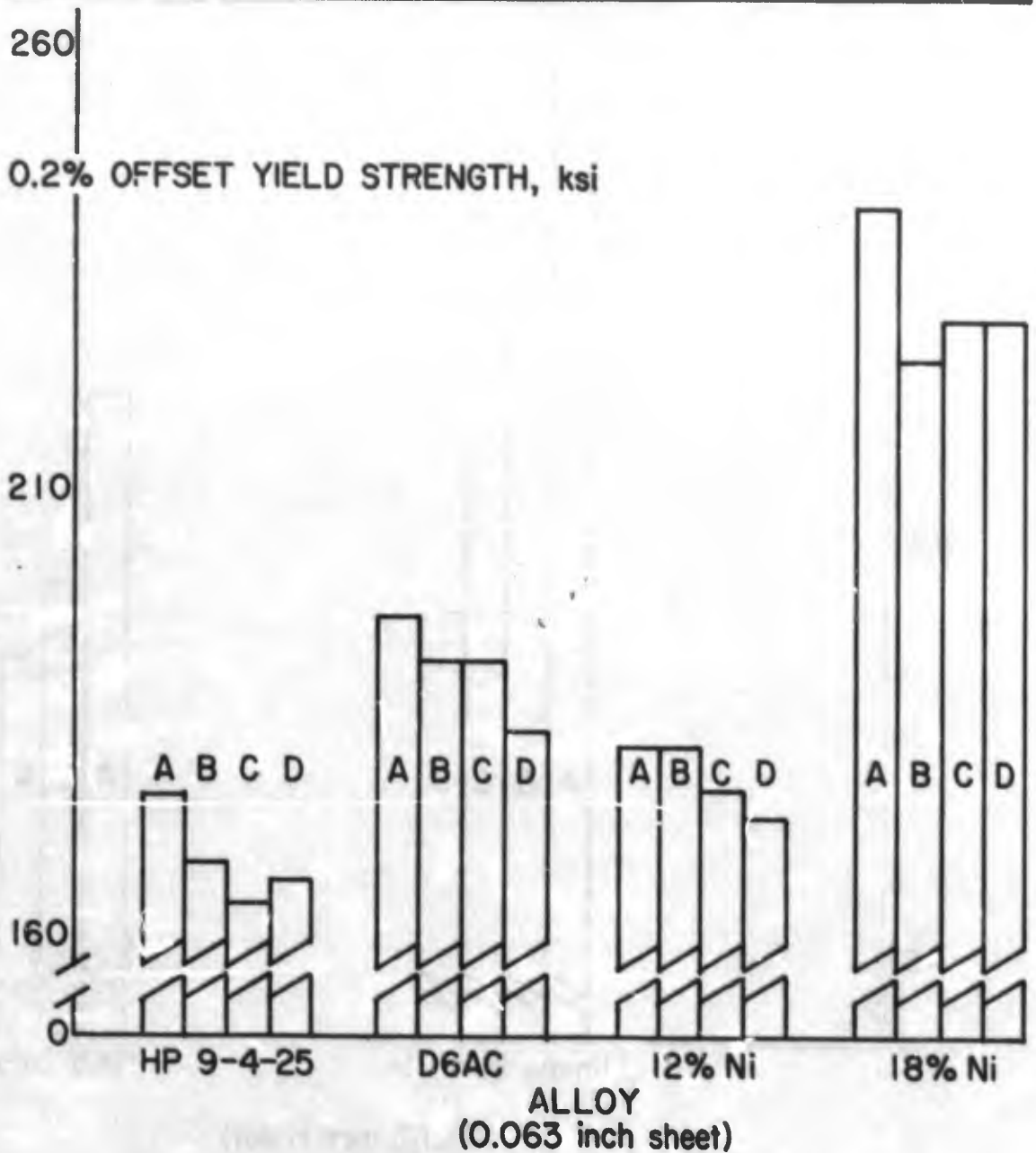
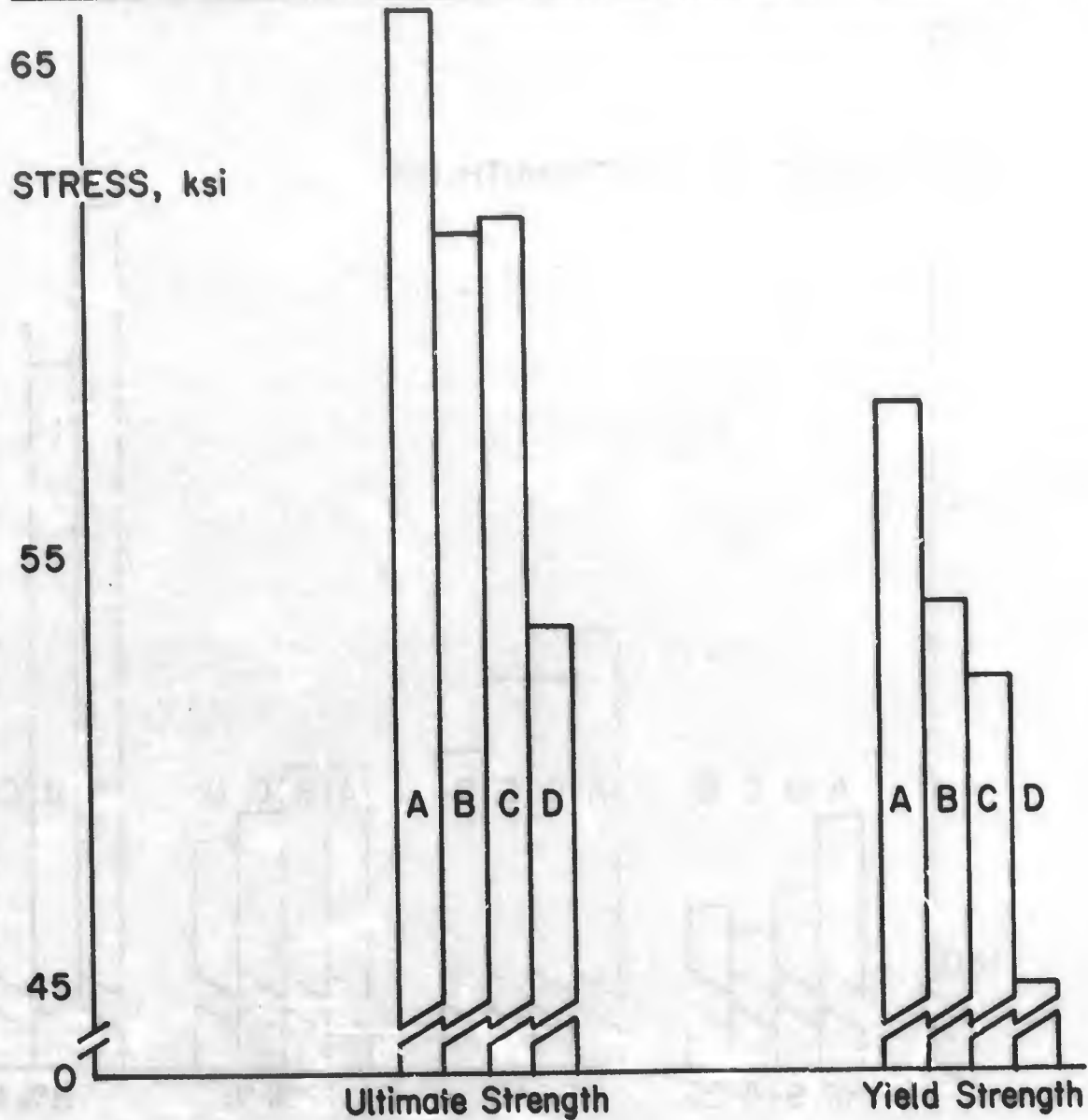


Figure 21. Effect of Explosive Deformation on the Corrosion Susceptibility under stress for Several High Strength Steel Alloys (200 hours exposure)

ALLOY CONDITION				
Specimen	As Received	Explosively Formed	Heat Treated	200 Hour Exposure
A	X		X	
B	X		X	X
C	X	X	X	
D	X	X	X	X



(0.063 inch sheet)

Figure 22. Effect of Explosive Deformation on the Corrosion Susceptibility under stress of 7039-T62 Aluminum Sheet (200 hours exposure)

TABLE VII

Stress Corrosion Results of Undeformed
Steel Plate Materials
(0.750-inch thick starting material)

Alloy	Exposure hours	Ultimate strength ksi		Yield strength ksi		% Elongation in two inches	
		Before	After	Before	After	Before	After
12Ni-5Cr-3Mo	100	209.5	204.9	208.7	204.9	5.5	4.5
	200	201.6	200.0	200.8	198.3	8.0	7.5
HP 9-4-25	100	195.0	190.2	177.5	180.3	10.0	10.0
	200	190.2	188.9	167.2	161.1	9.0	12.5
D6AC	100	214.0	214.0	210.0	192.0	11.0	11.0
	200	211.0	213.0	205.0	206.0	9.5	9.5
18% Ni	100	240.0	239.0	224.0	207.0	5.5	5.5
	200	249.0	248.0	222.0	229.0	7.0	5.0

In the deformation of 0.750-inch plate to produce suitable material for evaluation, die damage was evident as a result of the high explosive charges required. Therefore, it was decided to use the sheet materials as criteria for resistance of plate because the plate results were equal to or better than those found for sheet in undeformed material. In addition, the deformed material produced from plate was needed for fracture-toughness evaluation, which was felt to be of greater importance to the Air Force.

In summary, the results suggest that for high stress applications under corrosive environment the 12Ni-5Cr-3Mo and HP 9-4-25 alloys would be used. Data for 1% nickel maraging steel show conclusively that air-melted material is affected by corrosive environment under stress, while vacuum-melted material shows almost complete resistance and can be added to the list of recommended alloys. Explosive deformation does not appear to significantly affect the stress-corrosion resistance of the alloys listed above, and the process can be used for fabrication without concern for detrimental effects.

c. Fracture-Toughness Behavior

The objective of the fracture-toughness test was to determine the effects, if any, of explosive forming on the plane-strain fracture toughness (K_{Ic}) characteristics of the program materials.

All materials were tested in the heat-treated condition in accordance with the general program thermal treatment schedule (See Table III).

The fracture-toughness properties of greatest interest were for materials with thicknesses corresponding closely to those of the formed domes of the program in order to relate the fracture toughness values directly to hardware. However, this was not possible for some of the materials in the 1/8-inch nominal-thickness range, due to their high toughness and relatively low yield strengths. Therefore, 1/4-inch nominal-thickness was selected as a minimum for the steel evaluation and 1/2-inch plate as minimum for the aluminum alloy.

Initial consideration was given to cutting sections from the formed program domes, then flattening them for fracture-

toughness test specimens. This method was discarded for the 1/4-inch materials because of the complex flattening difficulties and the obvious question of whether the flattening effects were greater than the forming effects to be evaluated. Moreover, no practical method could be applied to determine the residual stress distribution after flattening and the complex effects on fracture-toughness values.

The flat-bottomed die described earlier was used to obtain explosively formed material. Through use of the flat-formed panels, machining problems and straightening effects were minimized, and photo-grid patterns on the panels could be used to indicate strains imposed by the explosive forming process. These strains were recorded to establish the particular strain history in the region of the induced flaw on each fracture-toughness specimen to permit a more accurate analysis of test data.

In the test portion of the program, the explosively deformed panels were cut into fracture-toughness specimens and compared with specimens of similar thicknesses from undeformed parent material for evaluation of effects of explosive forming on the fracture-toughness characteristics of each material. Most of the undesirable variables that could affect the base-line parity of this comparative program were minimized by using one heat of material for all tests in a given thickness; duplicate heat-treatment sequences for both conditions; identical specimen design and processing; and standardized rates of specimen loading (100,000 psi/min) during test. No attempt was made to duplicate the percentage of biaxial stretch of the explosively deformed material with the parent control material because this value varied across the face of the formed panels and should be reflected in any significant shift in fracture toughness between it and the parent material.

The specific type of fracture-toughness specimen selected was the surface-crack (part-through crack) specimen because this type of flaw provided higher conditions of restraint for thinner materials than other types of specimen flaw design.

Specimen design limitations were developed from the Irwin expression for plane-strain fracture toughness. (See Section II 2.c.).

All of the program specimens permitted sufficient flaw depth with appropriate temperature selection for three of the 1/4-inch steel materials. The lowering of test temperature to -110°F decreased the $\frac{K_{Ic}}{YS}$ value and consequently increased the effective plane-strain region in the midzone of the specimens with smaller a_{cr} required.

Specimen gage widths permitted sufficient latitude in flaw shape while remaining within the limitations of $\frac{W}{3}$ maximum for $2c$, and $\frac{B}{2}$ maximum for (a).

For aluminum alloy specimens, surface cracks were induced in the test specimens by first grinding a small slot. This slot was notched further with a sharp razor cut and then fatigue propagated by flexural cycling (Figure 23). The average surface tensile stress during flexure was controlled below 30,000 psi to prevent plastic flow at the front of the advancing crack.

For the steel alloy specimens, the surface cracks were induced by a combination of small arc burn (35 watt-second input, using a 1/16-inch-diameter carbon-steel electrode) and a shallow starter notch approximately 0.015 inch deep by 0.150 inch wide. The notch was a safety measure against propagation of multiple cracks from the arc-burn spot.

A flexural-fatigue cycling fixture was constructed to be adaptable for all program specimens. The three-point loading fixture, shown in Figure 23, was mounted on a BLH* SF10-U fatigue machine, which provided 30 cps loading frequency.

To save time during the fatigue cycling, crack initiation was induced in some steel test specimens at an elevated flexural stress level slightly below 0.8 TYS. Because some plastic flow could occur at the nose of the fatigue crack at high stress levels due to residual stresses in the explosively formed material, the initial flaws were further fatigue advanced at a stress level below 0.4 TYS until full flaw size was attained.

The 7039-T62 aluminum alloy specimens needed no reduced center gage section because they were designed with a width-to-thickness ratio high enough to permit easy gripping

*Baldwin-Lima-Hamilton Corporation

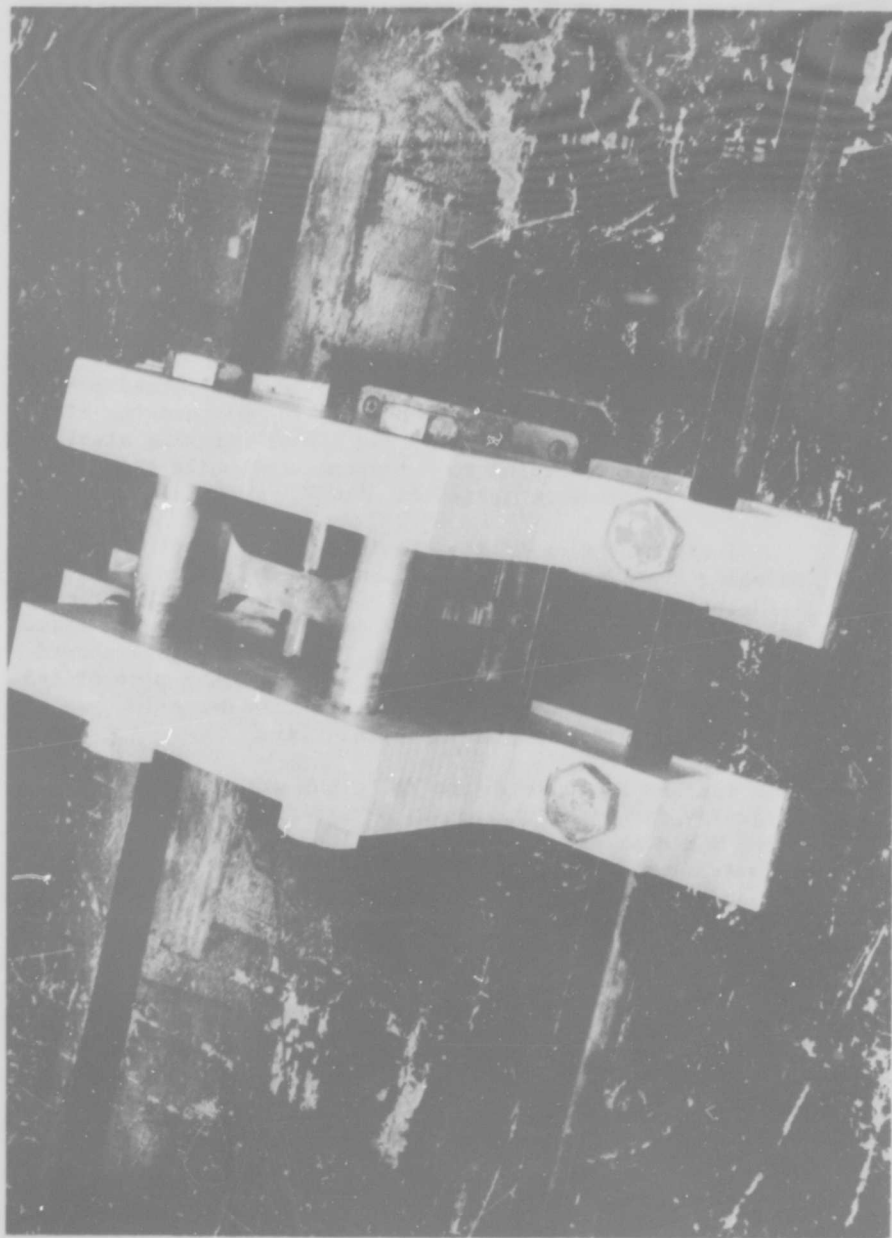


Figure 23. Three Point Flexural Loading Fatigue Fixture with $3/4$ -inch 18% Ni Maraging Steel Specimen Shown

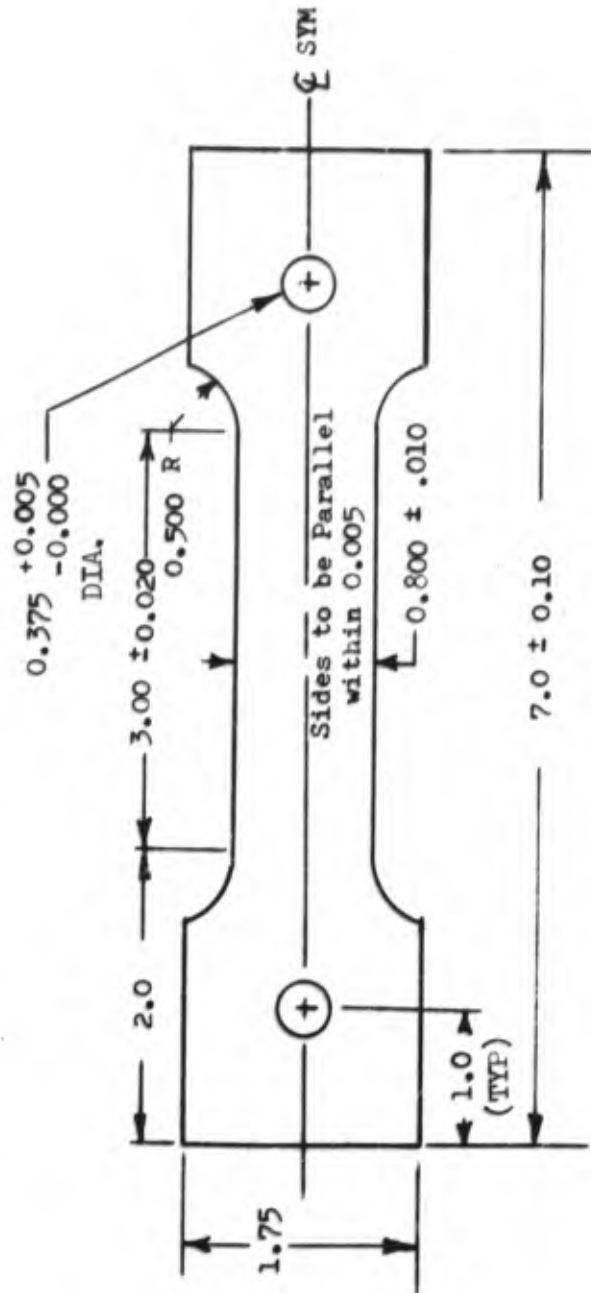
with flat wedge grips in a 150,000-pound BLH testing machine. However, the 1/4-inch steel specimens required reduced gage areas for adequate gripping. The typical specimen design for the 18% Ni maraging steel (1/4-inch) is shown in Figure 24. The specimen design for the 1/4-inch HP 9-4-25 steel, 12% Ni maraging steel, and the D6AC steel is shown in Figure 25. The 1/4-inch 18% Ni maraging steel material was difficult to grip with flat wedge grips alone; therefore, a combination pin and grip loading was used to conserve material from the limited sized flat-formed panels. Pin loading was used for the 3/4-inch 18% Ni maraging steel specimens. The aluminum alloy and 18% Ni maraging steel specimens were tested at room temperature, while the remaining steel alloys were tested at -110°F.

Instrumentation of the aluminum and 1/4-inch 18% Ni maraging steel specimens was accomplished by strain gages (1/4-inch length) bonded to the back surface of the fracture-toughness specimens directly in line with the induced flaw. At the onset of slow crack growth (pop-in) the gage showed a deviation from linearity on the stress-strain plot of the test machine's autographic recorder. This deviation was usually a distinct jog in the strain axis.

Another instrumentation technique was developed specifically for detecting pop-in of 1/4-inch steel materials. A BLH TSM dual extensometer (with long arms) was fitted with offset arm ends to reduce the 7/8-inch minimum gage length to 1/4-inch. These arm ends used phonograph needles for point contact against the test specimens. Two small center-punch indentations were placed 1/4-inch apart, centered across the surface crack of the test specimens. These indentations formed receptacles for the needle tips of the extensometer arms. At 1000X strain magnification, the system described served the same function as the strain gage for detecting pop-in. However, the system was less costly than the strain gage system -- only the needle tips were broken at specimen fracture. Replacement cost for the needles was approximately 1% of the strain-gage cost.

While testing the 1/4-inch 18% Ni maraging steel specimens, it became evident that visual observation of surface dimpling adjacent to the ends of the specimen flaw at pop-in correlated equally well with the instrumented strain-tracing techniques. This observation proved true for the 12% Ni maraging steel specimens tested at -110°F. Because

All Dimensions in Inches



Material Thickness 1/4 Nominal

Figure 24 1/4-Inch 18% Ni Maraging Steel Specimen Design

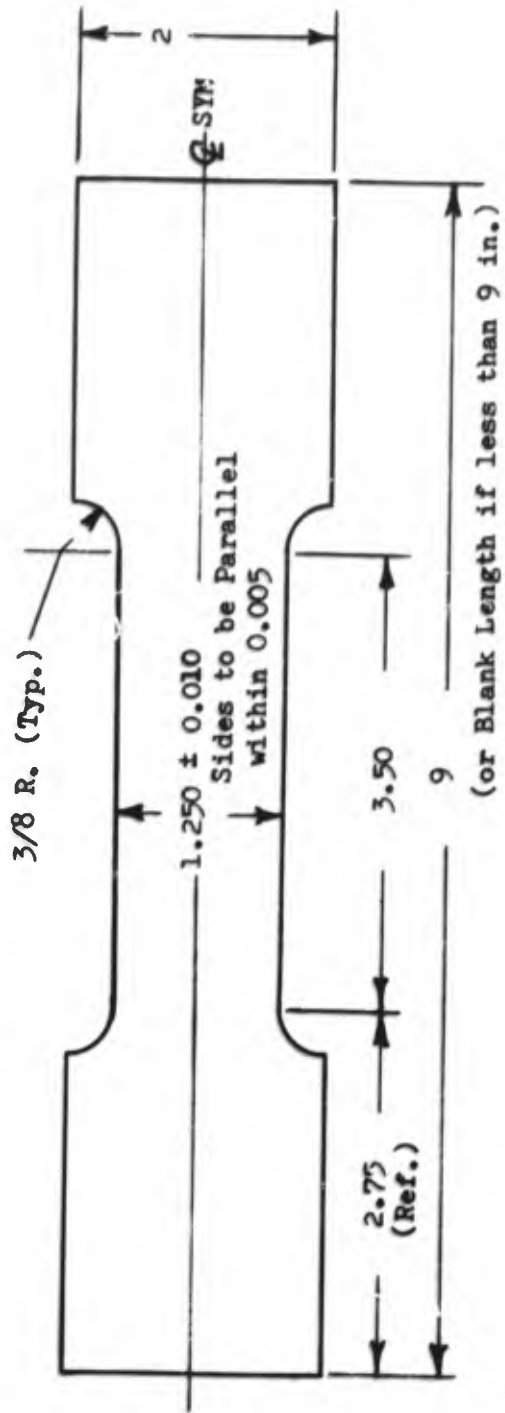


Figure 25 Specimen Design for High Strength Steels

no time was lost in hooking up instrumentation, the visual method was also better for the cold tests. An electrical-impulse signal switch actuated by the observer marked the pop-in point along the test machine load trace on an autographic recorder.

No instrumentation was necessary for the 1/4-inch D6AC steel specimens tested at -110°F nor for the 3/4-inch 18% Ni maraging steel specimens at room temperature, because these fractures were complete plane-strain type failures and no significant percentage of mixed-mode behavior was evident. Figure 26 shows a typical fracture surface for the 1/4-inch D6AC steel material. Specimen flaw dimensions were measured visually after fracture and K_{Ic} values computed from the Irwin equation previously described.

CO₂ (dry ice) powder was used as a dry cooling medium for the low-temperature tests to avoid the problem of wetting effects on crack advance behavior arising from the use of liquid baths at -110°F for fracture-toughness tests.

Parent metal tensile-test specimens were instrumented with extensometers at room temperature and strain gages at -110°F. These baseline data from undeformed material for each alloy are presented in Tables VIII through XII.

Two panels of 7039-T62 aluminum alloy were explosively formed in the 3/4-inch thickness, and one in the 1/2-inch thickness. Because of geometry limitations, all 3/4-inch longitudinal specimens were cut from one panel and all transverse from the other. Only transverse specimens were cut from the 1/2-inch panel for thickness comparison. Five specimens were machined in the longitudinal and six in the transverse grain orientation from parent 3/4-inch stock to obtain a 0.62-inch nominal thickness. This allowed comparison in similar widths to the specimens from the explosively formed panels. Two specimens were machined in the 0.570-inch thickness range to match the longitudinal specimens from the 3/4-inch formed panel. Two longitudinal parent-metal specimens were left in the original panel thickness (0.744-inch) for effect-of-thickness study. Five longitudinal and six transverse specimens were machined from the 1/2-inch parent material to the 0.410-inch nominal thickness range to match the explosively formed panel.

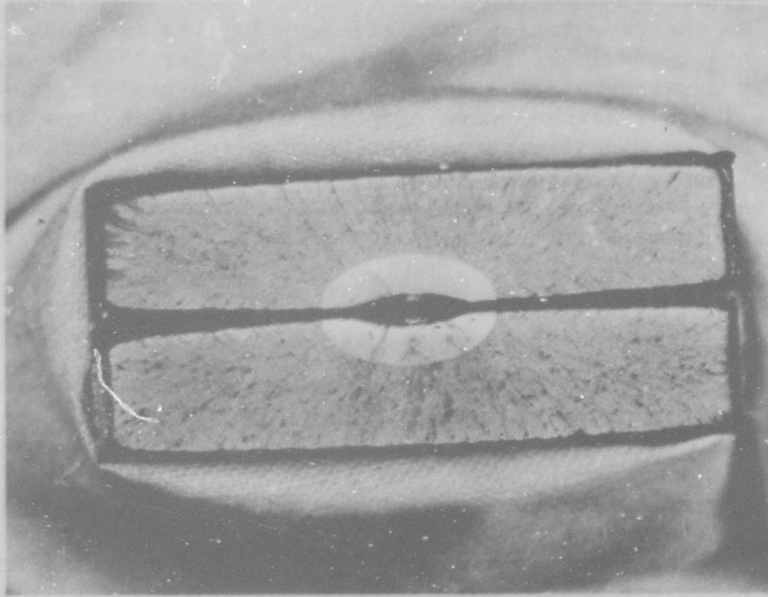


Figure 26. Typical Fracture Surface for the
1/4-Inch D6AC High-Strength Steel

TABLE VIII

Undeformed 7039-T62 Aluminum Alloy Tensile Properties
3/4-inch Nominal Thickness (Room Temperature)

Grain orientation	Specimen No.	Thickness inch	Width inch	0.2% Offset yield strength ksi	Ultimate tensile strength ksi	% Elongation in two inches
Longitudinal	1	0.740	0.749	54.30	63.14	18.0
	2	0.740	0.751	53.99	63.16	18.0
	3	0.742	0.751	54.83	62.90	18.0
	Average			54.37	63.07	18.0
Transverse	1	0.720	0.740	54.43	63.81	16.0
	2	0.723	0.738	53.75	62.69	15.5
	3	0.721	0.736	53.89	62.28	15.5
	Average			54.02	62.93	15.7

TABLE IX

Parent Tensile Properties for Undeformed 1/4-Inch
Nominal Thickness 18% Ni Maraging Steel* (Room Temperature)

Grain orientation	Specimen No.	Thickness inch	Width inch	0.2% Offset yield strength ksi	Ultimate tensile strength ksi	% Elongation in two inches
Longitudinal	1	0.2640	0.496	237.4	256.4	9.5
	2	0.2641	0.498	239.6	257.0	9.5
	Average			238.5	256.7	9.5
Transverse	1	0.2628	0.496	237.4	255.8	9.5
	2	0.2631	0.496	240.8	258.3	8.5
	Average			239.1	257.1	9.0
*Aged 3 hours @ 900°F						

TABLE X

Parent Tensile Properties for Undeformed 1/4-Inch
Nominal Thickness 12% Ni Maraging Steel* (-110°F)

Grain orientation	Specimen No.	Thickness inch	Width inch	0.2% Offset yield strength ksi	Ultimate tensile strength ksi	% Elongation in two inches
Longitudinal	1	0.2740	0.980	205.86	209.52	10.0
	2	0.2750	0.4993	202.11	207.57	10.0
	3	0.2723	0.5000	207.04	211.09	10.0
	Average			205.00	209.39	10.0
Transverse	1	0.2758	0.4946	203.45	206.38	9.5
	2	0.2728	0.4990	206.10	208.67	9.5
	3	0.2761	0.4960	210.01	214.02	9.5
	Average			206.52	209.69	9.5

*Aged 3 hours @ 900°F

TABLE XI

Parent Tensile Properties for Undeformed 1/4-Inch
Nominal Thickness HP 9-4 Steel* (-110°F)

Grain orientation	Specimen No.	Thickness inch	Width inch	0.2% Offset yield strength ksi	Ultimate tensile strength ksi	% Elongation in two inches
Longitudinal	1	0.2646	0.5006	190.19	203.77	16.0
	2	0.2640	0.5015	191.84	200.76	14.0
	3	0.2637	0.5010	190.01	204.39	14.0
	Average			190.68	202.97	14.8
Transverse	1	0.2550	0.4963	187.60	205.37	14.0
	2	0.2555	0.4970	186.61	204.72	13.0
	3	0.2555	0.4935	186.36	202.62	13.0
	Average			186.86	204.24	13.3

* Heat treated with double temper according to program schedule

TABLE XII

Parent Tensile Properties for Undeformed 1/4-Inch
Nominal Thickness D6AC Steel* (-110°F)

Grain orientation	Specimen No.	Thickness inch	Width inch	0.2% Offset yield strength ksi	Ultimate tensile strength ksi	% Elongation in two inches
Longitudinal	1	0.2570	0.4992	206.94	222.14	13.0
	2	0.2559	0.5000	206.25	219.53	13.0
	3	0.2543	0.4995	209.45	221.85	14.0
	Average			207.55	221.17	13.3
Transverse	1	0.2573	0.5012	207.75	222.48	11.0
	2	0.2571	0.4996	205.61	218.07	11.5
	3	0.2551	0.5014	204.85	222.05	14.0
	Average			206.07	220.87	12.2
* Heat treated according to program schedule						

Analysis of the 7039-T62 data from Tables XIII through XVI shows a comparatively wide variation in K_{Ic} values.

From these data the conclusions are: no distinct trend in behavior due to explosive forming is evident; no interaction effects between flaw orientation and percentage of forming strain in the explosively formed material exist to a significant degree; and the effects of thickness on the K_{Ic} values of the parent material are greater than the corresponding effects in the explosively formed material.

The general lowering of K_{Ic} values with decreasing material thickness is characteristic of geometry dependence below the minimum thickness for which K_{Ic} is a true materials property.

The 1/4-inch 18% Ni data were examined for a statistical comparison of explosive forming effects on K_{Ic} values (Tables XVII through XVIII). A two-way analysis of variance was performed on a selected portion of the program data. This analysis is based on a null-hypothesis approach, using a fixed-effects model. (22)

Selection of samples for the analysis was made from the following considerations:

- 1) The transverse orientation is of the greatest concern for the program, and;
- 2) Data from specimens with the most valid flaw geometry should yield the best comparisons.

Following this guide, three specimens from each explosively formed panel and six parent-metal specimens were compared. The model is shown in Table XIX with K_{Ic} values coded to an arbitrary origin of 100.

Conclusions of the analysis of variance are:

- 1) At the 0.05 level of significance, the difference in data between explosively formed and parent material is marginal; no significant difference between samples and their interactions is indicated;

TABLE XIII

Room-Temperature Fracture Toughness Properties
For Parent Transverse 7039-T62 Aluminum Alloy

Finished thickness inch	Width inch	Pop-in stress psi	Crack depth Crack width inch	Crack shape factor Q	Apparent fracture toughness K_{Ic} (Ksi $\sqrt{\text{In.}}$)
0.627	3.25	50,600	0.215/0.635	1.52	37.09
0.626	3.25	50,400	0.212/0.625	1.52	36.67
0.626	3.25	48,700	0.235/0.715	1.50	37.58
0.627	3.25	49,600	0.238/0.755	1.47	38.88
0.631	3.23	46,100	0.270/0.825	1.52	34.09
				Average	36.86
0.410	3.38	47,330	0.180/0.582	1.45	32.50
0.410	3.38	48,780	0.185/0.610	1.42	34.34
0.409	3.38	50,650	0.165/0.600	1.32	34.93
0.409	3.38	51,380	0.120/0.410	1.38	29.53
0.409	3.38	44,900	0.187/0.665	1.35	32.59
0.409	3.38	44,500	0.175/0.550	1.49	29.73
				Average	32.27

TABLE XIV

Room-Temperature Fracture Toughness Properties for
Explosively Deformed Transverse 7039-T62 Aluminum Alloy

Finished thickness incl.	Width inch	Pop-in stress psi	Crack depth Crack width inch	Crack shape factor Q	Apparent fracture toughness K_{Ic} $K_{si}\sqrt{In.}$	Strain-flaw* orientation %
0.624	3.25	48,770	0.242/0.765	1.47	38.58	5.0 A, 5.0B
0.625	3.25	45,700	0.248/0.770	1.49	36.35	4.5 A, 4.5B
0.623	3.25	44,200	0.242/0.750	1.52	34.40	5.0 A, 4.5B
0.624	3.25	46,840	0.225/0.695	1.48	35.62	6.5 A, 6.0B
				Average	36.23	
0.411	3.38	49,860	0.165/0.675	1.22	35.75	3.0 A, 9.0B
0.411	3.38	46,900	0.165/0.620	1.29	32.70	2.5 A, 4.0B
0.412	3.38	48,310	0.167/0.595	1.34	33.26	5.0 A, 6.0B
0.411	3.38	48,450	0.160/0.630	1.26	33.67	4.0 A, 4.0B
0.411	3.38	45,430	0.165/0.635	1.29	31.68	3.0 A, 6.0B
				Average	33.41	

* A Denotes deformation of explosively formed panel normal to surface flaw.

B Denotes deformation of explosively formed panel parallel with surface flaw.

TABLE XV

Room-Temperature Fracture Toughness Properties
For Parent Longitudinal 7039-T62 Aluminum Alloy

Finished thickness inch	Width inch	Pop-in stress psi	Crack depth Crack width inch	Crack shape factor Q	Fracture toughness K_{Ic} (Ksi $\sqrt{\text{In.}}$)
0.744	3.25	48,820	0.210/0.660	1.48	35.85
0.743	3.25	49,730	0.222/0.675	1.49	37.43
				Average	36.64
0.625	3.25	51,650	0.235/0.590	1.79	36.47
0.626	3.25	48,620	0.270/0.790	1.57	39.31
0.623	3.25	49,410	0.230/0.605	1.70	35.42
0.624	3.25	49,780	0.265/0.755	1.60	38.66
0.626	3.25	50,860	0.260/0.710	1.65	38.37
				Average	37.64
0.574	3.25	49,950	0.265/0.775	1.57	40.0
0.570	3.24	50,680	0.215/0.640	1.52	37.12
				Average	38.56
0.410	3.38	49,860	0.195/0.630	1.44	35.77
0.410	3.38	50,970	0.163/0.585	1.35	34.53
0.409	3.38	48,080	0.195/0.540	1.62	32.53
0.410	3.38	49,640	0.195/0.635	1.42	35.86
				Average	34.67

TABLE XVI

Room-Temperature Fracture Toughness Properties for
Explosively Deformed Longitudinal 7039-T62 Aluminum Alloy

Finished thickness inch	Width inch	Pop-in stress psi	Crack depth Crack width inch	Crack shape factor Q	Fracture toughness, K _{IC} (Ksi√In.)	Strain-flaw* orientation %
0.623	3.25	49,650	0.250/0.680	1.66	37.57	6.0 A, 5.0 B
0.624	3.22	45,460	0.260/0.745	1.61	35.62	5.5 A, 5.0 B
				Average	36.60	
0.571	3.25	45,130	0.252/0.752	1.54	35.59	4.5 A, 7.0 B
0.570	3.25	46,300	0.265/0.735	1.65	36.24	8.0 A, 8.0 B
0.570	3.25	41,280	0.255/0.745	1.62	31.91	5.0 A, 8.0 B
				Average	34.58	

* A Denotes deformation of explosively formed panel normal to surface flaw.

B Denotes deformation of explosively formed panel parallel with surface flaw.

TABLE XVII

Fracture-Toughness Data for 1/4-Inch 18% Ni Maraging Steel - Room Temperature

Specimen No.	Thickness inch	Area inch ²	Pop-in stress ksi	Fracture stress Yield stress	$\frac{a}{2c}$	Shape factor Q	Apparent fracture toughness K_{Ic} (Ksi√in.)
L1 L2 L3 L4 L5 L6 L7 Longitudinal	0.263	0.2122	229.0	0.96	0.352	1.55	107.6
	0.264	0.2115	225.5	0.95	0.373	1.67	104.9
	0.256	0.2033	229.2	0.96	0.409	1.78	100.5
	0.263	0.2088	232.75	0.98	0.386	1.73	100.6
	0.263	0.2109	234.7	0.98	0.311	1.43	101.3
	0.264	0.2078	211.74	0.89	0.311	1.47	108.2
	0.264	0.2053	217.25	0.91	0.333	1.53	105.6
						Average	104.1
T1 T3 T4 T5 T6 T7 Transverse	0.265	0.2104	235.3	0.98	0.444	1.89	94.4
	0.267	0.2120	234.0	0.97	0.364	1.63	101.1
	0.264	0.2075	231.8	0.97	0.364	1.63	100.1
	0.262	0.2096	228.5	0.96	0.314	1.44	105.1
	0.262	0.2080	214.66	0.90	0.333	1.53	109.6
	0.264	0.2128	222.74	0.93	0.327	1.50	100.3
							Average
Parent material							

TABLE XVIII

Fracture-Toughness Data for 1/4-Inch 18% Ni Maraging Steel - Room Temperature

Explosively deformed material	Specimen No.	Thick inch	Area inch ²	Pop-in stress ksi	Fracture stress		a/c	Shape factor Q	Apparent fracture toughness, K _{Ic} Ksi√In.	Strain-flaw orientation %
					Yield stress	stress				
Explosively deformed material	Longitudinal Panel AL T1 T2 T3 T4 T5 T6 T7 T8	0.255	0.2017	220.38	0.92	0.321	1.48	106	0.5 A, 5.0 B	
		0.256	0.2035	231.94	0.97	0.338	1.55	115.9	1.0 A, 3.0 B	
		0.256	0.2033	227.00	0.95	0.344	1.56	106.3	1.5 A, 2.5 B	
		0.258	0.2110	230.57	0.97	0.335	1.52	97.8	1.5 A, 2.5 B	
		0.259	0.2059	206.38	0.87	0.259	1.28	113.0	1.5 A, 2.5 B	
		0.261	0.2114	228.48	0.96	0.314	1.44	104.9	1.0 A, 2.5 B	
		0.260	0.2085	230.46	0.97	0.346	1.55	111.1	0.5 A, 3.0 B	
		0.258	0.2064	235.22	0.99	0.357	1.58	100.0	1.0 A, 5.0 B	
		Average						Average	106.9	
	Transverse Panel AL T1 T2 T3 T4 T5 T6 T7 T8	0.259	0.2113	230.95	0.97	0.327	1.49	110.7	3.0 A, 1.5 B	
		0.257	0.2038	231.60	0.97	0.348	1.51	104.0	3.0 A, 0.5 B	
		0.260	0.2057	234.56	0.98	0.311	1.50	98.8	3.5 A, 1.5 B	
		0.252	0.2066	225.07	0.94	0.333	1.52	106.8	4.0 A, 0.5 B	
		0.258	0.2064	234.25	0.98	0.333	1.50	105.5	3.0 A, 4.0 B	
		0.258	0.2064	229.65	0.96	0.309	1.42	109.5	2.5 A, 3.0 B	
		0.258	0.2087	234.07	0.98	0.357	1.59	103.6	2.5 A, 2.0 B	
		0.258	0.2069	217.01	0.91	0.300	1.42	115.1	3.0 A, 1.0 B	
		Average						Average	106.8	

*A Denotes deformation of explosively formed panel normal to surface flaw.

B Denotes deformation of explosively formed panel parallel with surface flaw.

TABLE XIX

Two-Way Analysis of Variance for 18% Ni
Maraging Steel Fracture-Toughness Values

	Explosively formed		Parent Material		Σ	\bar{X}
Panel A1	1T	10.7	T1	5.6		
	2T	4.0	T2	1.1		
	4T	6.8	T4	0.1		
		21.5		-4.4	17.1	2.85
Panel A2	1T	5.5	T5	5.1		
	2T	9.5	T6	9.6		
	3T	3.6	T7	0.3		
		18.6		15.0	33.6	5.6
	40.1		10.6	50.7		
	\bar{X}	6.7		1.77		

Hypothesis: No significant difference	Squares	Degrees of freedom	Mean square	F Ratio	F 0.05	F 0.01
(A) Between samples	22	1	22	1.6	5.32 Accept	Accept
(B) Between parent & Explosively formed	72	1	72	5.24	5.32 Marginal	Reject
(C) A X B	41.8	1	41.8	3.2	Accept	Accept
Error	109.91	8	13.73			

- 2) At the 0.1 level of significance, a difference in data between explosively formed and parent material is indicated, but none is indicated between samples and their interactions.

The particular level of significance used to evaluate the analysis of data is left to the choice of the examiner for a specific application. As a matter of laboratory engineering practice, the level chosen for this comparison was with $F = 0.05$ as maximum. With this criterion, no conclusive difference is seen to exist between explosively formed and parent-metal K_{Ic} values.

As in the previous case, no interaction effects between specimen flaw orientation and the biaxial strain variations from the explosively formed photo-gridded panels exist to a significant degree.

Analysis of data for the 1/4-inch D6AC steel, Tables XX and XXI, leads to conclusions similar to those for the 18% Ni maraging steel—that is, no effects of explosive forming are evident in the fracture-toughness properties for the material. Although the fracture-toughness values for the 12% Ni maraging steel and HP 9-4 steel at -110°F were consistent, dry-ice temperature proved to be an unfortunate choice for the D6AC steel. The K_{Ic} values obtained were from a temperature region where rapid changes in fracture behavior occur for relatively small temperature changes. Consequently, the D6AC data show more variation than would have been evident at a higher temperature such as -60°F .

Analysis of the HP 9-4 steel fracture-toughness data, Tables XXII and XXIII, shows no effects of explosive forming on the K_{Ic} values of the material. Effects of specimen-flaw orientation in relation to biaxial-forming strain variations are not shown to exist to a level of engineering significance.

The data for the 1/4-inch 12% Ni maraging steel are shown in Tables XXIV and XXV. The analysis for this material produced no obvious explosively formed property effects on the K_{Ic} values or biaxial strain/flaw orientation effects. This material retained an unusually high degree of fracture-toughness behavior at -110°F and caused extreme difficulty in fatigue cracking the induced flaws.

TABLE XX

Fracture-Toughness Data for 1/4-Inch D6AC Steel at -110°F

Specimen No.	Thickness inch.	Area inch ²	Pop-in stress ksi	Fracture stress Yield stress	$\frac{a}{2c}$	Shape factor Q	Apparent fracture toughness K_{Ic} (Ksi $\sqrt{\text{in.}}$)
L1 L2 L3 L4 L5 L6 L7 Longitudinal	0.2550	0.319	146.0	0.71	0.265	1.36	74.3
	0.2595	0.324	186.0	0.90	0.265	1.29	95.8
	0.2595	0.325	118.0	0.57	0.269	1.43	62.3
	0.2605	0.326	110.4	0.53	0.293	1.50	51.3
	0.2550	0.320	118.0	0.57	0.281	1.48	56.7
	0.2560	0.320	114.8	0.55	0.289	1.50	60.6
	0.2570	0.323	127.7	0.67	0.275	1.41	69.6
						Average	67.2
T1 T2 T3 T4 T5 T6 Transverse	0.2605	0.326	143.4	0.70	0.212	1.22	67.0
	0.2600	0.325	163.1	0.79	0.303	1.48	82.7
	0.2600	0.327	133.8	0.65	0.290	1.48	64.3
	0.2610	0.326	143.4	0.69	0.294	1.47	72.9
	0.2650	0.332	142.2	0.69	0.307	1.49	64.3
	0.2620	0.327	162.8	0.79	0.243	1.27	84.6
						Average	72.6

Parent material

TABLE XXI

Fracture-Toughness Data for 1/4-Inch D6AC Steel at -110°F

Explosively deformed material		Specimen No.	Thick inch	Area inch ²	Pop-in stress ksi	Fracture stress Yield stress	$\frac{a}{2c}$	Shape factor Q	Apparent fracture toughness, K _{IC} Ksi√In.	Strain-flow * orientation	
Longitudinal	Panel A1	L2	0.2510	0.3150	201.6	0.97	.290	1.37	100.7	2.5% A, 3.5% B	
		L3	0.2485	0.3112	157.5	0.76	.290	1.43	77.0	3.0% A, 3.5 B	
		L4	0.2505	0.3840	189.1	0.91	.286	1.38	99.3	3.0% A, 3.5 B	
		L6	0.2470	0.3096	138.2	0.67	.267	1.38	64.9	1.5% A, 2.5 B	
	Panel A2	L7	0.2460	0.3076	160.3	0.77	.258	1.32	77.0	1.5% A, 4.5 B	
		L8	0.2370	0.2966	166.0	0.80	.300	1.45	80.6	1.5% A, 6.0 B	
		Average							83.2		
		Average								72.6	
	Transverse	Panel A1	T1	0.2470	0.3089	137.58	0.67	.314	1.50	72.6	5.0% A, 4.0 B
			T2	0.2470	0.3096	159.40	0.77	.259	1.33	71.3	3.5% A, 2.5 B
			T3	0.2475	0.3094	133.48	0.65	.303	1.51	67.0	3.5% A, 3.0 B
			T4	0.2500	0.3128	162.24	0.79	.286	1.41	75.3	3.5% A, 3.5 B
Panel A2		T5	0.2560	0.3205	130.27	0.63	.313	1.53	65.0	3.0% A, 5.0 B	
		T6	0.2465	0.3082	138.25	0.67	.273	1.39	68.6	4.0% A, 1.5 B	
		T7	0.2470	0.3105	153.78	0.75	.290	1.44	75.0	2.5% A, 1.5 B	
		T8	0.2490	0.3127	148.70	0.72	.261	1.34	86.8	3.0% A, 1.0 B	
Average								72.7			

* A Denotes deformation of explosively formed panel normal to surface flaw.

B Denotes deformation of explosively formed panel parallel with surface flaw.

TABLE XXII

Fracture-Toughness Data for 1/4-Inch HP 9-4 Steel at -110°F

Specimen No.	Thickness inch	Area inch ²	Pop-in stress ksi	Fracture stress Yield stress	$\frac{a}{2c}$	Shape factor	Apparent fracture toughness K_{Ic} (Ksi√in.)
Longitudinal	L2	0.3205	120.12	0.63	0.309	1.53	61.3
	L3	0.3223	172.20	0.90	0.286	1.36	91.0
	L4	0.3217	167.86	0.88	0.282	1.36	93.1
	L5	0.3254	161.34	0.85	0.302	1.45	79.2
	L6	0.3259	156.49	0.82	0.303	1.45	80.2
	L7	0.3291	161.05	0.85	0.326	1.51	72.0
	L8	0.3270	172.78	0.91	0.290	1.39	85.7
	Average						
Transverse	T1	0.2376	177.05	0.91	0.302	1.42	86.9
	T2	0.3250	133.85	0.72	0.304	1.50	65.7
	T3	0.3273	180.26	0.97	0.305	1.42	88.4
	T4	0.3213	157.17	0.84	0.304	1.46	82.2
	T5	0.2996	175.23	0.94	0.290	1.38	87.2
	T6	0.2991	170.51	0.91	0.319	1.45	87.3
	T7	0.3217	169.41	0.91	0.263	1.28	88.6
Average							83.8

Parent material

TABLE XXIII

Fracture-Toughness Data for 1/4-Inch HP 9-4 Steel at -110°F

Specimen No.	Thick inch	Area inch ²	Pop-in stress ksi	Fracture stress Yield stress	$\frac{a}{2c}$	Shape factor Q	Apparent fracture toughness, K _{IC} Ksi inch	Strain-flaw* orientation
Longitudinal Explosively deformed material	L1	0.3070	161.24	0.85	0.294	1.41	83.7	2.5% A, 3.5% B
	L3	0.3070	179.15	0.94	0.286	1.36	94.7	1.5 A, 2.5 B
	L4	0.3051	176.99	0.93	0.302	1.42	89.3	1.5 A, 5.5 B
	L5	0.3022	158.84	0.83	0.311	1.48	78.5	4.0 A, 4.0 B
	L6	0.2977	181.39	0.95	0.289	1.37	89.6	4.0 A, 4.5 B
	L7	0.2964	167.00	0.88	0.289	1.39	94.5	4.5 A, 6.0 B
	L8	0.3061	171.51	0.90	0.297	1.41	86.8	3.5 A, 3.0 B
	Average						88.2	
Transverse Explosively deformed material	T1	0.3130	166.13	0.89	0.273	1.33	92.3	3.5% A, 2.0% B
	T2	0.2898	170.80	0.91	0.287	1.38	90.5	3.5 A, 1.5 B
	T3	0.3129	148.61	0.80	0.295	1.43	73.9	3.5 A, 1.5 B
	T4	0.3090	155.34	0.83	0.296	1.42	83.6	3.5 A, 1.0 B
	T6	0.2932	163.71	0.88	0.299	1.42	82.6	6.5 A, 4.5 B
	T8	0.2964	167.00	0.89	0.300	1.42	88.5	6.5 A, 5.0 B
	T9	0.2964	180.50	0.97	0.310	1.43	88.3	8.0 A, 6.5 B
	Average						85.7	

*A Denotes deformation of explosively formed panel normal to surface flaw.

B Denotes deformation of explosively formed panel parallel with surface flaw.

TABLE XXIV
Fracture-Toughness Data for 1/4-Inch 12% Ni Maraging Steel at -110°F

Specimen No.		Thickness inch	Area inch ²	Pop-in stress ksi	Fracture stress Yield stress	a/2 _c	Shape factor Q	Apparent fracture toughness K _{Ic} (Ksi√in.)
Longitudinal	L1	0.2740	0.3439	187.85	0.92	0.287	1.37	110.6
	L2	0.2740	0.3436	197.18	0.96	0.370	1.65	110.0
	L3	0.2725	0.3432	198.13	0.97	0.311	1.44	99.3
	L4	0.2720	0.3374	194.13	0.95	0.293	1.38	105.4
	L5	0.2740	0.3424	194.21	0.95	0.309	1.43	102.6
	L6	0.2730	0.3414	194.05	0.95	0.275	1.42	97.9
							Average	104.3
Transverse	T1	0.2740	0.3420	192.25	0.93	0.328	1.50	96.8
	T2	0.2740	0.3444	195.99	0.95	0.298	1.49	106.2
	T4	0.2735	0.3432	193.04	0.94	0.311	1.45	106.0
	T5	0.2780	0.3471	187.27	0.91	0.307	1.44	103.2
	T6	0.2760	0.3469	190.26	0.92	0.289	1.38	113.9
	T8	0.2735	0.3413	202.90	0.98	0.286	1.35	107.7
							Average	105.6
Parent material								

TABLE XXV

Fracture-Toughness Data for 1/4-Inch 12% Ni Maraging Steel at -110°F

Specimen No.	Thick-ness inch	Area inch ²	Pop-in stress ksi	Fracture stress Yield stress	$\frac{a}{2c}$	Shape factor Q	Apparent fracture toughness, K _{1c} Ksi√In.	Strain-flaw* orientation
Panel A1 Longitudinal	L1	0.3400	188.24	0.92	0.250	1.24	100.0	1.5% A, 3.0% B
	L2	0.3389	190.32	0.93	0.288	1.37	102.7	1.5 A, 3.0 B
Panel A2 Longitudinal	L3	0.3355	178.09	0.87	0.310	1.47	103.3	2.0 A, 6.0 B
	L4	0.3398	185.14	0.91	0.396	1.40	99.4	1.5 A, 5.5 B
	L5	0.3410	187.68	0.92	0.276	1.33	99.4	1.5 A, 5.0 B
						Average	101.0	
Panel A3 Transverse	T1	0.3338	178.25	0.86	0.291	1.40	99.6	
	T3	0.3367	189.34	0.92	0.274	1.32	105.2	3.5 A
Panel A4 Transverse	T4	0.3233	194.09	0.94	0.262	1.28	97.5	5.5 A, 1.5 B
	T5	0.3080	187.50	0.91	0.342	1.57	103.1	5.0 A, 1.5 B
	T7	0.3405	187.95	0.91	0.271	1.34	97.6	5.5 A, 1.0 B
						Average	100.6	

*A Denotes deformation of explosively formed panel normal to surface flaw.

B Denotes deformation of explosively formed panel parallel with surface flaw.

The 3/4-inch 1.8% Ni maraging steel data are shown in Tables XXVI and XXVII. No significant effects of explosive forming on K_{Ic} properties are shown by analysis of the data.

Complete comparison of flaw orientation with respect to biaxial strain was not possible for this material because the grid markings in one direction were impossible to record after the forming process. As expected, the 3/4-inch material exhibited the most consistent fracture toughness behavior of all the program materials.

The general summation that must be made from review of all the program data is that the effects of thermal treatment after forming, specimen geometry, and normal testing variation have combined effects equal to or greater than possible shifts in plane-strain fracture-toughness behavior due to explosive forming of the program materials.

2. THEORETICAL ANALYSIS

Typical measured strains and contour shapes for five blanks are discussed as the basis for process predictability. Theoretical results have been computed from a numerical analysis of the response of a flat, circular blank to an impulsive load. This analysis is outlined in Part IV of the First Annual Report of the Center for High Energy Forming.*

There are empirical relations available in the literature that predict the specific impulse of explosive charges as a function of charge weight and distance from the charge. When the impulse derived from these formulae is used as input data in the computer program, the draw depth predicted by theory is always higher than the measured value by a few percent up to 35 percent. Although there are possible explanations for this discrepancy, this question will not be considered here.

The procedure adopted to compute the results in this report was to adjust the impulse used as input for the computer program until the computed draw depth at the apex was in close agreement with the measured value on the deformed part. Once the computed and measured draw depths agree, it is found that theory and experiment are in relatively good agreement for the deflected shape and for radial and circumferential strains.

Results are plotted in Figures 27 through 31 for five specimens. Physical parameters associated with each shot are listed

*Contract DA-19-066-AMC(266)X under the sponsorship of the Advanced Research Projects Agency, Washington, D.C.

TABLE XXVI

Fracture-Toughness Data for 3/4-Inch 18% Ni Maraging Steel - Room Temperature

Specimen No.		Thickness inch	Area inch ²	Pop-in stress ksi	Fracture stress Yield stress	$\frac{a}{2c}$	Shape factor Q	Apparent fracture toughness K_{Ic} (Ksi $\sqrt{\text{in.}}$)	
Parent material	Longitudinal	L1	0.6172	222.78	0.93	0.396	1.78	105.5	
		L2	0.6176	225.06	0.89	0.362	1.64	106.6	
		L3	0.6158	211.92	0.88	0.370	1.68	100.8	
		L4	0.6156	196.96	0.82	0.367	1.68	98.3	
		L5	0.7047	0.6154	210.43	0.88	0.372	1.69	103.7
		L6	0.7040	0.6142	221.67	0.92	0.357	1.61	107.7
							Average	103.8	
Parent material	Transverse	T1	0.6183	214.70	0.89	0.356	1.62	106.6	
		T2	0.6133	220.53	0.92	0.372	1.67	110.4	
		T3	0.6153	201.93	0.84	0.377	1.72	101.9	
		T4	0.6164	222.66	0.93	0.322	1.48	110.0	
		T5	0.7016	0.6160	222.16	0.93	0.375	1.67	108.7
		T6	0.7040	0.6186	227.13	0.93	0.375	1.67	111.1
		T7	0.7035	0.6124	221.26	0.93	0.339	1.53	107.5
							Average	108.0	

TABLE XXVII

Fracture-Toughness Data for 3/4-Inch 18% Ni Maraging Steel - Room Temperature

Specimen No.	Thick-ness inch	Area inch ²	Pop-in stress ksi	Fracture stress Yield stress	$\frac{a}{2c}$	Shape factor Q	Apparent fracture toughness, K _{IC} Ksi√In.	Strain-flaw* orientation
L1	0.7048	0.6122	227.46	0.95	0.334	1.51	115.2	, 3.0%B
L2	0.6733	0.5888	213.15	0.89	0.359	1.62	110.5	, 4.5%B
L3	0.6953	0.6000	232.91	0.97	0.341	1.55	110.7	, 1.0 E
						Average	112.1	
T1	0.7060	0.6193	226.87	0.95	0.307	1.44	108.1	, 1.0%B
T2	0.6750	0.5931	228.46	0.95	0.344	1.54	116.4	, 2.0 B
T3	0.6980	0.6124	219.62	0.91	0.373	1.68	112.1	4.0% A ; 1.5 B
T4	0.6980	0.6140	228.01	0.95	0.365	1.60	116.6	, 1.0 B
T5	0.7040	0.6019	210.58	0.88	0.365	1.63	109.1	, 1.0 B
						Average	112.1	

*A Denoted deformation of explosively formed panel normal to surface flaw.

R Denotes deformation of explosively formed panel parallel with surface flaw.

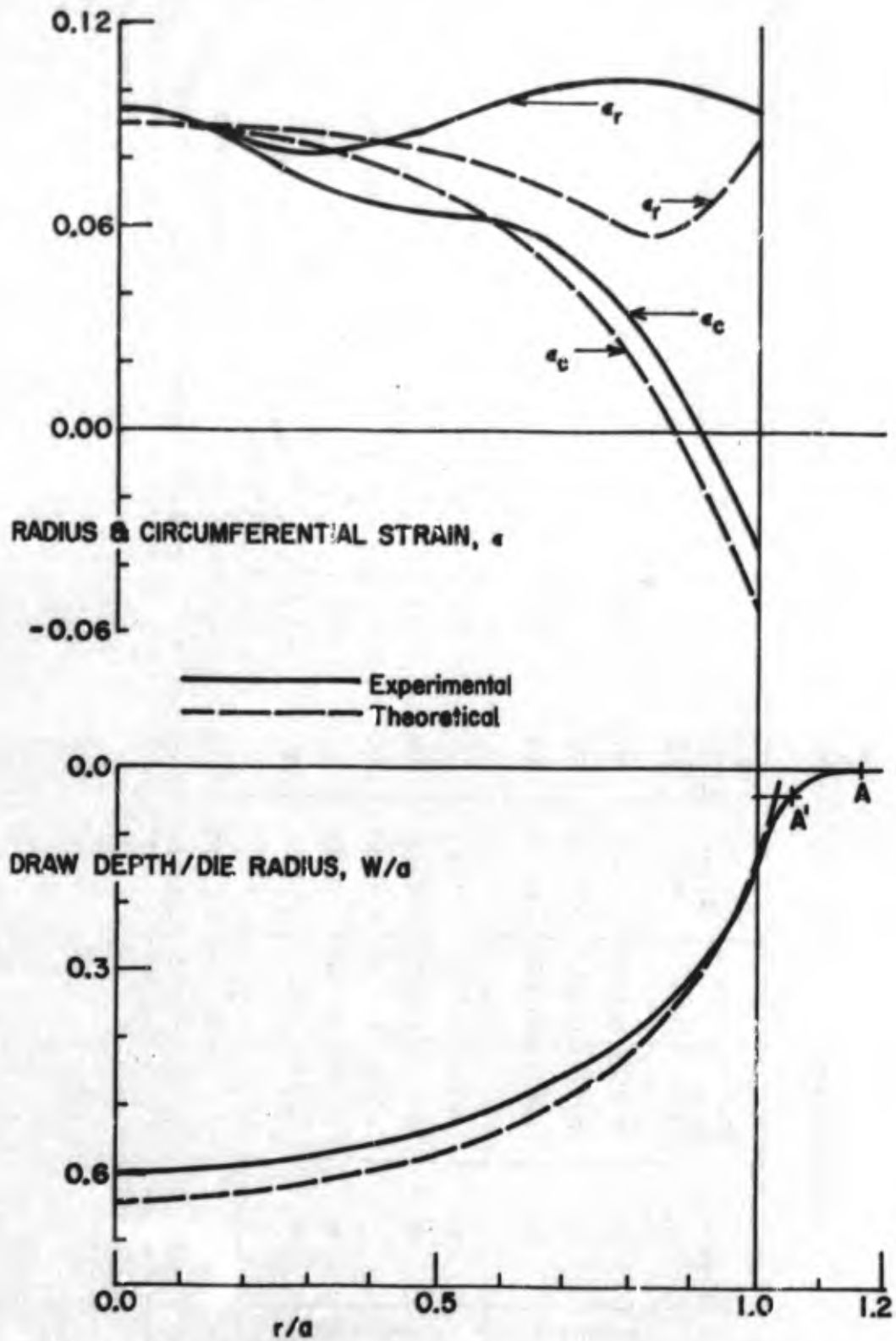


Figure 27 Experimental vs Theoretical Strain and Contour Data, Specimen 1

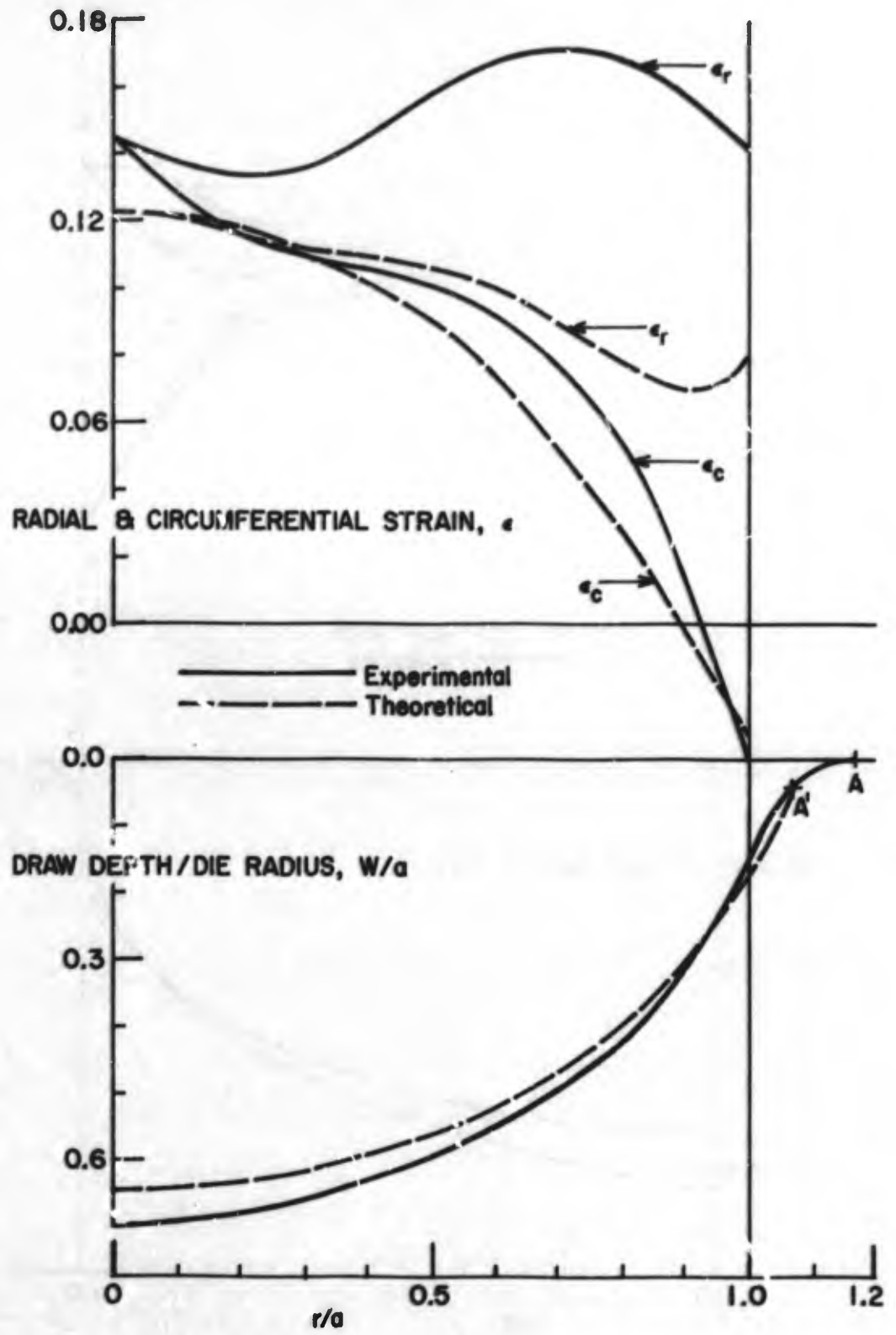


Figure 28 Experimental vs Theoretical Strain and Contour Data, Specimen 2

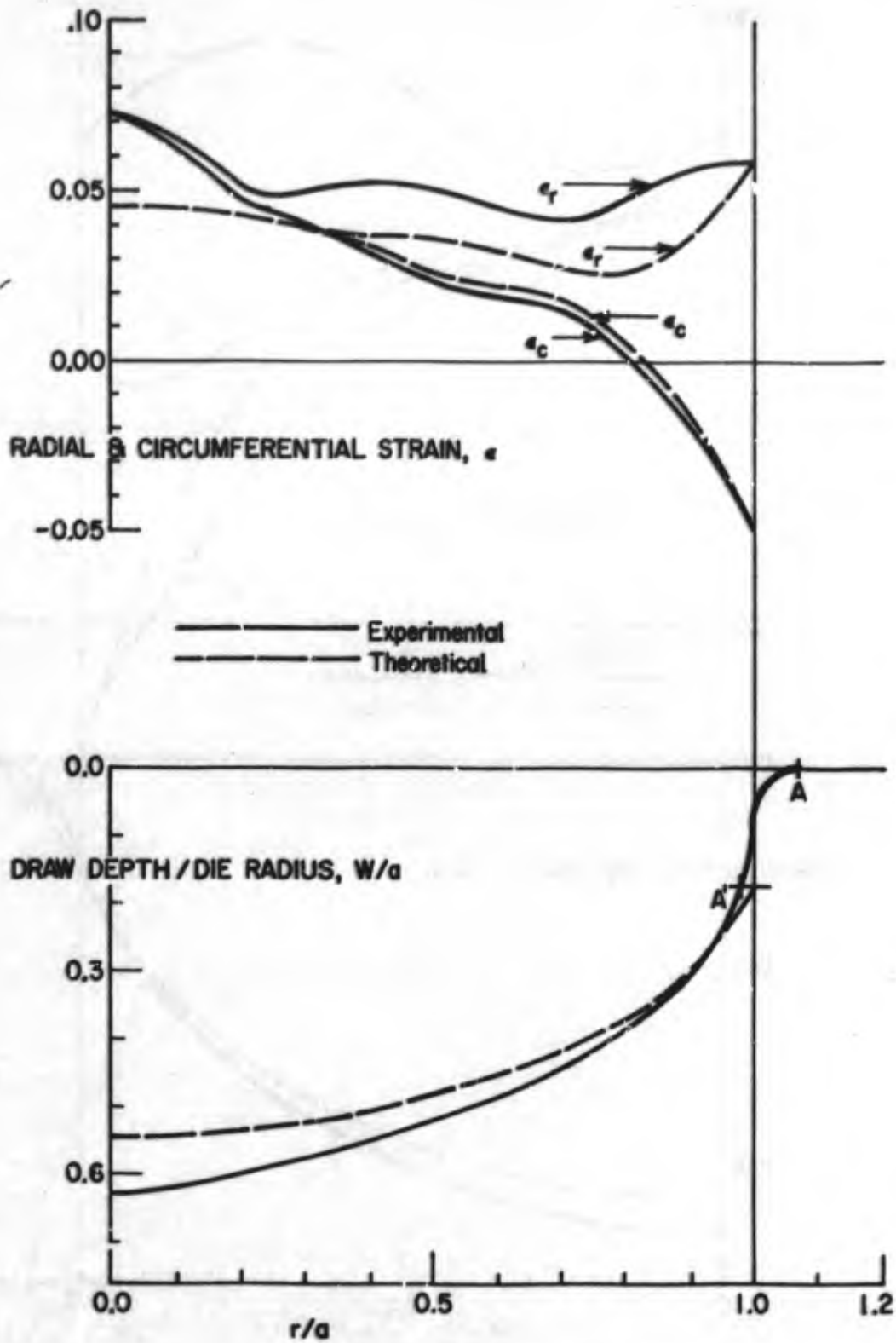


Figure 29 Experimental vs Theoretical Strain and Contour Data, Specimen 3

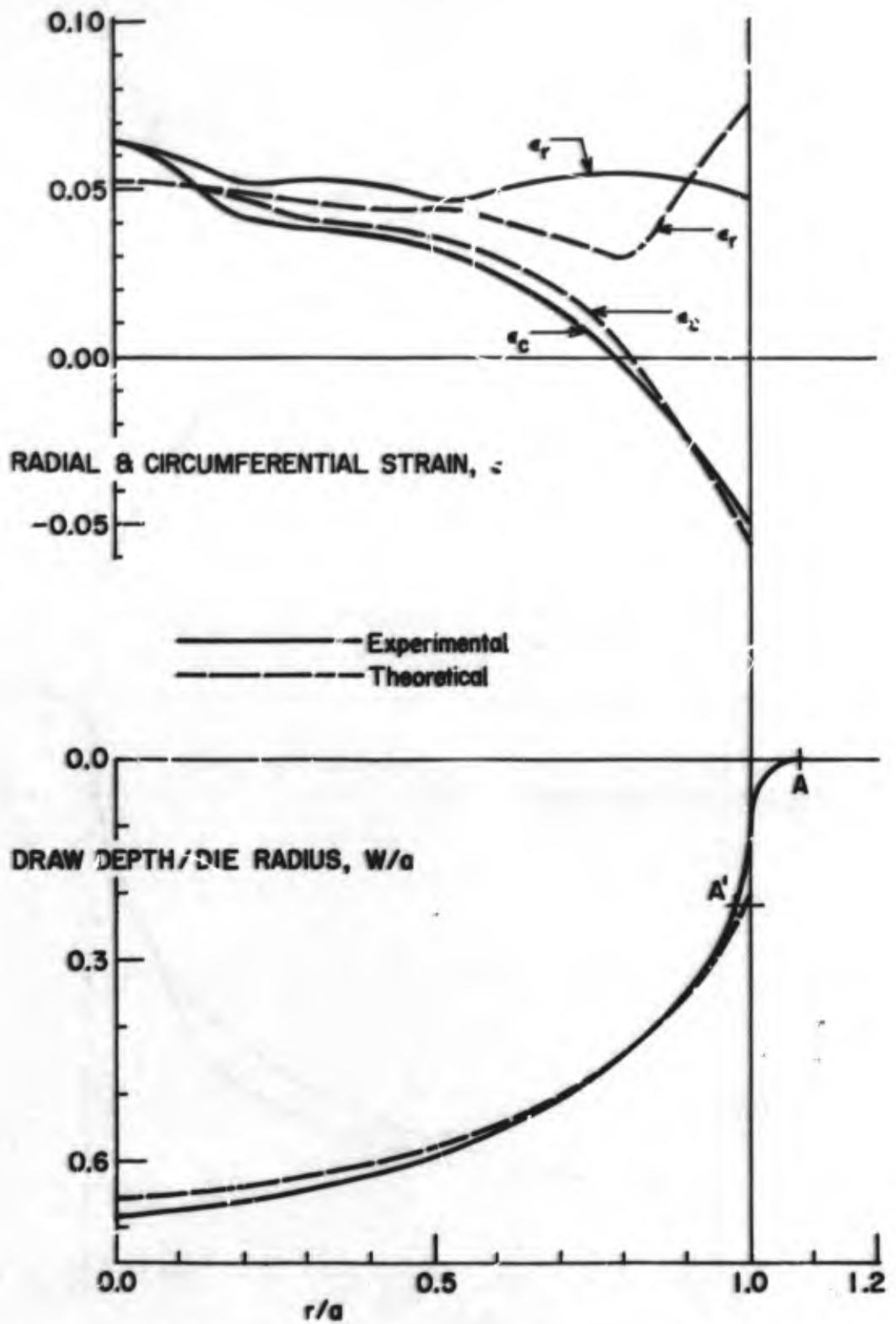


Figure 30 Experimental vs Theoretical Strain and Contour Data, Specimen 4

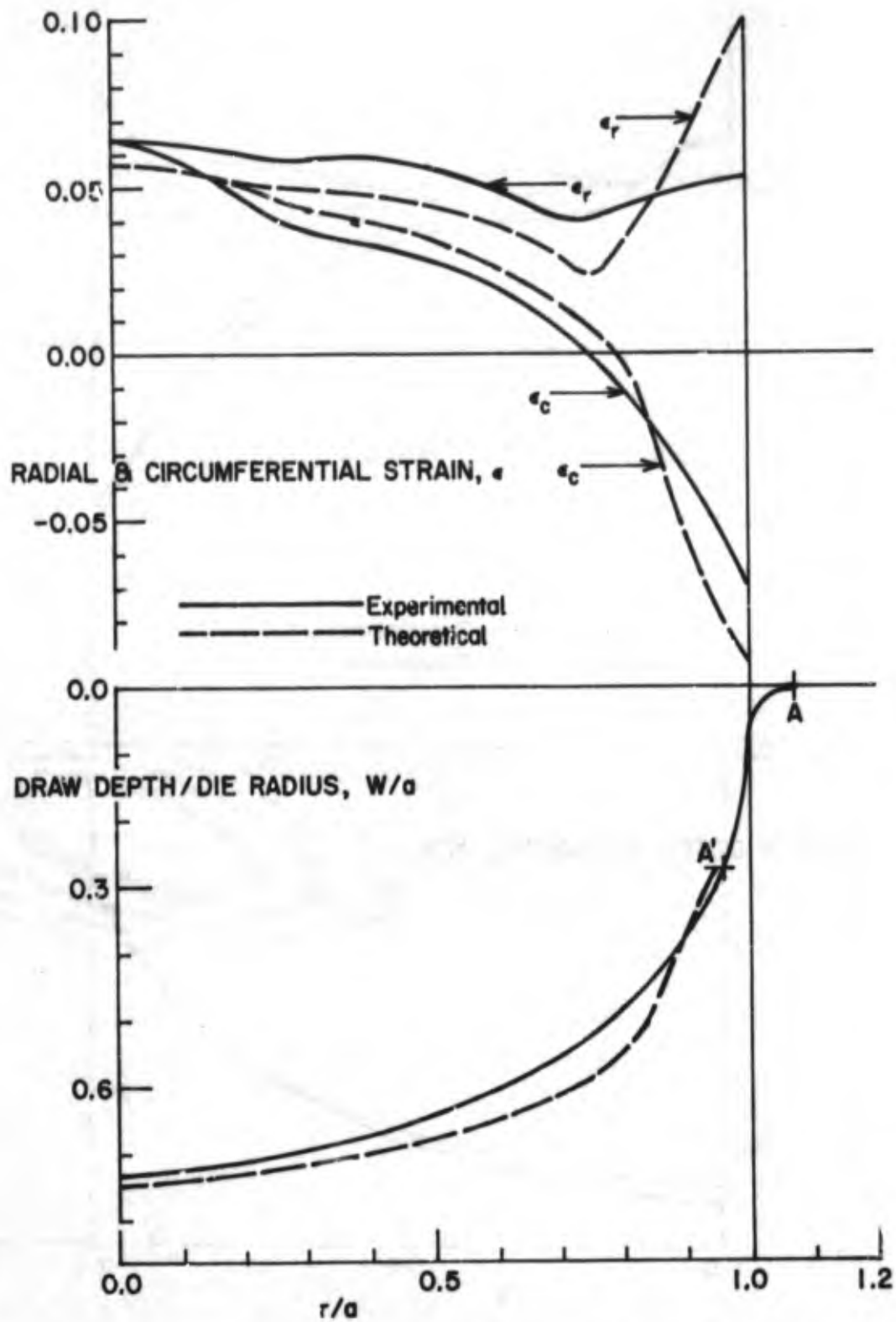


Figure 31 Experimental vs Theoretical Strain and Contour Data, Specimen 5

in Table XXVIII. The lower curves in each figure show the deflected shape of the blank drawn to scale. The upper curves represent the strain distribution. The computed circumferential strains ϵ_c agree better with experiment than the radial strain ϵ_r . Part of this is because the circumferential strain is directly related to the radial displacement, u , and the measured value of u at $r = a$ is used as a boundary condition in the program. The boundary condition brings the circumferential strains into good agreement near the edge. The measured strains increase noticeably near the apex of the shell, $r = 0$, while the computed values do not reflect this. It has been observed before that this effect is noticeable when the stand-off distance, L , from the charge to the blank is comparatively short. Possibly the theory would show this trend also if the membrane theory used in the analysis were replaced with a bending theory. The poorest agreement on any specimen for the deflected shape is for No. 5, which also has the largest draw depth. This suggests using large finite-deflection theory, rather than the simpler finite-deflection theory.

In summary, the computer program at this time cannot predict on a rational basis the charge requirements to produce a given draw depth. However, when the desired draw depth is known, the program can calculate the strains that will be in the formed part. If the computed strains fall below the maximum strains measured in static tests of the material, it can be concluded that the part can be made without a tearing failure in the material.

3. EXPLOSIVE FORMING

A major share of the technical effort was spent in developing formability limits for the five alloys and establishing relationships between explosive charge and metal draw depth. These relationships were derived from shots in six-inch-diameter dies using material thicknesses ranging from 0.020-inch to 0.125-inch. A 24-inch-diameter die was used for all of the alloys to verify subscale results. For the 7039 aluminum, a full-scale verification test of subscale results used an existing 120-inch-diameter free-forming tool. The following sections describe the experiments conducted and the results obtained in each case. Each alloy is discussed separately and the results are summarized at the end of the section.

a. 7039 Aluminum

(1) Formability Limits

The 7039 aluminum alloy is reported to be a highly formable material by the manufacturer. This claim was verified during the development of formability limit curves. Using unlubricated blanks, it was not possible to deep draw the 7039-O aluminum into a hemisphere in one forming operation. However, draw-depth ratios up to 0.375 can be obtained in one operation from metal thicknesses ranging from 0.032 to 0.125-inch. Figure 32 shows the formability limit curve for 7039 aluminum using a ratio of blank diameter to die opening diameter of 1.58 ($B/D = 1.58$). A similar curve for a $B/D = 1.4$ is presented in Figure 33. Because existing tooling was being used to verify subscale forming data, it was necessary to develop formability limit curves for two sizes of blanks: one to be used for draw-depth ratios (W/D) to 0.400 and the second for use in forming parts to draw-depth ratios up to 0.600.

There was little tendency for the alloy to buckle at any thickness. This resistance to buckling was attributed primarily to the very high stiffness of the forming die used. Even with very little clamping force around the blank periphery, flange buckling was nonexistent. In fact, reduction in hold-down ring thickness from $1\frac{1}{2}$ inches to $1/4$ inch was possible before blank wrinkling became a significant problem. Blank failures were usually tensile tearing at the apex of the formed piece or shearing at the die draw radius. Figure 34 shows the former type of failure. Notice the lack of pull-in. When excessive charges were used, there was little or no movement of the metal under the clamping ring. Another type of failure that results mainly from a blank of insufficient diameter for the draw depth desired is shown in Figure 35. There is obviously a lower limit for the size of blank used to form a given deep drawn part. For parts no deeper than a $W/D = 0.400$, a $B/D = 1.36$ to 1.4 is the minimum size to consider. Smaller blanks either pull unevenly because of inherent instability or become swallowed by the die to produce a part of insufficient size to be trimmed. On the other hand, parts of hemispherical depth or greater ($W/D = 0.5$ to 0.6) can be successfully formed using $B/D = 1.5$ to 1.6. The particular blank size chosen depends on the amount of cupping or stretching achieved during explosive forming. If the blank becomes too large, i.e.,

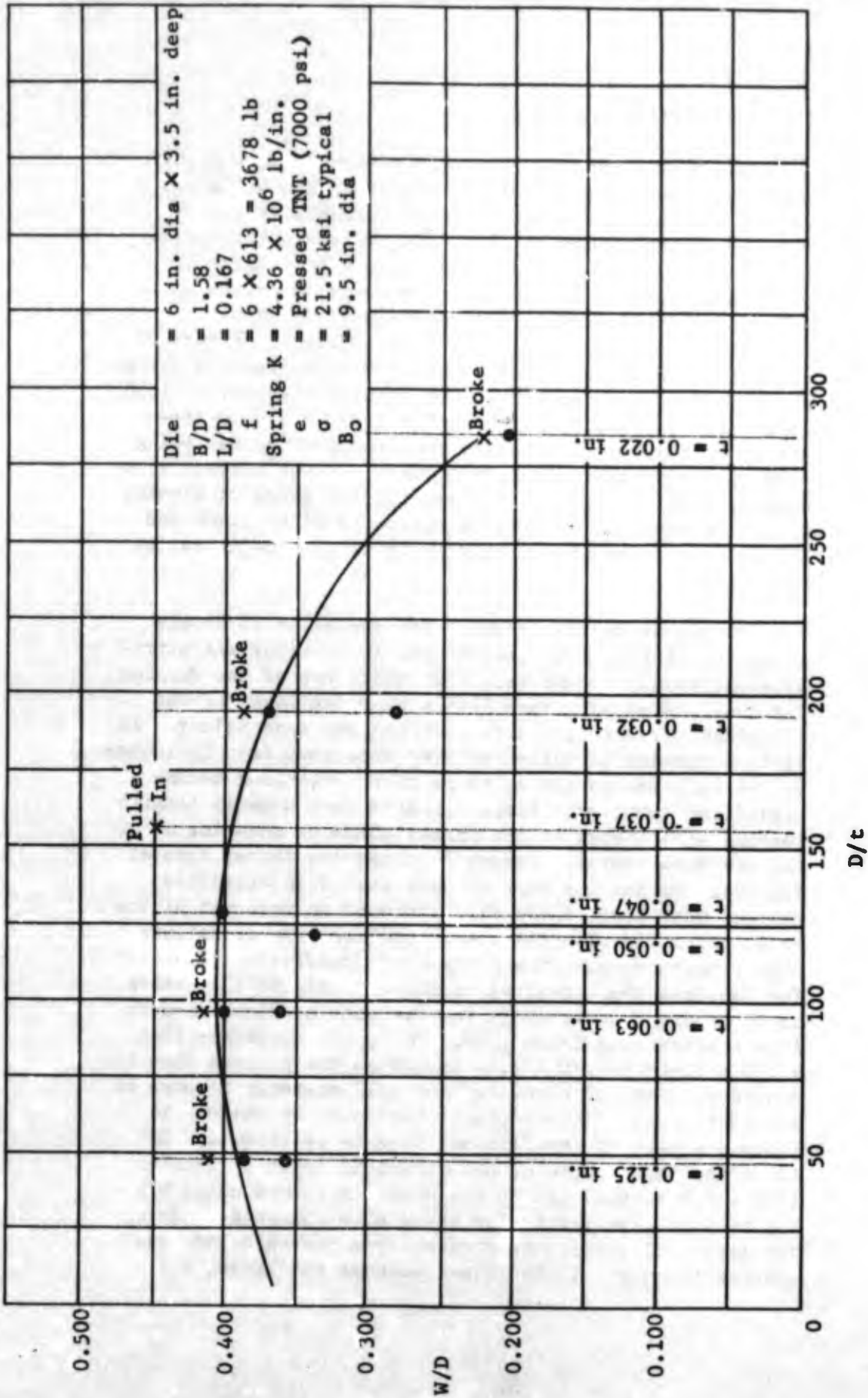


Figure 32 7039-0 Aluminum Formability Limit Curve

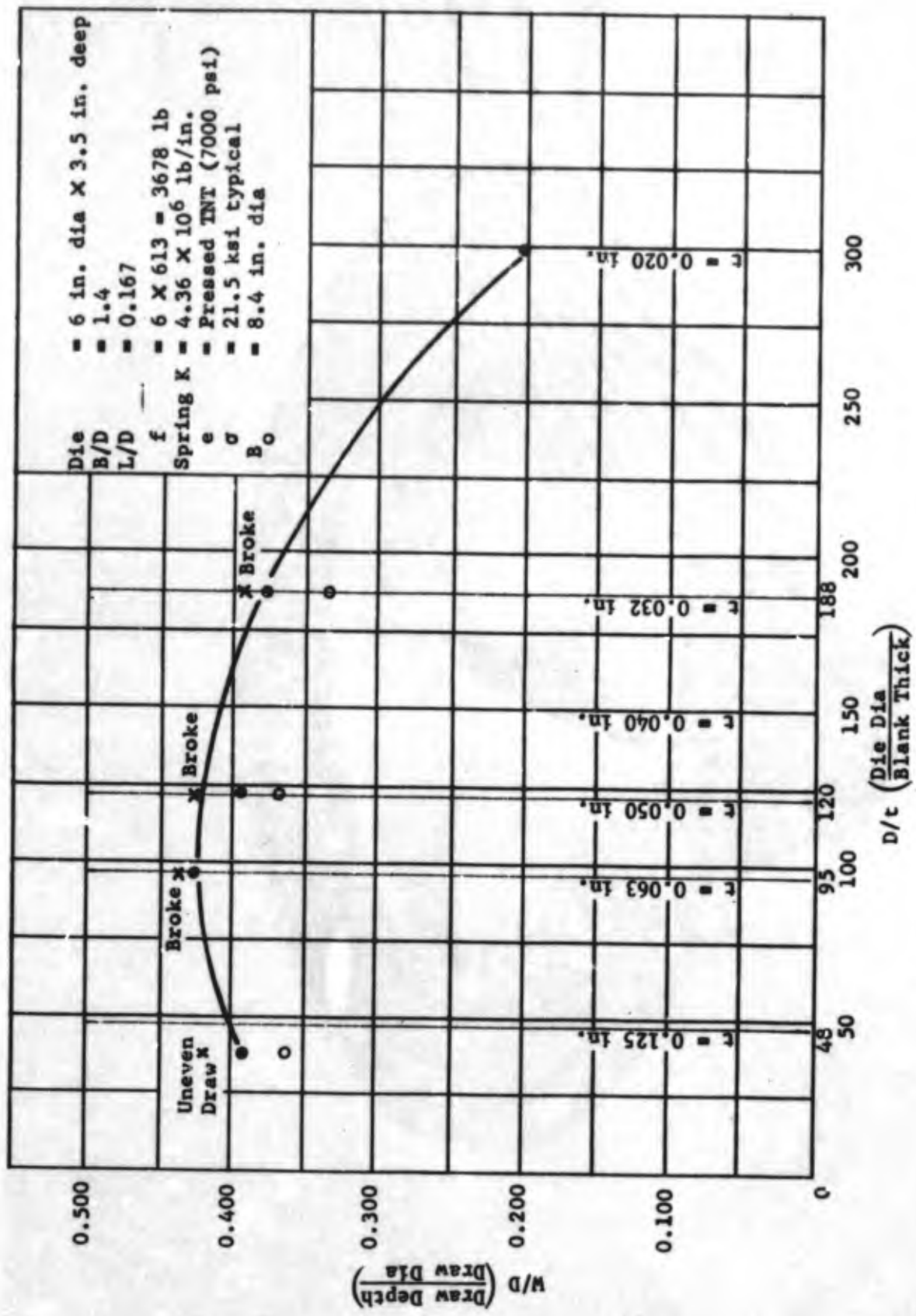


Figure 33 7039-O Aluminum Formability Limit Curve

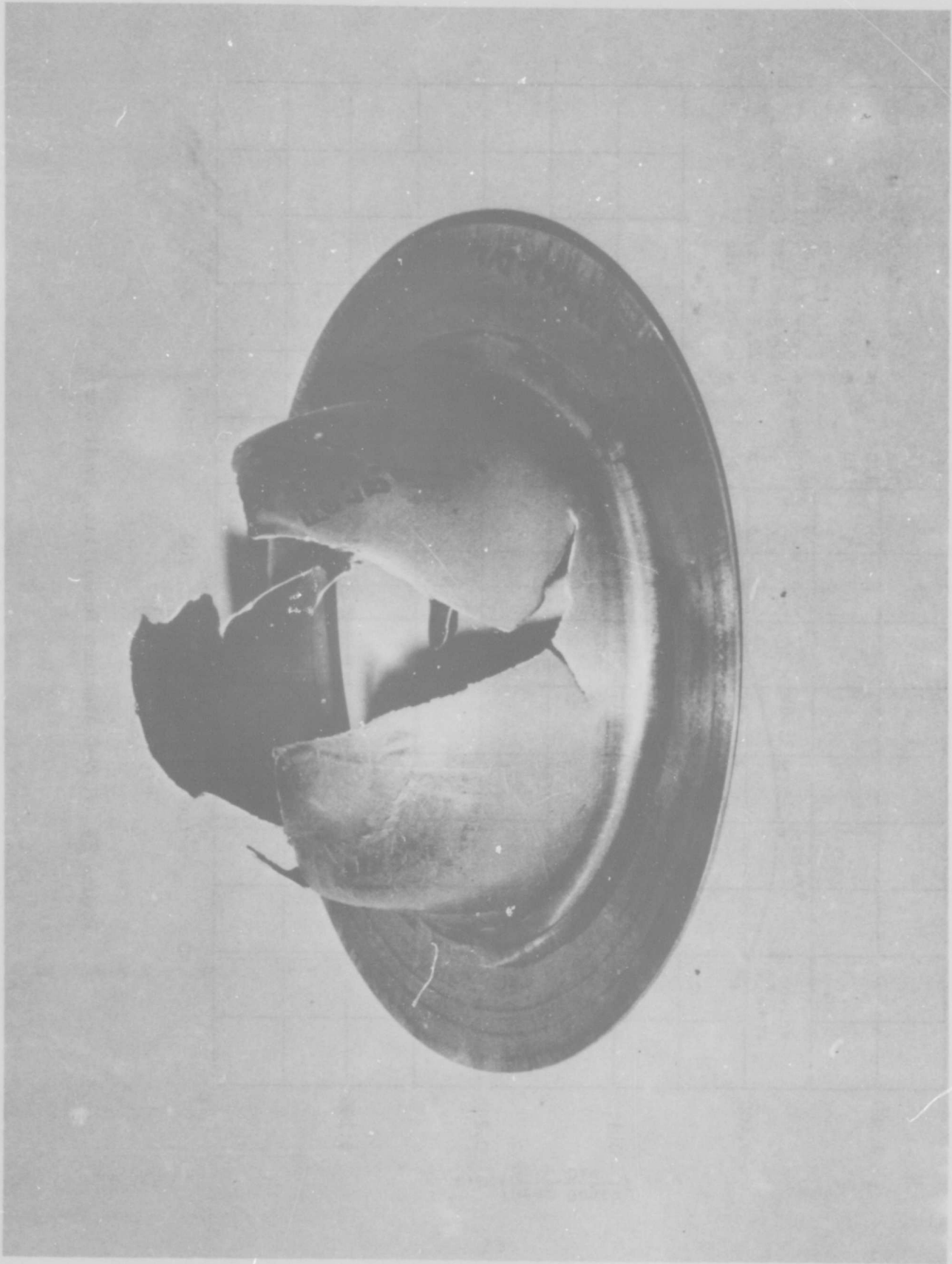


Figure 34. Typical Tensile Fracture of 7039-O Aluminum Caused by an Excessive Explosive Charge.

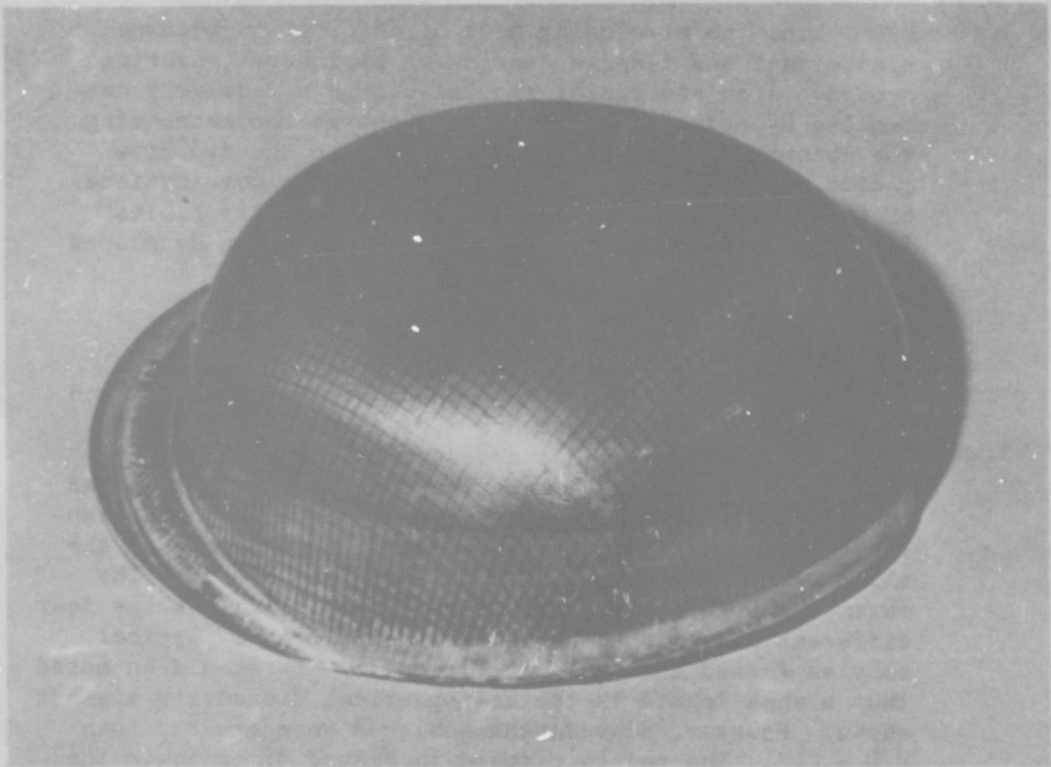


Figure 35. A Typical Failure of 7039-0 Aluminum Caused by Use of Too Small a Blank.

$B/D > 1.6$, the stretching mode of deformation becomes predominant and tensile tearing or peripheral shearing occurs. Apex and radial strains can be effectively controlled by reducing the explosive charge and increasing the number of forming steps, lubricating the die draw radius, reducing the clamping pressure, or combinations of these techniques. All data for formability limits for this alloy and the steel compositions were developed using unlubricated blanks.

(2) Explosive Charge Estimation

The charge required to reach a given draw depth and the charge necessary to reach a given draw depth to a specified contour are not necessarily the same. Thus, it is important to establish the maximum charge required to produce full-contour parts for use in a standard manufacturing operation. Three different thicknesses of the alloy were formed using dies of different depths. The maximum charge necessary to form each material in the four different dies was established by experiment. Typical samples formed are shown in Figure 36. It should be noted that blanks formed in the hemispherical die cavity are not shown. However, draw depths achieved were greater than $W/D = 0.3$. The points circled in Figure 37 indicate the draw depths obtained by essentially free-forming parts in the hemispherical die cavity. It was not possible to form full hemispheres in one forming operation without lubrication of the blank. When lubricated, the 7039-O aluminum could be fully formed in one operation. However, the large charge needed could not be scaled to full-scale requirements (156-inch diameter) within the abilities of existing facilities in the country. Optimum forming sequences must be developed to arrive at charge sizes more appropriate for available facilities. Optimization of the forming sequence was beyond the scope of the present contract.

(3) Verification of Subscale Forming Data

The 7039-O aluminum was the only alloy that was formed in dies to 120 inches in diameter. Because of the need to use existing tooling for the full-scale verification, exact scaling conditions could not be reproduced for all die sizes. However, the variations in parameters that were present were subsequently found to



Figure 36 Deformed Specimens of T039-0 Aluminum Sheet Used to Establish the Relation Between Explosive Charge and Metal Draw Depth

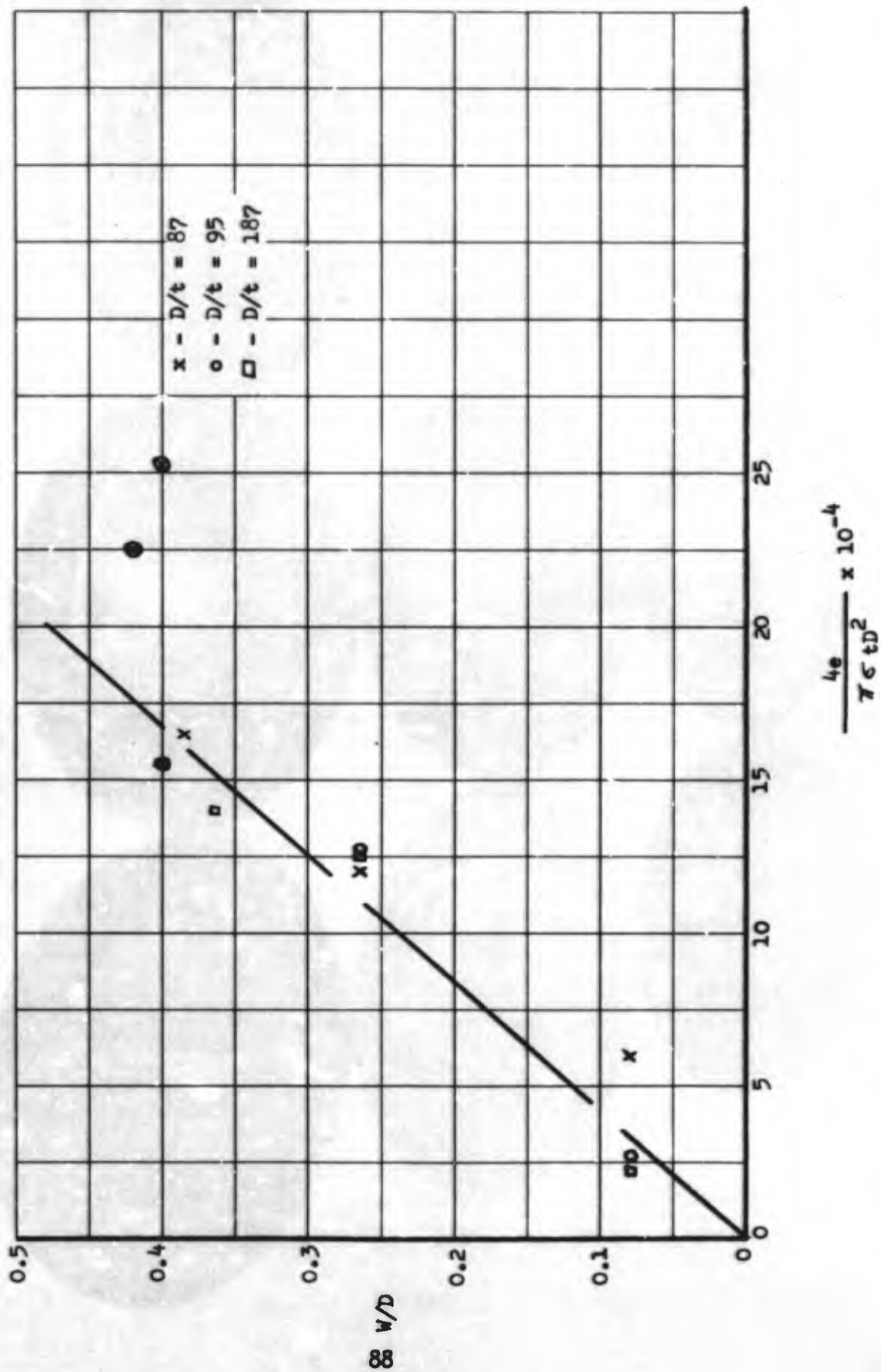


Figure 37 Estimation of Charge as a Function of Metal Draw Depth for 7039-O Aluminum Sheet

be of little significance for the deep drawing of aluminum. Table XXIX presents data used in the scaling verification experiments. It should be noted that the die details for the six-inch-diameter tool were not directly scalable to the larger sizes. Because both the high-strength steels and aluminum alloys were being studied on the same tooling, it was necessary to construct the six-inch die of sufficient stiffness to prevent flange wrinkling of the steels during explosive forming. This provided significantly more stiffness than required to prevent wrinkling of the aluminum alloy. The die stiffness has little influence on the depth of draw, part contour or pull-in achieved during forming. Lack of similitude with respect to hold-down ring thickness and clamp mass, therefore, was not instrumental in significantly modifying blank response to deformation.

Even though the six-inch and 24-inch die experiments involved different die conditions, the excellent scalability of data can be seen by comparing blanks B and C. Predicted draw depth and pull-in were 7.72 inches and 29.60 inches, respectively. Actual values obtained were 7.75 inches and 29.32 inches, or less than a 1% error. The good agreement resulted even though a calculated adjustment in charge weight was required because of thickness differences. To permit scaling to the 120-inch diameter die, a minimum blank thickness of 0.150-inch could be used for the 24-inch-diameter die. Thus, the use of 0.0375-inch material was required for the six-inch die but was unavailable from the producer.

It should be noted that a number of experiments were conducted in the 24-inch scale die that were not in direct scale to either the six-inch-diameter die or the 120-inch-diameter die. This was a result of the requirement for a change in explosive for the full-scale experiments. All of the subscale work on the six-inch die was accomplished by pressed TNT charges. When Picatinny Arsenal was requested to produce full-scale charges (25 pounds) it was discovered that recrystallized TNT necessary for pressing the charges was unavailable. Subsequent inquiries of Navy, Air Force, and Army sources substantiated the unavailability on a national basis.

Because of the problems with explosive, it was decided to use a TNT derivative, 50/50 Pentolite. Thus,

TABLE XXIX
Scaling Verification Experiments on 7039-O Aluminum

Die size in.	C _t in.	K lb/in	f lb/clamp	B _o in.	B _l in.	t in.	h in.	e grains	W/D	W
A	1/2	1,250,000	135	8.4	7.5	0.032	54	5RDX +	0.290	1.74 (1)
B	1/2		135	8.4	7.4	0.032	54	Cap.	0.322	1.93
C	1		1620	33.6	29.32	0.150	42	1175	0.323	7.75 (1)
D	1		1620	33.6	28.56	0.150	42	1300	0.347	8.32 (1)
24 E	1	50,000	1620	33.6	28.38	0.150	42	1350	0.353	8.47 (1)
F	1		1620	33.6	29.46	0.150	42	1350	0.315	7.56
G	1		1620	33.6	29.42	0.150	42	1350	0.336	8.06
H	1		1620	33.6	27.70	0.150	54	1400	0.379	9.10
I	.6		1950	33.6	27.67	0.150	37.5	1350	0.383	9.20
120 J	3	500,000	41,250	168.0	*	0.770	188.0	25 lbs	0.387	46+
K	3		48,750	168.0	(138.35) 135.0	0.780	188.0	24 lbs	0.373	44 3/4

(1) No air curtain.

Note: $B/D = 1.4$ $L/D = 0.167$ $\rho < 1$

cast charges were made at Martin Marietta for adjustment shots on the 24-inch die to permit the fabrication of properly sized full-scale charges. Experiments D, E, G, and H were used to properly adjust charge weight. Based on the results of the one-fifth-scale tests, the 25-pound charges were made by Picatinny Arsenal. Comparison of experiments H and J shows the results. Actual draw depth and predicted draw depth agreed to within 3%. However, blank pull-in values were quite diverse. Due to problems with the clamping and sealing arrangement on experiment J, the blank pulled completely into the die cavity. An analysis of results clearly showed the problem areas, and experiments verified the analysis. Test I was then conducted to produce, as accurately as possible, direct scalability to the full-scale die using conditions adjusted from an analysis of the first full-scale-part results. The full-scale charge was ground under water to reduce its weight to 24 pounds as suggested by Test I. Subsequent forming produced very acceptable results, although blank instability caused by uneven draw on one segment of the part was still evident. Blank pull-in agreed with predicted values within 2%, while draw-depth agreement was within 3%. Figure 38 shows a one-fifth scale and full-scale part after forming. The slight waves in the large part are due to the blank making contact with rib stiffeners in the free-forming tool. This did not detract from the demonstration of scaling.

One serious discrepancy between the 24-inch and 120-inch dies was the use of an O-ring groove and rubber O-ring on the 24-inch die, and the use of a rubber gasket on the full-scale die. This method of sealing the large die was found to contribute significantly to blank movement. Because the gasket was bonded to the draw ring, the blank sat on the gasket and, even with very high clamping pressure, did not contact the draw ring except in an area near the entrant radius to the die. Thus, when the explosive force was applied, the blank slid freely into the die cavity because of the lack of frictional restraint around the blank periphery.

In the free forming of full-scale parts under this contract, blank instability was a serious problem. The situation was complicated by the use of as-rolled blanks with insufficient control of waviness. With small diameter blanks, i.e., $B/D < 1.40$, the tendency toward uneven pull-in is high. When a small blank is formed in a

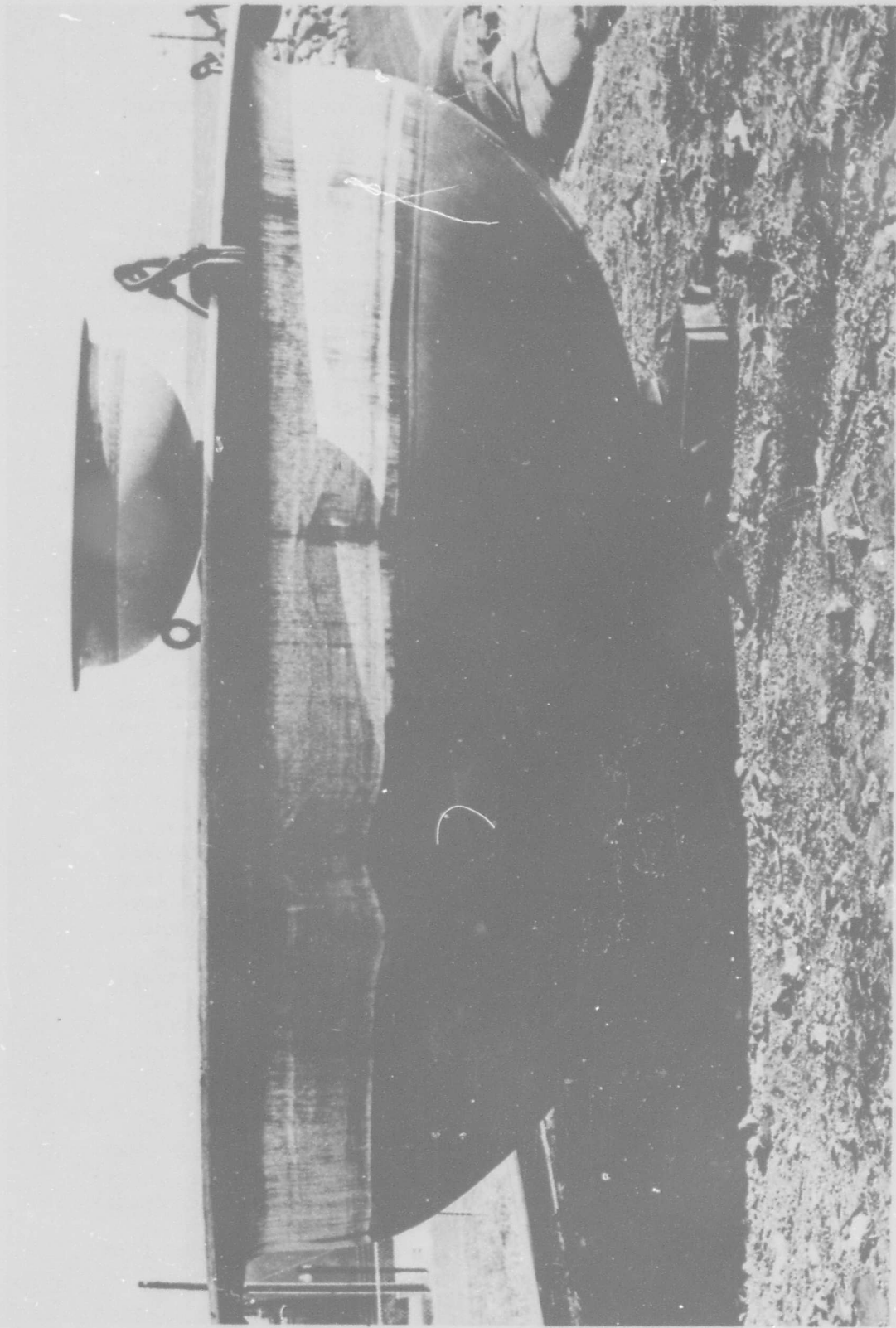


Figure 38 Scaling Verification Results for 7039-O Aluminum Using 24-inch and 120-inch Diameter Dies.

die with a machined cavity, some stability is gained as the blank contacts the die wall during deformation. In addition, the contact of the blank apex before die filling also acts to stabilize the blank. In free forming, these methods of stabilizing the blank are not possible. Therefore, stability can only be gained by frictional restraint created by contact of the blank with the draw ring and hold-down ring. On the first full-scale shot, the sealing gasket prevented intimate contact of blank and die surfaces. Maximum frictional restraint was provided on the second shot by sealing the die at the blank periphery and increasing the clamping force. Even with these optimized conditions for free forming, the waviness of the blank prevented uniform blank restraint over a small section of the die periphery and the blast wave from the explosion caused one of the clamping ring segments to move outward, thus relieving the restraining force on the blank. The blank thus pulled in to the die entrant radius over a four-foot section, causing uneven pull-in. This partial release of pressure on the blank accounts for the deviation in final blank diameter from predicted values. Figures 39 through 41 show the sequence of operations leading to the formed piece.

In spite of the experimental problems encountered as a result of tooling variations, it is felt that scaling of forming results has been sufficiently demonstrated.

b. HP 9-4-25 Steel

(1) Formability Limits

The high-strength HP 9-4-25 alloy showed excellent formability, and draw-depth ratios over 0.450 were achieved with one forming operation. For 0.022-inch-thick material, draw-depth ratios of 0.425 could be reached without tensile fracture. However, when draw-depth ratios of 0.325 and greater were reached, severe buckling became evident. These buckles would render the part useless, but the impressive drawability of the alloy in such thin section was noteworthy. After forming, elongations were measured along the curved surface of the part using pregridded material. In two inches of measured length over the part, apex elongations up to 15.5% were recorded. This compares with 12.5% elongation in two inches obtained from uniaxial test specimens.



Figure 39 Lifting of 120-inch Diameter Free Forming Tool for Explosive Forming.



Figure 40 Explosive Standoff Installation for Full Scale Forming.

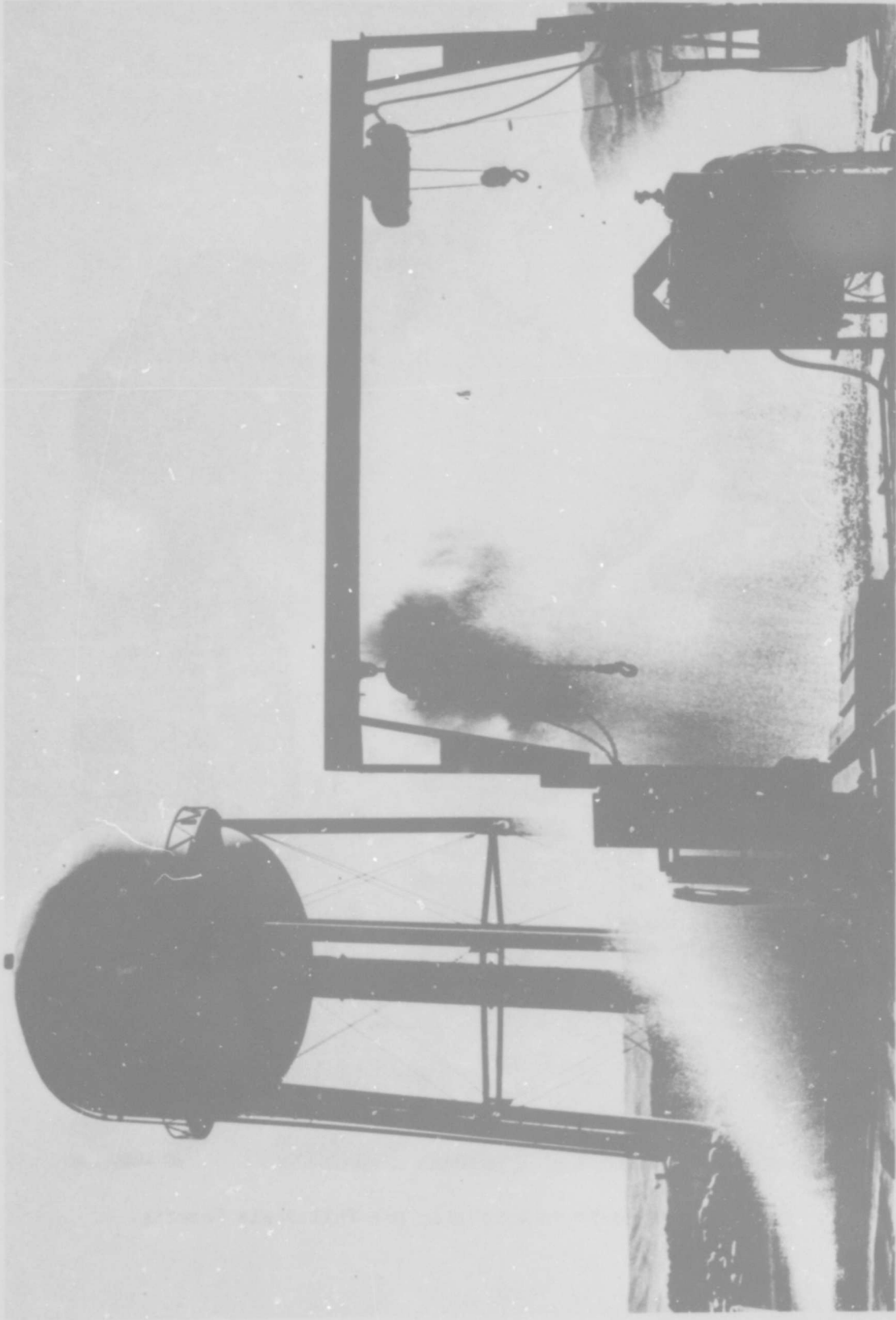


Figure 41 Full Scale Explosive Forming Shot Using 25 Pounds of 50/50 Cast Pentolite.

Material 0.024 inch thick buckled when a draw-depth ratio of 0.400 was reached. As the part was drawn deeper, the buckles disappeared and usable parts were obtained. The elimination of buckling was undoubtedly due to high tensile stretching of the blank as failures occurred above a draw-depth ratio of 0.425, not appreciably above the point at which buckling was first observed.

Stock 0.043 inch thick could be formed without concern for buckling at any draw depth. However, problems with uneven blank pull-in were encountered when draw-depth ratios greater than 0.430 were reached. The uneven pull-in may account for the deep draws obtained with this thickness metal. It was interesting to note that for blanks chemically cleaned before forming, as part of preparation for photogripping, fracture occurred at draw-depth ratios greater than 0.400. The data suggest that care must be taken in cleaning because embrittlement may result from hydrogen pickup from solutions used for surface treatment.

Figure 42 shows the formability limit curve developed for the BP 9-4-25 alloy using unlubricated blanks.

(2) Explosive Charge Estimation

Controlled forming experiments were conducted on three separate dies of different draw depth to establish the minimum charge required to deform blanks to full die contour. Figure 43 shows deformed material after charge evaluation. The wrinkling tendency of the 0.022-inch-thick material for the deeper draws is shown on the right side of the photograph. The photo-grid used to record specimen strain after deformation can be clearly seen on each specimen. The results of the charge estimation experiments are shown in Figure 44. Rather good agreement exists for data obtained from different thicknesses of material. The data adhere well to a straight line for a variety of charge sizes and metal draw depths. The greatest scatter occurs for shallow draw depths, i.e., $W/D < 0.2$. The variation in data, which was noticed for all of the materials in the program, is undoubtedly a result of metal springback. The high elastic properties of high-strength materials prevent large blank deformation at shallow draw depths, and thus, large variations

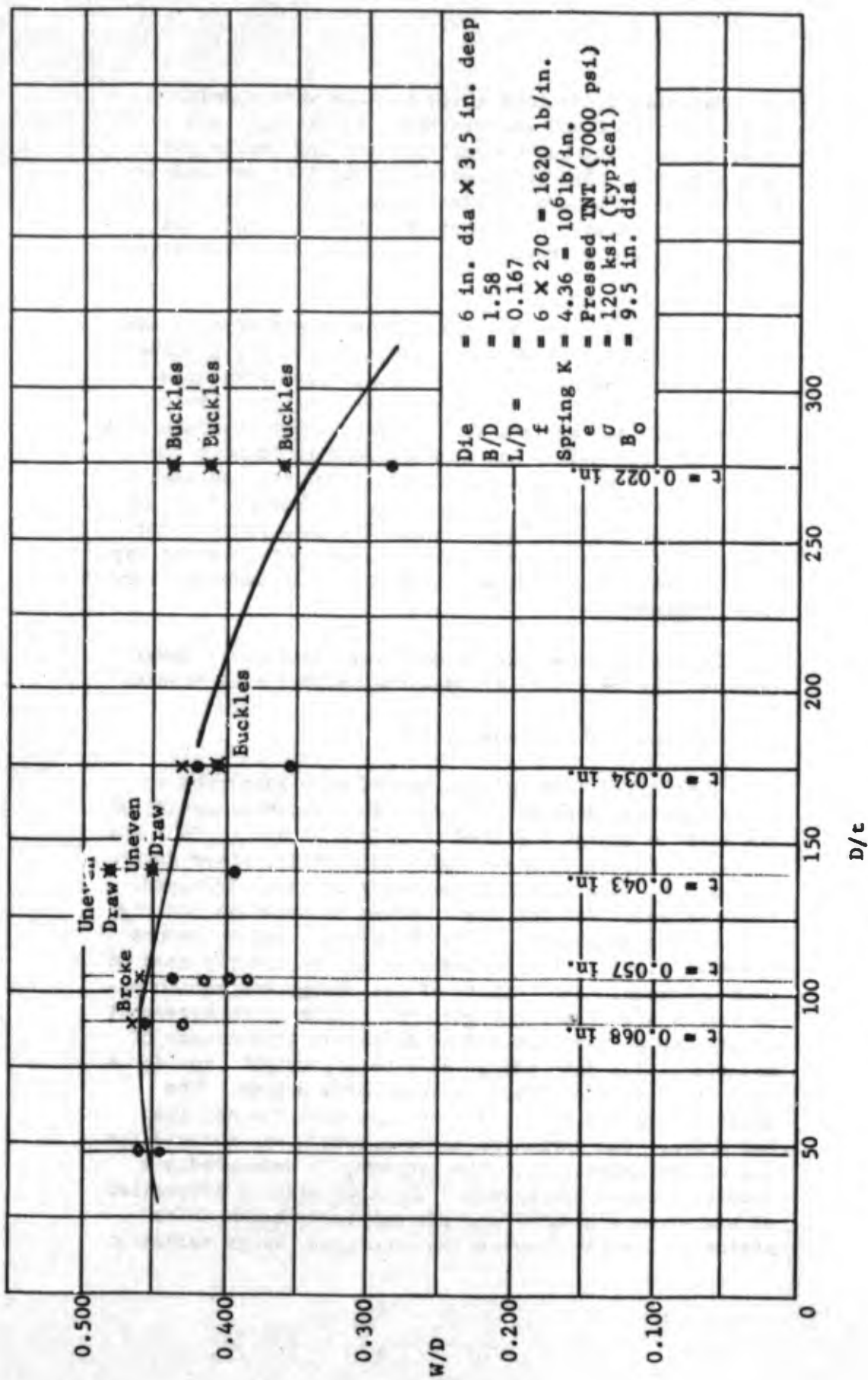


Figure 42 HP9-4-25 Steel Formability Limit Curve (B/D = 1.58)



Figure 43 Deformed Specimens of HP9-4-25 Steel Sheet Used to Establish the Relation Between Explosive Charge and Metal Draw Depth

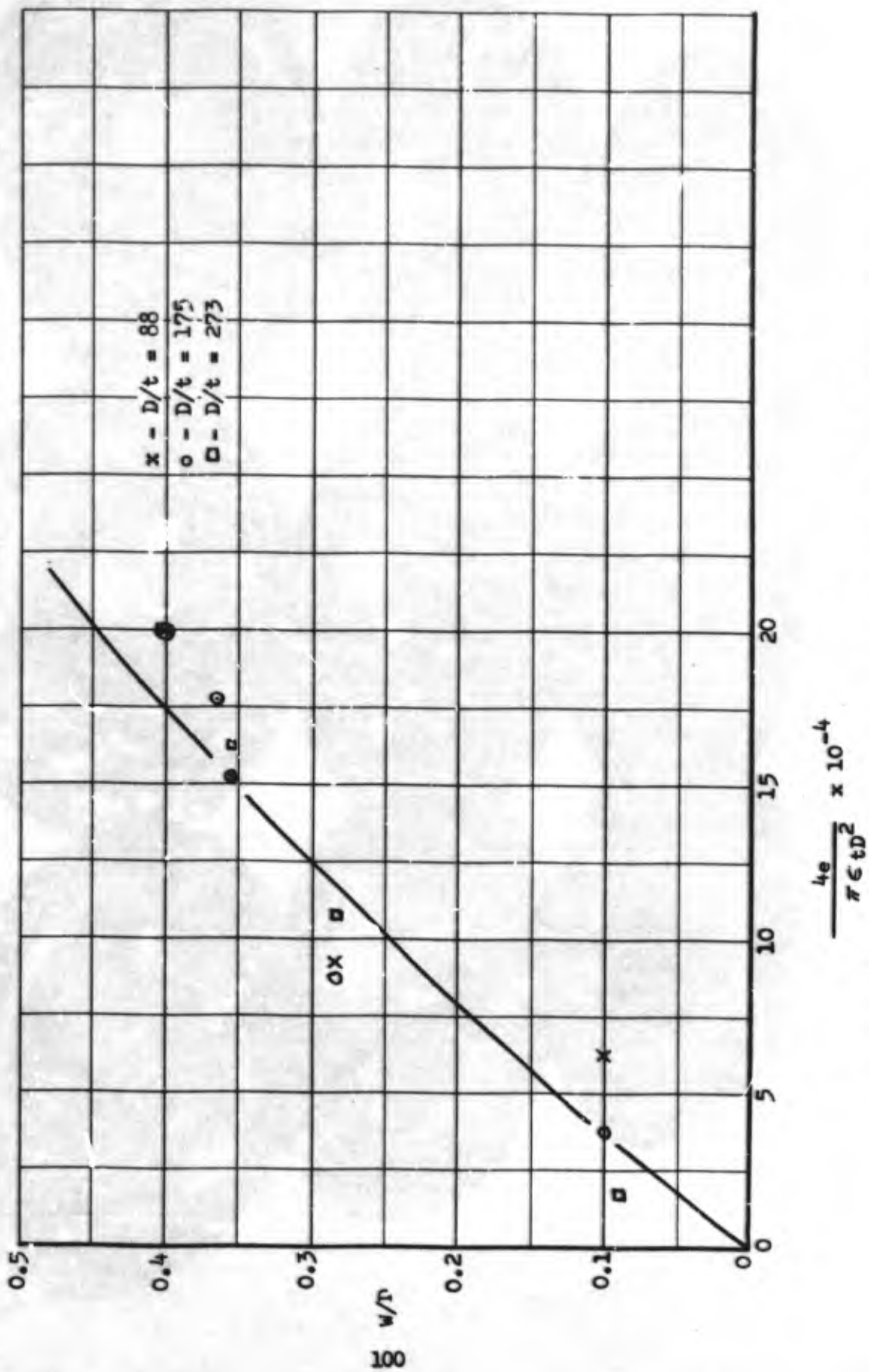


Figure 44 Estimation of Charge as a Function of Metal Draw Depth for HP 9-4-25 Steel Sheet

in explosive charge can result in identical draw depth. Even though one might expect greater elastic rebound of the blank from the die surface with higher explosive charges, deflection of the die can negate the effect of rebound and produce the same final part contour.

(3) Verification of Subscale Forming Experiments

To demonstrate the validity of data produced on the six-inch forming dies, experiments were conducted on a 24-inch-diameter die using material of appropriate thickness and yield strength. The Martin Marietta 24-inch-diameter Meehanite die was not adequate for the necessary forming studies. Therefore, the Phase III die was used. This die was designed with sufficient stiffness to prevent flange buckling of the high-strength steel sheet. The buckling of blanks during deformation must be prevented because either the buckles will progress into the die cavity as the blank is formed deeper or predicted draw depth will not be achieved.

The results of scaling verification tests are presented in Table XXX.

The excellent scaling results can be seen by comparing the first two experiments. The average variation in blank pull-in and draw depth from predicted values was about 0.4% and 1.5%, respectively. The last two experiments were essentially unscaled with respect to blank thickness because the charges used were based on subscale thicknesses of 0.040 inch. Tolerance variation was as much as 0.006 inch, which resulted in a variation of 0.024 inch on the full scale. Thus, the much deeper draw evident for the 24-inch-diameter experiments was a result of overshooting based on a blank thickness less than subscale tests showed necessary. Because there was a 12-to-16-week schedule for material delivery from the producer, it was necessary to order material early to meet program schedules. The requested thicknesses for the 24-inch die tests were not completely as specified, thus giving a deviation from required thicknesses that could not be controlled. Previous experience with adjustment of charges based on variations in thickness was used with highly satisfactory results as shown in Table XXX.

TABLE XXX

Scaling Verification: Results for HP 9Ni-4CO-.25. High-Strength Steel

Test	B ₀ in.	B ₁ in.	6-inch die		W in.	f lb	B ₀ (in.)	B ₁ in.	24-inch die		W in.	f lb
			t ₀ in.	e grains					t ₀ in.	e grains		
1	9.5	8.3	0.035	144.5	2.18	1620	37.75	32.6	0.158	0.150	8.56	25,900
2	9.5	8.3	0.035	144.5	2.18	1620	37.75	32.75	0.158	0.150	8.65	25,900
3	9.5	8.3	0.035	194.5	2.48	1620	37.75	29.4	0.160	0.150	10.76	25,900
4	9.5	8.4	0.035	124.5	2.00	1620	37.75	34.0	0.160	0.150	7.93	25,900

Dimensionless parameters													
	B ₁ /B ₀	W/D	L/D	D/t	B/D		B ₁ /B ₀	% Deviation	W/D	% Deviation	L/D	D/t	α t ₀ Deviation
1	0.875	0.353	0.167	171	1.58		0.870	0.6	0.357	1.1	0.167	152	11
2	0.875	0.353	0.167	171	1.58		0.873	0.2	0.360	2.0	0.167	152	11
3	0.875	0.413	0.167	171	1.58		0.785	11.0	0.450	8.2	0.167	150	12
4	0.885	0.334	0.167	171	1.58		0.902	1.9	0.330	1.4	0.167	150	12

c. D6AC Steel

(1) Formability Limits

Figure 45 is the formability limit curve for the D6AC alloy steel sheet. It is possible to obtain draw-depth ratios of more than 0.450 with the alloy in one forming operation using unlubricated blanks. This is comparable to the excellent formability achieved with the HP 9-4-25 alloy. The buckling resistance of the material is good at any thickness above 0.020 inch. For a given draw depth the charge requirements are somewhat lower than for the 18% nickel maraging steel but comparable to those needed to deep draw HP 9-4-25 and 12Ni-5Cr-3Mo. Figure 46 shows typical D6AC parts formed from 0.032- and 0.040-inch-thick stock. The absence of flange wrinkles and excellent part surface is noteworthy.

(2) Estimation of Explosive Charge

Figure 47 is the charge estimation curve for the D6AC alloy. There was considerable scatter at both the low and high ends of the curve. The variations in data points at the low end of the curve have been explained previously. No logical explanation can be presented for the scatter in values for large draw-depth ratios. Charges selected from the estimation curves for scaling verification experiments were found to be very accurate as described in the next section. The general relationship, which reveals that explosive charge scales as the cube of the scale factor, is accurate. The scatter in charge-estimation curve data for different D/t ratios is a measure of the accuracy of interpolating charge weights based on blank volume.

(3) Verification of Subscale Forming Data

The results of verification experiments were satisfactory. Table XXXI summarizes the data for the six- and 24-inch-diameter forming tests. The data showed more variation from predicted values than HP 9-4-25 steel. Comparing the first and third experiments, one can see that the percent variation for blank pull-in and draw depth is 4% and 14.5%, respectively. In general, the material for the 24-inch die tests was thicker than required and therefore predicted charges caused underforming of the parts. The second and fourth tests

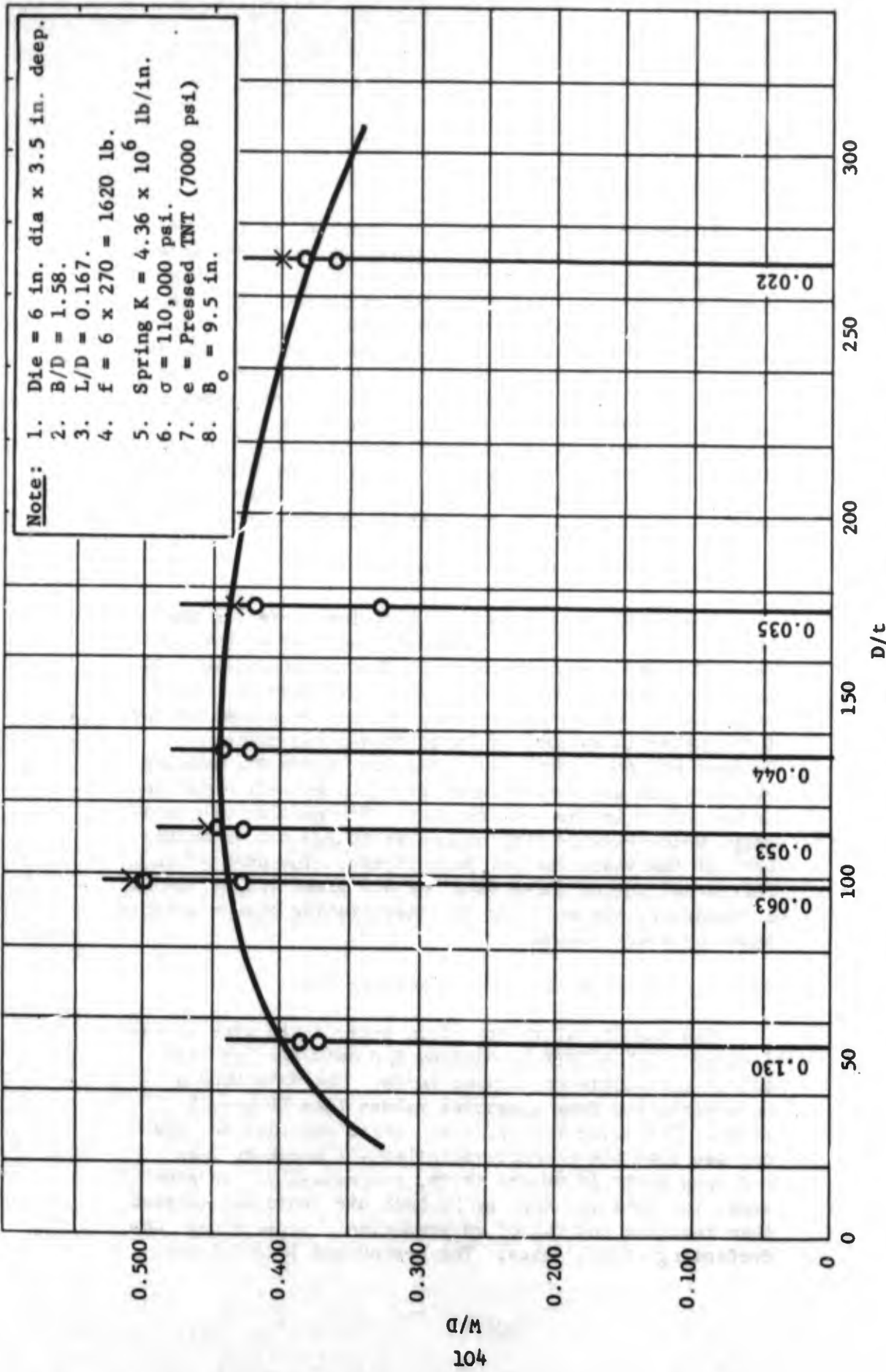


Figure 45 Formability Limits for D6AC Alloy Steel

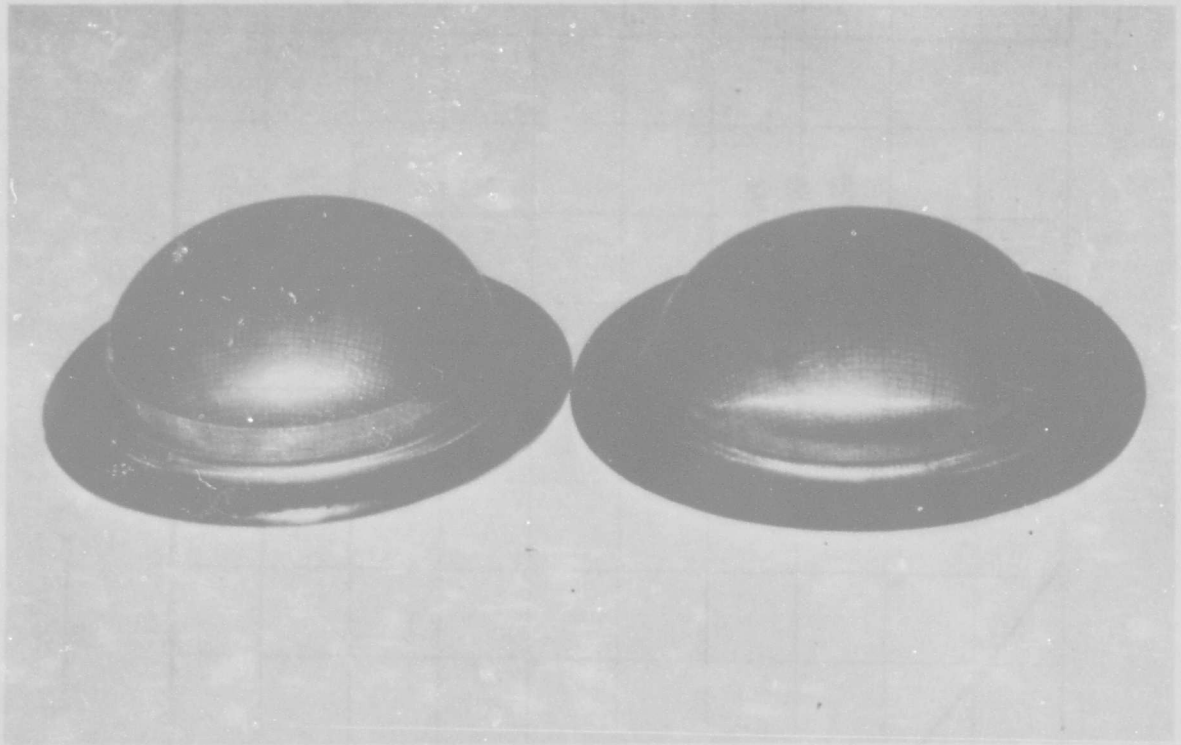


Figure 46 Typical Formed Parts from Thin Gage D6AC Steel Sheet

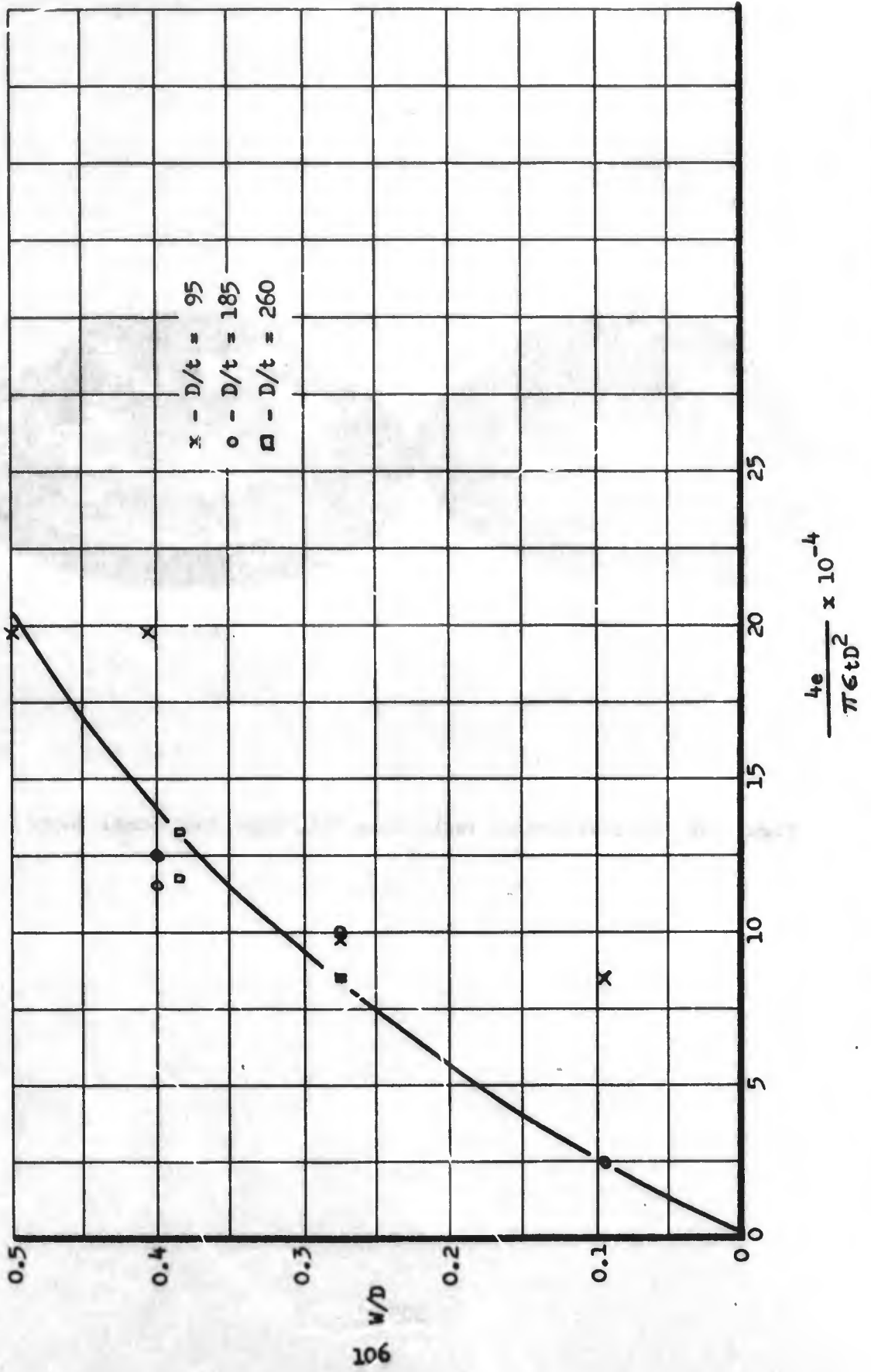


Figure 47 Estimation of Charge as a Function of Metal Draw Depth for D6AC Steel Sheet

TABLE XXI

Scaling Verification Results for D6AC High-Strength Steel

Test No.	6-Inch Die							24-Inch Die						
	B_o in.	B_l in.	t_o in.	c grains	W in.	f lb	B_o in.	B_l in.	t_o in.	Req. t_o in.	e grains	W (in.)	f lb	
1	9.5	8.7	0.034	114.5	1.95	1620	37.75	33.7	0.160	0.136	7075	7.6	25,900	
2	9.5	8.6	0.032	124.5	2.38	1620	37.75	33.0	0.160	0.128	7975	8.34	25,900	
3	9.5	8.6	0.032	124.5	2.38	1620	37.75	33.1	0.158	0.128	7975	7.97	25,900	
4	9.5	8.45	.034	144.5	2.38	1620	37.75	32.2	0.158	0.136	9250	9.26	25,900	

Dimensionless parameters											
B_l/B_o	W/D	L/D	D/t	B/D	B_l/B_o	% Deviation	W/D	% Deviation	L/D	D/t	% Deviation
1	0.915	0.325	0.167	1.58	0.895	2.2	0.318	2.2	0.167	150	15.3
2	0.905	0.397	0.167	1.58	0.875	3.3	0.347	12.5	0.167	150	21.0
3	0.905	0.397	0.167	1.58	0.878	3.0	0.332	16.4	0.167	152	18.8
4	0.890	0.397	0.167	1.58	0.853	4.2	0.386	2.8	0.167	152	16.5

were used to establish charge size based on thickness differences and yield-strength variations. Buckling and uneven draw resulted in meaningless values for final blank diameter and draw depth for the fourth experiment. It started to become evident at this stage of the scaling verification program that the Phase III die was not retaining the clamping stiffness available during the early experiments. Weld cracks around the shim pads and channel stiffener members permitted flange wrinkling to become unsatisfactory. The die was reworked to permit subsequent forming.

d. 12Ni-5Cr-3Mo Maraging Steel

(1) Formability Limits

The 12Ni-5Cr-3Mo maraging steel had to be reprocessed to permit satisfactory deep drawing (See Section 1 a). Even with correct thermal treatment, the alloy is not as formable as the 7039, HP 9-4-25, or D6AC materials. The lower formability is particularly noticeable in the thinner gages, as shown in Figure 48. However, the restricted drawing possible with these blanks can be attributed to the poorer quality of material. Because the 12Ni-5Cr-3Mo alloy is not generally produced in thicknesses less than about 0.063 inch, and because hand mills were used to roll the original billets, surface and property values were not as closely controlled as production mill output. Some difficulties were experienced with sheet warpage because sealing of the blank to permit evacuation of the die cavity requires a relatively flat blank. Adequate clamping force could be applied to the blank before final torque selection to permit die-cavity sealing, therefore, no further problems were encountered. As indicated in Figure 48, the 12Ni-5Cr-3Mo alloy could not be formed in one operation to full hemispherical depth. However, full hemispheres were produced using a two-shot forming sequence. Figure 49 shows a hemisphere of 12Ni-5Cr-3Mo together with hemispheres from the other steel alloys in the program. It should be explained that, although all of the steels under study could be formed into full hemispheres using a two-shot forming sequence, the large explosive charges required would result in extremely large charges on the full scale, which would exceed the capacity of the largest existing facilities in the United States. For example,

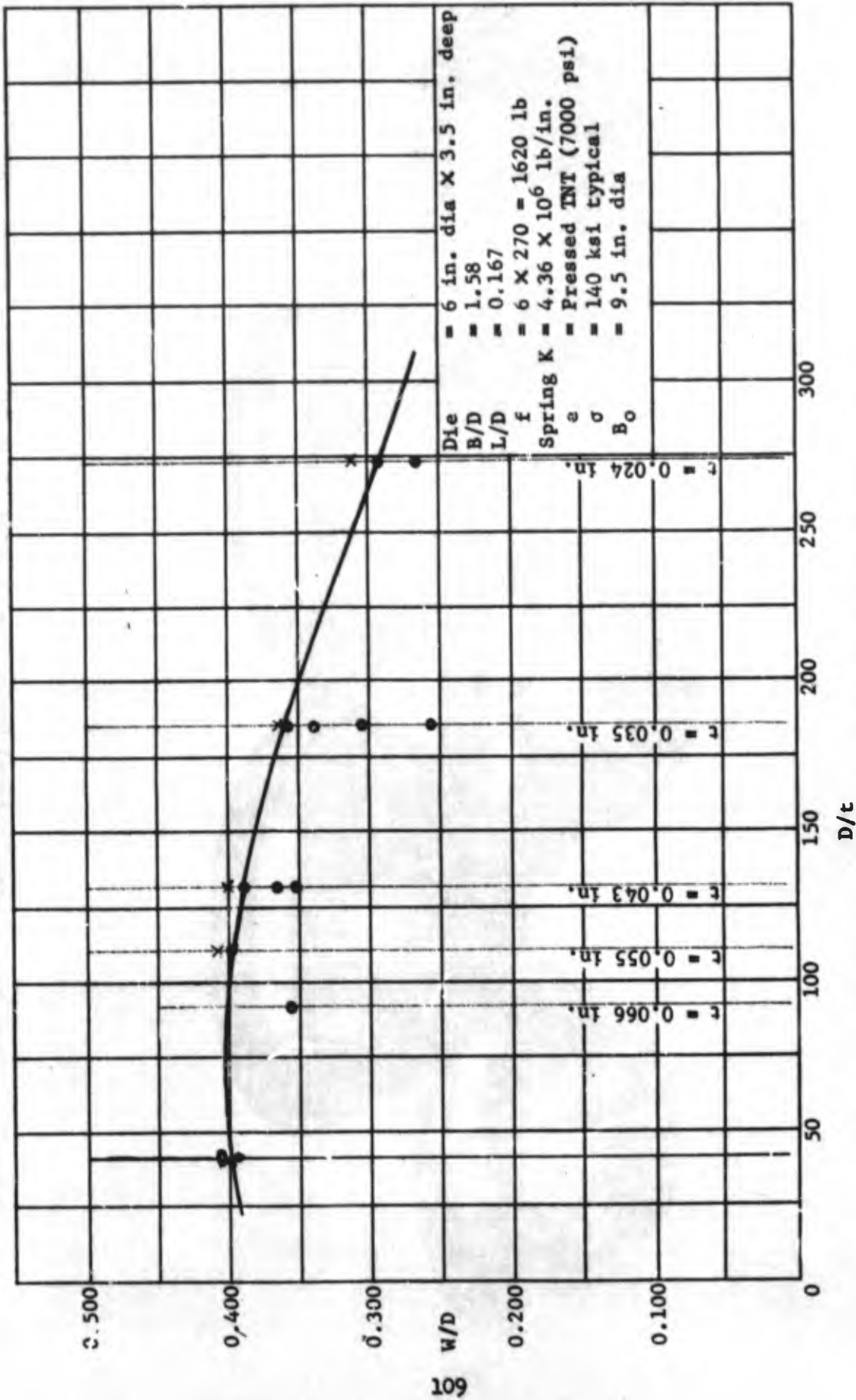


Figure 48 Formability Limits for 12N1-5Cr-3Mo Maraging Steel

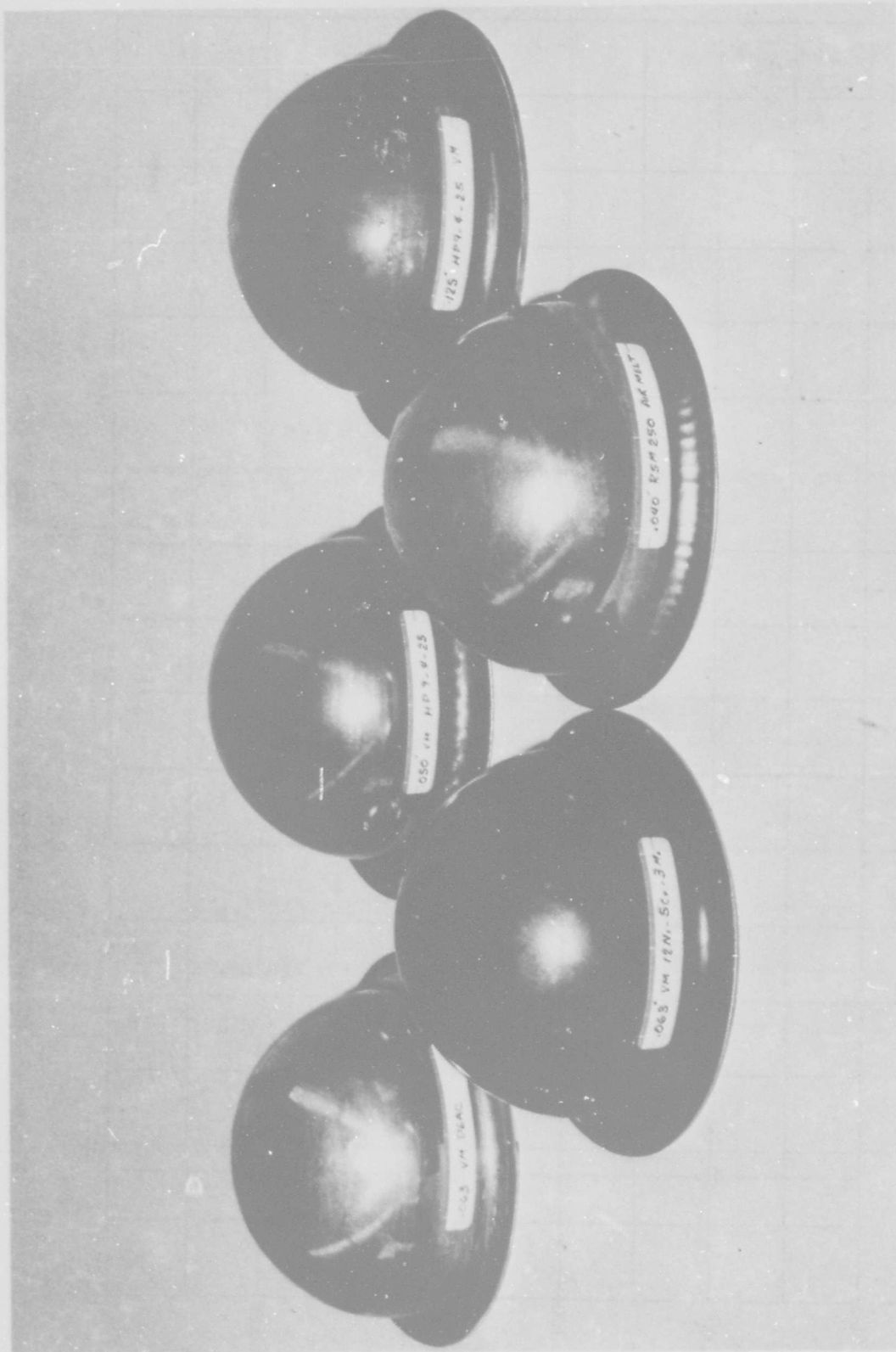


Figure 49 Steel Hemispheres Produced During the Program Using Multiple Forming Sequences.

the first forming shot for the 12Ni-5Cr-3Mo 0.063-inch-thick alloy on the six-inch die required 400 grains. This would scale to 1003 pounds to permit the forming of 0.975-inch-thick plate on a 156-inch diameter. Even though there is a large charge requirement one can still accomplish the forming by using barges or shipyard facilities and conduct the forming in the ocean. However, another more practical approach is to break up the charge into several smaller charges to permit the forming of hemispherical parts in 5 to 10 operations or less. This method was tried on the HP 9-4-25 alloy using charges that would be more reasonable for existing facilities. A three-shot sequence using 100-grain charges (scalable to 250 pounds) produced a full hemisphere. More work is necessary to optimize the forming sequence to permit the use of charges of less than 100 pounds for full-scale part fabrication. It is our opinion that a 6- to 8-shot forming sequence can be developed for any of the steels being studied, which will permit the full-scale forming of parts using charges of 50 to 75 pounds.

(2) Estimation of Explosive Charge

The relation of metal draw depth to explosive charge for the 12Ni-5Cr-3Mo maraging steel is shown in Figure 50. However, the data scatter is less than for the materials previously discussed. In general, the charges required to produce a given draw depth are similar to those required for the HP 9-4-25 and D6AC.

The accuracy of charges used for scaling verification tests selected from the charge-estimation curves can be seen by studying the results outlined in the next section.

(3) Scaling Verification Experiments

Table XXXII presents the results of scaling verification experiments for the 12Ni-5Cr-3Mo alloy. The predictions for blank pull-in and draw depth were quite good. Variations of experimental from predicted values of 4 to 6% and 4 to 7%, respectively, were found. The material was quite formable in the 0.160-inch thickness. In fact, the ductility was noticeably improved for the thicker blanks over those used in subscale experiments.

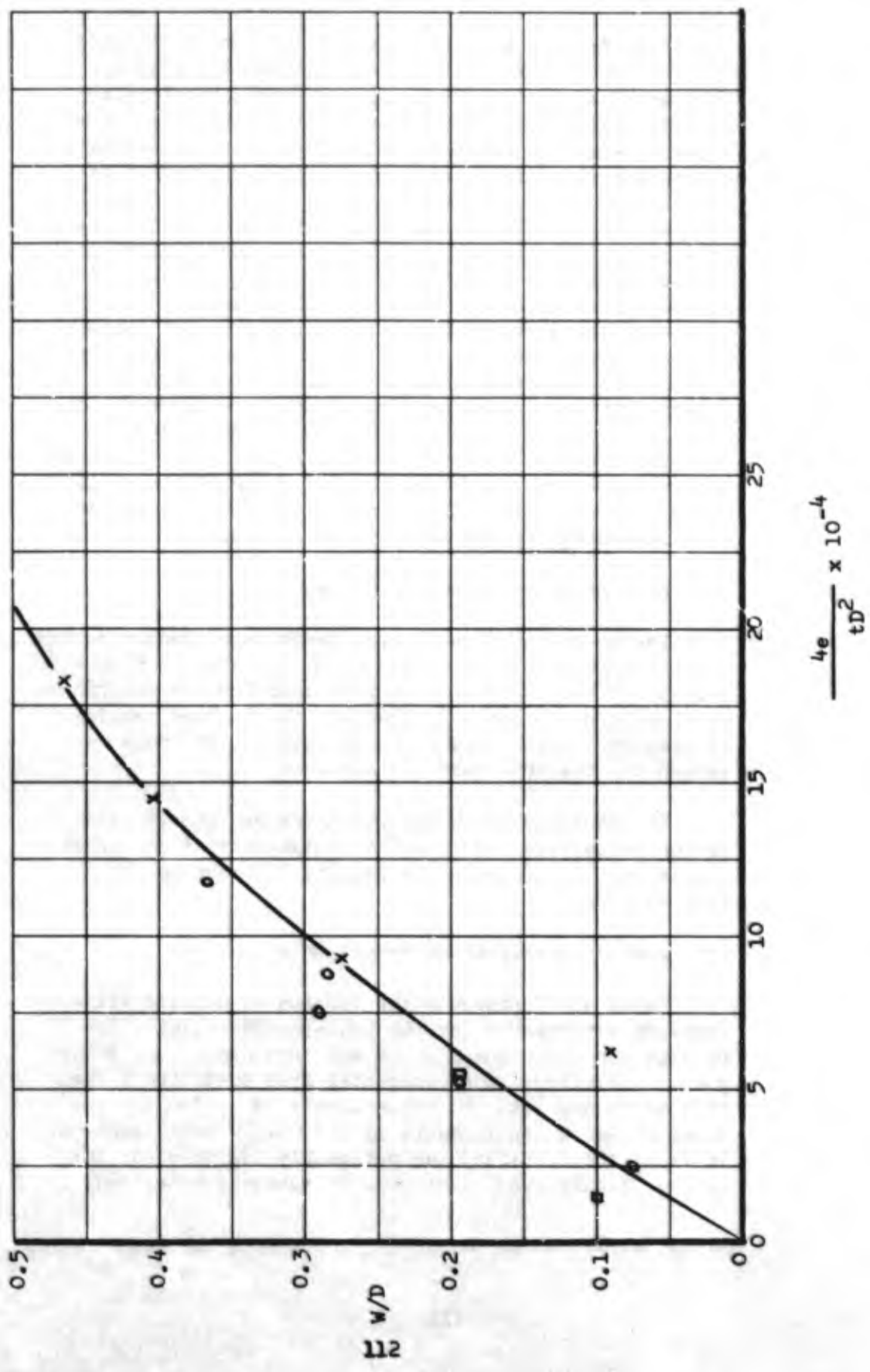


Figure 50 Estimation of Charge as a Function of Metal Draw Depth for 12Ni-5Cr-3Mo Maraging Steel

TABLE XXXII

Scaling Verification Tests for 12Ni-5Cr-3Mo Maraging Steel

Test No.	6-inch die						24-inch die						
	B _o in.	B ₁ in.	t _o in.	e grains	W in.	f lb	B _o in.	B ₁ in.	t _o in.	Req. t _o in.	e grains	W in.	f lb
1	9.5	8.65	0.034	154.5	2.18	1620	37.75	33.0	0.162	0.136	9890	9.4	25,900
2	9.5	8.65	0.034	154.5	2.18	1620	37.75	32.44	0.159	0.136	9890	9.06	25,900
3	9.5	8.60	0.035	154.5	2.18	1620	37.75	31.45	0.157	0.140	9890	9.53	25,900
4	9.5	8.60	0.035	144.5	2.05	1620	37.75	32.75	0.160	0.140	9250	8.77	25,900

Dimensionless parameters											
B ₁ /B _o	W/D	L/D	D/t	B/D	B ₁ /B _o	% Deviation	W/D	% Deviation	L/D	D/t	% Deviation
1	0.910	0.364	0.167	158	0.874	0.4	0.391	6.9	0.167	148	16
2	0.910	0.364	0.167	158	0.864	0.6	0.378	3.7	0.167	151	14
3	0.906	0.364	0.167	158	0.840	0.7	0.396	8.1	0.167	153	11
4	0.906	0.342	0.167	158	0.873	0.3	0.366	6.5	0.167	150	13

e. 18% Nickel Maraging Steel

(1) Formability Limits

The formability of the air-melted 18% nickel maraging steel was less than any of the other steels. In addition, the charge requirement was greatest for the alloy to produce specific draw depths when compared with the other materials. Because research under a previously funded Martin Marietta program had shown good forming characteristics for air-melted stock, the bulk of subscale testing used that material. However, to permit a comparison between air-melted and vacuum-melted sheet, 0.063-inch material that had been vacuum melted was obtained from Republic Steel. Unfortunately the quality of surface on the vacuum-melted material was very poor, which resulted in premature failures during forming. Figure 51 shows a cold-formed part that has a crack extending from the flange area into the drawn area of the part. These cracks were a result of severe surface striations in the rolled material caused by improper processing at the mill. The striations were built-in stress risers that contributed to part failure before appreciable deep drawing had occurred. Figure 52 is the formability limit curve for the 18% nickel maraging steel. Notice that the vacuum-melted material had much less formability than the air-melted stock. It was later found that the vacuum-melted sheet we had obtained from Republic Steel was a rejected lot shipped to Martin Marietta by mistake.

Even though most of the formability data were generated using air-melted material, the large charge requirements and more restricted formability suggested that much could be gained if material used in subsequent forming was produced from properly processed vacuum-melted material. In addition, the striking resistance of vacuum-melted material to stress corrosion compared to the air-melted sheet substantiated the need for the vacuum processed metal. It should be noted that blank material used on the 24-inch-diameter die was vacuum melted and had excellent surface condition and properties. Formability achieved was much superior to the previous material used on the small dies.

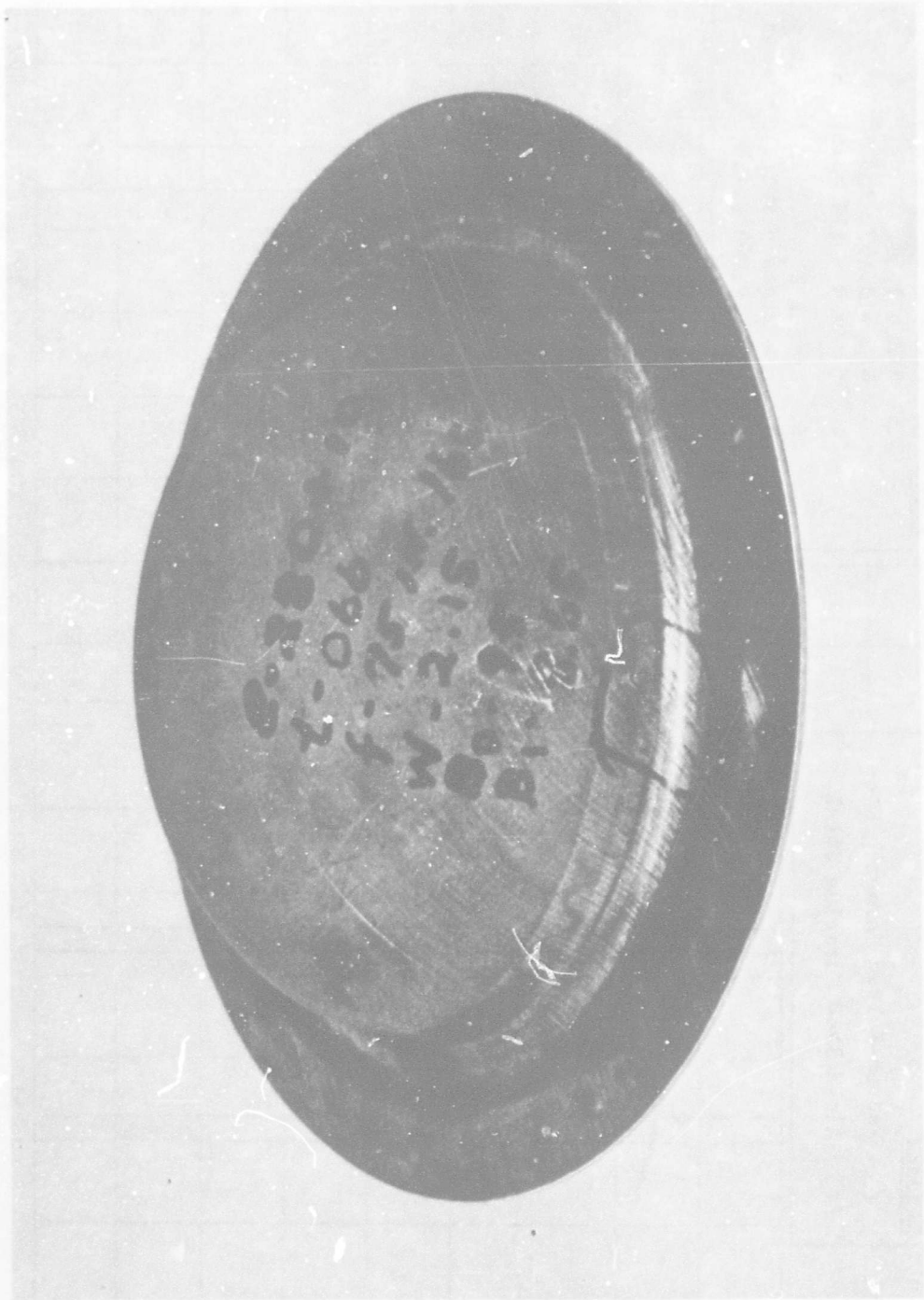


Figure 51 Failure of Formed Vacuum Melted 18% Nickel Maraging Steel Along Surface Striations Caused by Rolling.

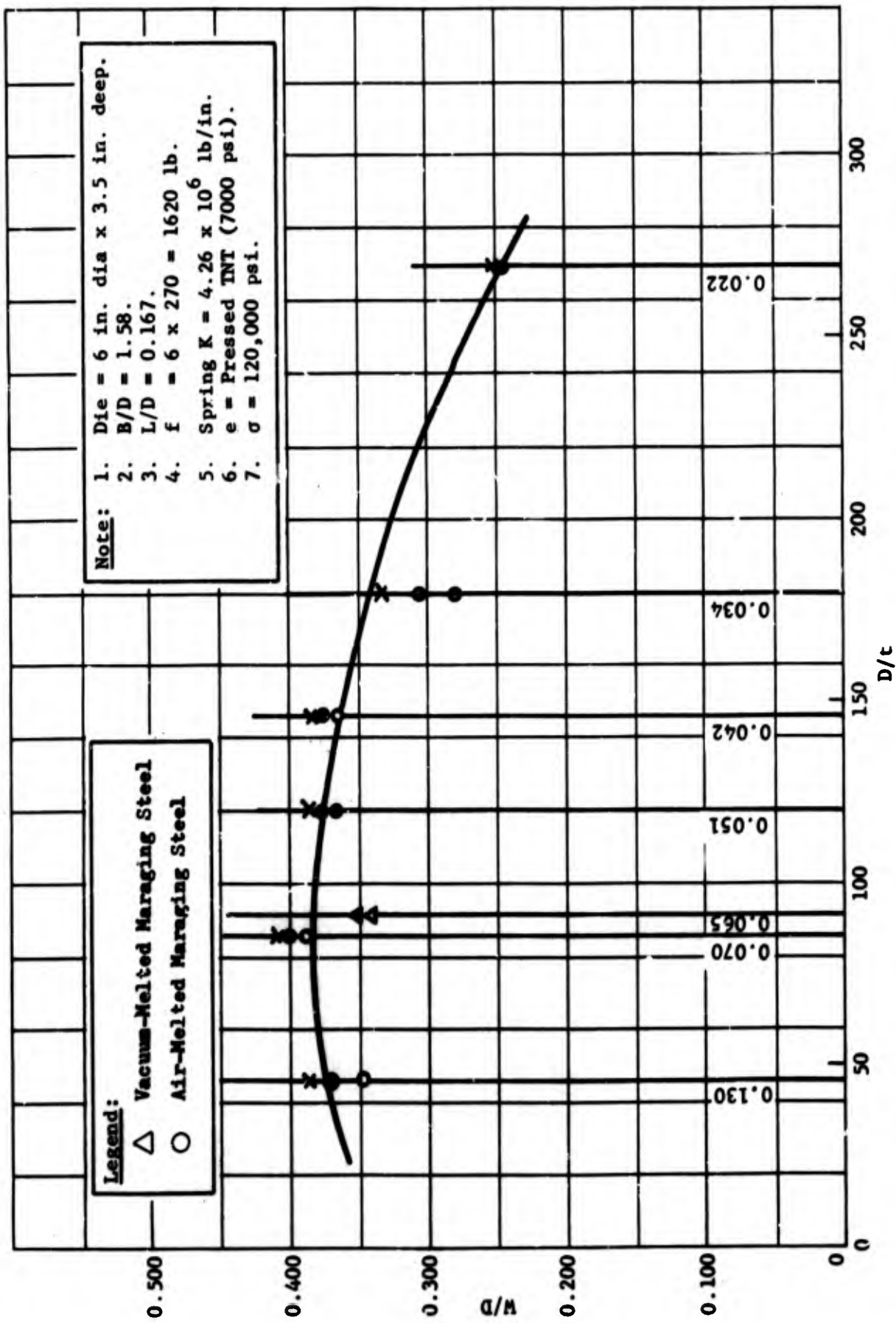


Figure 52 Formability Limits for 18% Nickel Maraging Steel

(2) Estimation of Explosive Charges

Charge-estimation data obtained from a measure of metal draw depth were quite accurate and plotted points adhered well to the curve shown in Figure 53. As mentioned previously, the charge requirements for deformation of the 18% nickel maraging steel were higher than for any of the other steels. It has been found from previous work with this alloy that the use of slower explosives enhances the formability. For example, if loose pentaerythritol tetranitrate (PETN) is used for forming, it is very difficult to restrict the metal strain to values below those required for fracture. However, the use of dynamite allows much deeper draws with lower total strain⁽²³⁾. In this program TNT, which has a detonation velocity intermediate to the other two explosives, was used. It is possible that TNT is still faster than the threshold velocity below which better metal formability exists, because restricted drawing was observed. Insufficient time and money in the program precluded establishment of the optimum explosive for use with the 18% nickel maraging steel.

(3) Scaling Verification Experiments

Empirical results were obtained on a 24-inch-diameter hemispherical die based on conditions established using a six-inch-diameter model die. The data were quite consistent and results from the subscale tests could be reproduced on the 24-inch size with very good accuracy. Table XXXIII summarizes the results. It can be seen that blank pull-in was reproduced within 3%, while the predicted draw depth varied by a like amount. The first two experiments listed in the table were directly scaled based on the use of an explosive charge of 124.5 grains on the six-inch-diameter scale. Repeatability was excellent. When larger charges are used, as shown by the third test, the variations from predicted results were somewhat greater. Blank pull-in was about 9.8% more than expected, while the draw depth obtained exceeded predicted values by 7%. The deeper draws achieved on the 24-inch die were unexpected because the thickness of material needed on the six-inch die required thinner blanks for the larger size. However, there were variations in mechanical properties between thin-gage and thicker parts, as mentioned previously. The material

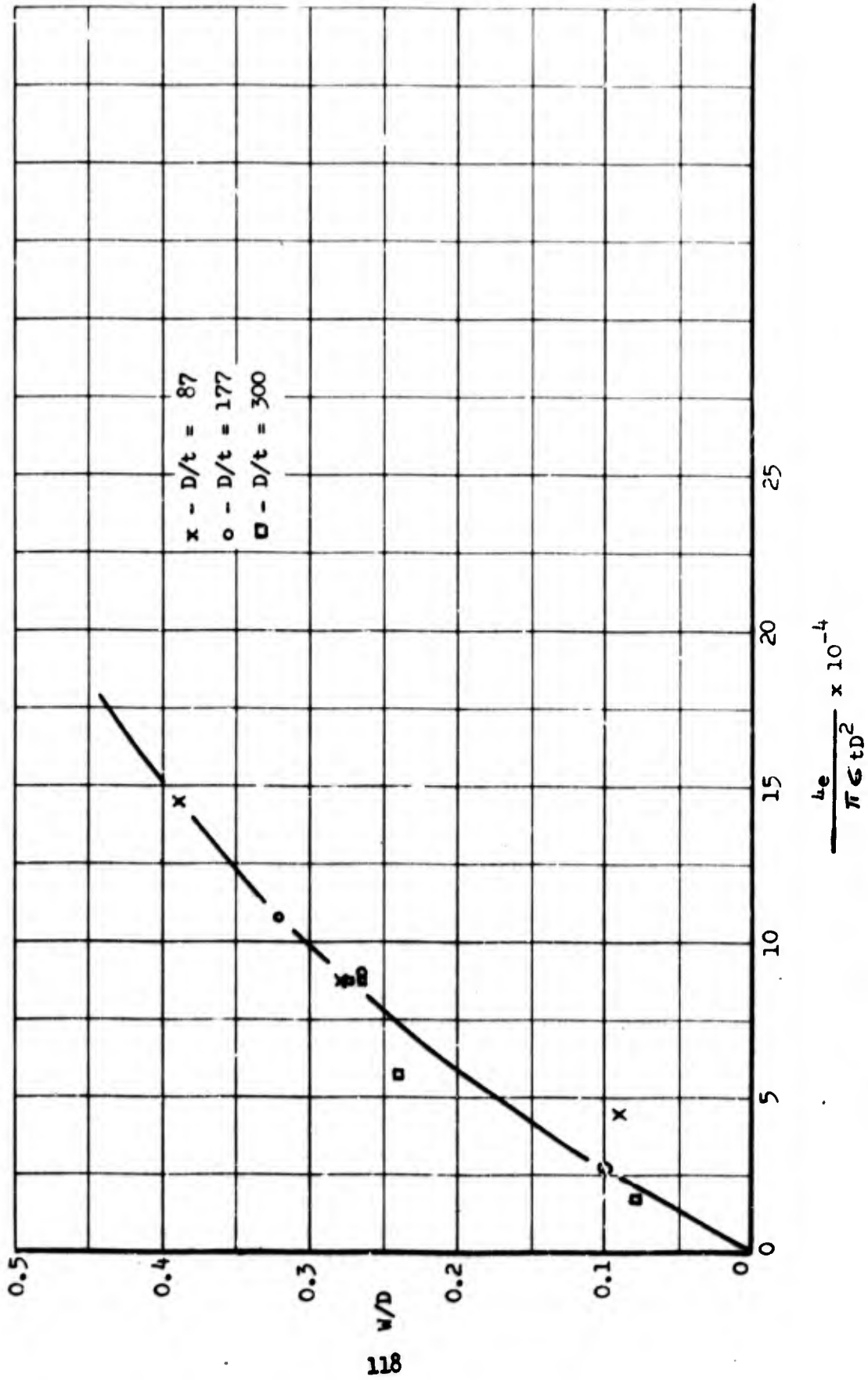


Figure 53 Estimation of Charge as a Function of Metal Draw Depth for 18% Nickel Maraging Steel Sheet.

TABLE XXXIII

Scaling Verification Tests for RSM 250 18% Ni Maraging Steel

Test No.	B ₀ in.	B ₁ in.	6-inch die		W in.	f lbs	B ₀ in.	B ₁ in.	24-inch die			W in.	f lbs
			t ₀ in.	e grains					t ₀ in.	Req. t ₀ in.	e grains		
1	9.5	8.6	0.034	124.5	1.95	1620	37.75	33.2	0.156	0.136	7975	8.09	25,900
2	9.	8.6	0.034	124.5	1.95	1620	37.75	33.25	0.156	0.136	7975	8.07	25,900
3	9.5	8.5	0.034	144.5	2.15	1620	37.75	32.7	0.156	0.136	9250	3.25	25,900
4	9.5	8.7	0.042	194.5	2.23	1620	37.75	26.0	0.155	0.168	12,475	Broke*	25,900

Dimensionless parameters

	B ₁ /B ₀	W/D	L/D	D/t	B/D	U ₁ /B ₀	% Deviation	W/D	% Deviation	L/D	D/t	% to Deviation
1	0.905	0.325	0.167	176	1.58	0.880	0.3	0.337	3.5	0.167	153	+13
2	0.905	0.325	0.167	176	1.58	0.880	0.3	0.336	3.6	0.167	153	+13
3	0.895	0.325	0.157	176	1.58	0.866	0.3	0.385	15.6	0.167	153	+13
4	0.915	0.372	0.167	143	1.58	0.688	2.5	---	---	0.167	154	- 7

*Lower yield strength of 0.150-inch material than that of 0.042-inch material coupled with charge scaled for 0.168-inch material caused blank failure.

used on the larger die had a lower yield strength and higher elongation than the thin blanks; therefore, explosive forming would tend to give larger draw depths and greater blank pull-in. The yield-strength effect appears to affect the charge requirement to a greater extent than the change in thickness. Accurate control of both thickness and blank yield strength for both the six-inch and 24-inch sizes would permit exact duplication of results, everything else being equal.

In summary, HP 9-4-25 was the most formable of any of the alloys studied, while the air-melted 18% nickel maraging steel had the least formability. The D6AC steel had by far the best formability at high diameter-to-thickness ratios with attendant high resistance to buckling. Thus, at $D/t > 130$, D6AC is recommended for deep drawing, while below this value HP 9-4-25 is superior. Strength advantage is gained using the D6AC alloy. Both alloys exhibit high fracture toughness and therefore the choice of either alloy for structural use depends largely on the service conditions encountered. Figure 54 summarizes the formability limits for the several alloys investigated.

With respect to the estimation of explosive charge requirements, Figure 55 presents empirical relationships of charge as a function of metal draw depth using pressed TNT. Three of the alloys (i.e., 12Ni-5Cr-3Mo, 18% nickel maraging steel, and D6AC steel) can be basically represented by a single curve, while the charge requirements for alloys HP 9-4-25 and 7039 aluminum are somewhat different and can be defined by a second curve.

If one wishes to form one of the alloys to a given draw depth, selection of a charge from the empirical curves yields predictable and accurate results. The data are excellent input to the computer program being developed at Martin Marietta, and should permit the accurate prediction of radial blank strains and metal thin-out from forming.

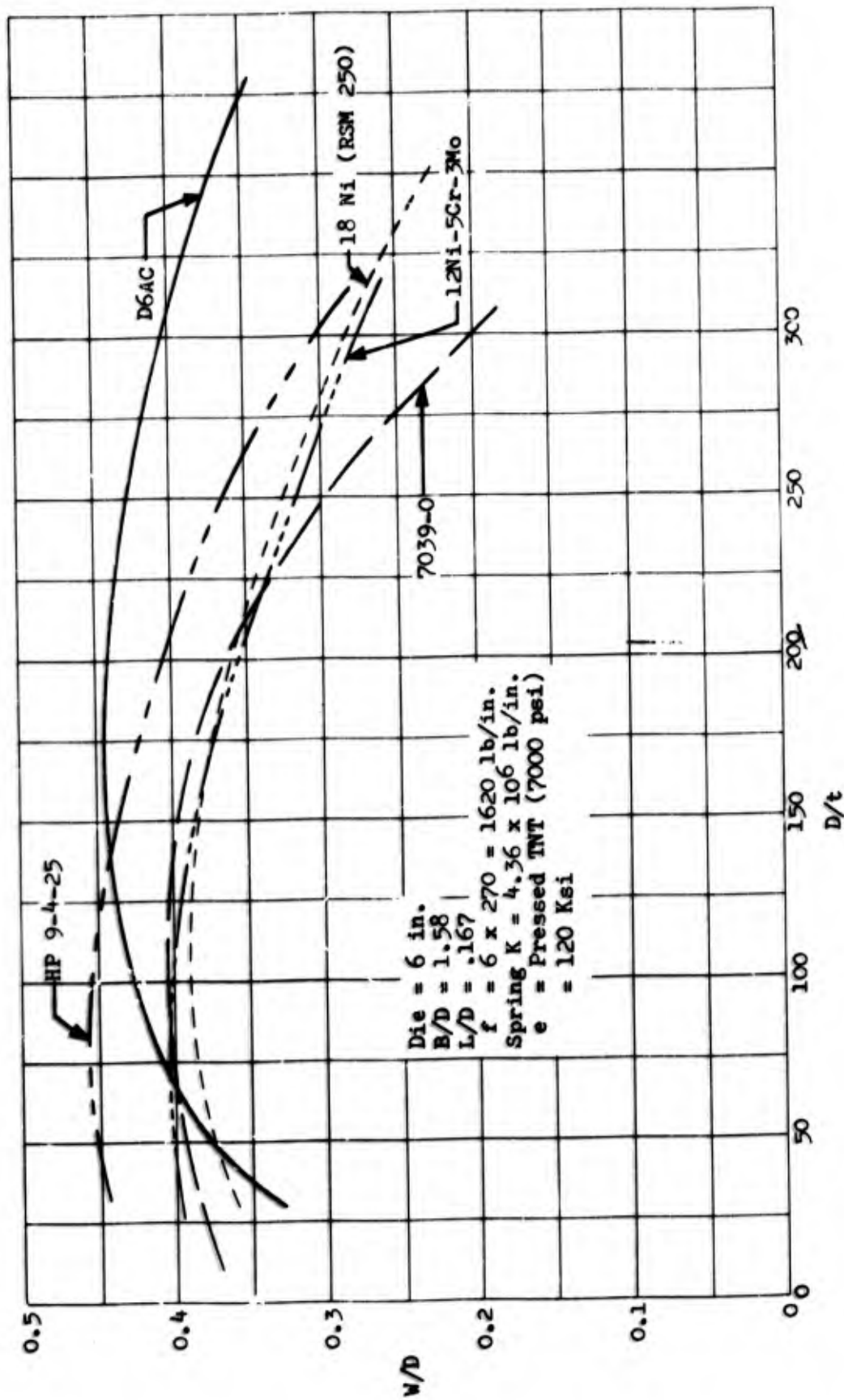


Figure 54. Summary of Formability Limit Curves

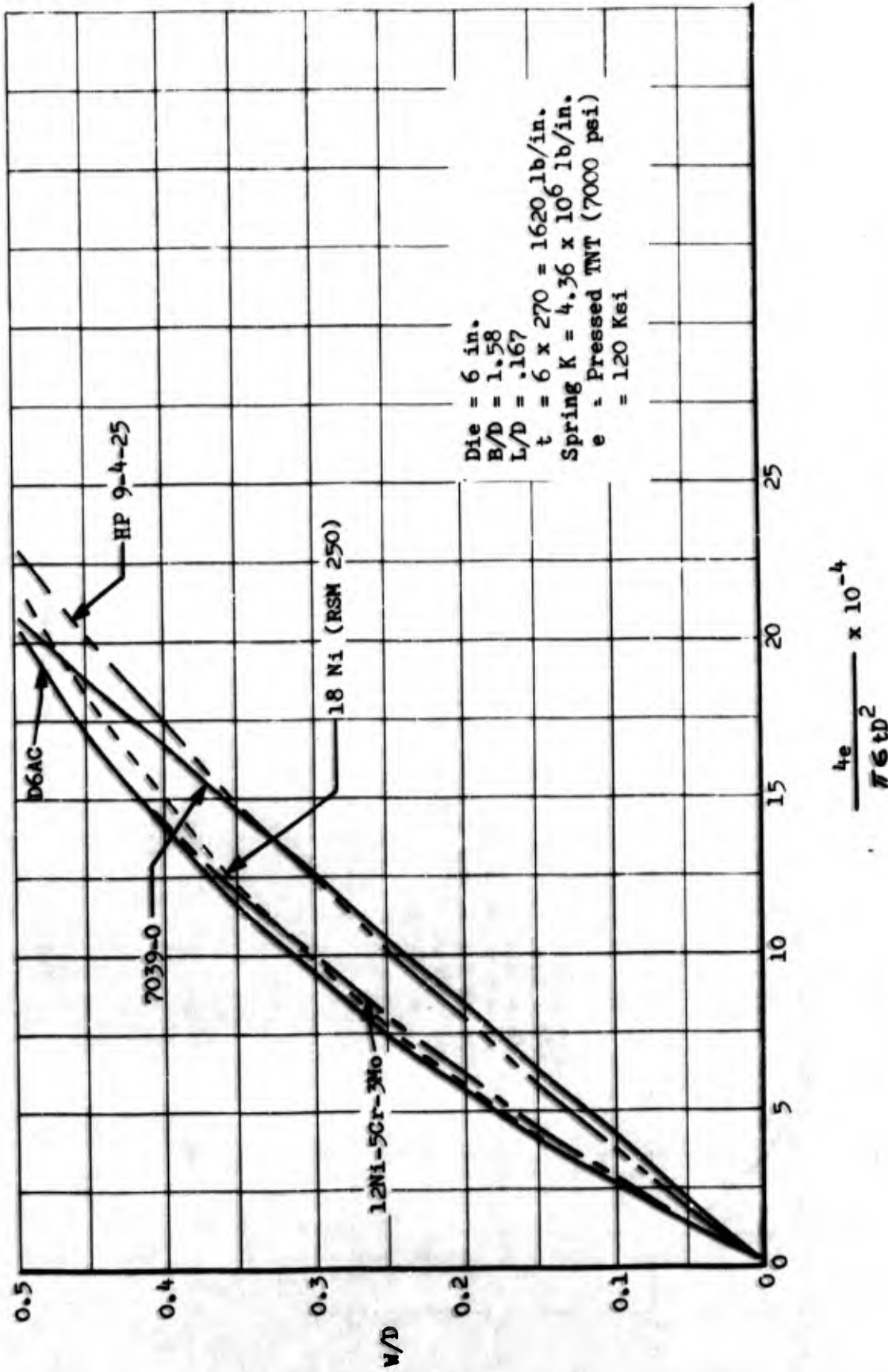


Figure 55. Summary of Charge Estimation for High Strength Alloys

SECTION IV

CRITERIA FOR DIE DESIGN

Since the inception of high-energy-rate forming techniques, the bulk of the technical die design efforts have been directed toward massive female forming tools constructed from castings or forgings. Standard design methods were used to produce suitable dies for forming, i.e., calculated loads were determined and large safety factors were used to arrive at the final die shape and size. For part sizes up to about 72 inches, the use of massive tooling does not pose many serious problems. However, when one is faced with the requirement for parts larger than 72 inches in diameter, conventional forming tools become unwieldy. Crane capacity becomes severely challenged, transportation of the tools from the point of manufacture to the place of use poses serious problems, and handling of the tools presents many difficult problems. With the inherent disadvantage of massive tooling relating to economics and handling capacity, different concepts must be considered for the fabrication of tools needed to form parts up to 50 feet in diameter.

During the past ten years, several unique concepts have been studied to permit the fabrication of metal components using light weight die construction. Aerojet General (24) developed a design in which ice was used as the forming surface. The concept made use of a steel shell in which a refrigeration system was installed. Water was poured into the steel shell and frozen by the cooling system. After the ice was formed, the specific die contour desired was either machined directly from the ice or a contoured plug was used that was removed after the water was frozen around it. Standard hold-down rings and clamping methods were used. Although the concept was unique, many of the problems encountered were difficult to solve, e.g., close contour control could not be maintained, if blank wrinkling occurred the ice could not withstand the high localized forces produced, sizing could not be conducted without causing severe damage to the ice surface, and materials of construction used in the ice container had to be carefully selected to prevent fracture as a result of ductile-brittle transition effects. Some offsetting advantages of ice dies are: die surface contours can be rapidly changed, repairs of forming surface damage can be made quickly, and the total die cost is relatively low. Because many problems remain to be solved with the use of ice dies, and fabrication of tough high-strength metals such as HP 9-4-25, 12 and 18% nickel maraging steels, D6AC steel could create serious problems with respect to tolerance

control and wrinkle prevention, further consideration of ice die techniques was dropped.

A second but more promising concept was suggested by Beyer (25) in which a metal shell was suspended in a pool so that it used water as the supporting medium for the die shell and at the same time the dynamic force was applied normal to the axis of the crane cable. Figure 56 illustrates the technique. The concept uses the incompressibility of water for necessary support and permits the use of a lightweight tool. The shell die approach has considerable merit and will be discussed more fully.

Beyer and his colleagues conducted numerous experiments using the shell die or "pendulum die" and extended the idea to evaluate die materials by using a massive support tool and a water annulus between the die base and the "replaceable" shell. Figure 57 shows the modified-shell die concept. The disadvantages of this latter die design became obvious for large parts. In the fabrication of the SeaLab end closures, the Navy successfully used the pendulum die concept, but a steel/concrete die form was used in place of a shell die. Only two shots were made in the die because it fractured on the second forming operation. However, the method produced the necessary parts and prevented a serious schedule slip in the SeaLab program.

In conventional forming pools available within the United States, a die suspended from a crane cable cannot be used effectively to form large parts due to the lack of water head over the die, which permits movement of water behind the die shell during the explosion with subsequent lack of support and possible severe die distortion. Thus, the concept appears to be limited to bodies of water in which significant water head can be provided over the die, i.e., the ocean. However, further extension of the shell die concept has been made at Martin Marietta with gratifying results.

In an effort to explosively form 10-foot-diameter ellipsoidal domes for the Titan II Improvement Program, a lightweight inexpensive die design was needed. After careful analysis of stresses, deflections, and supporting methods, it was decided to use a fiberglass shell bolted to a rigid steel understructure that would contain stiff metal springs to react to forming loads. A steel draw ring and hold-down ring were designed and "shoe clamp" holding devices designed. The die produced two domes from 0.750-inch-thick 2014-O aluminum plate in one forming operation for each dome. The domes were used for engineering evaluation and testing. The results showed that the domes were superior to domes of

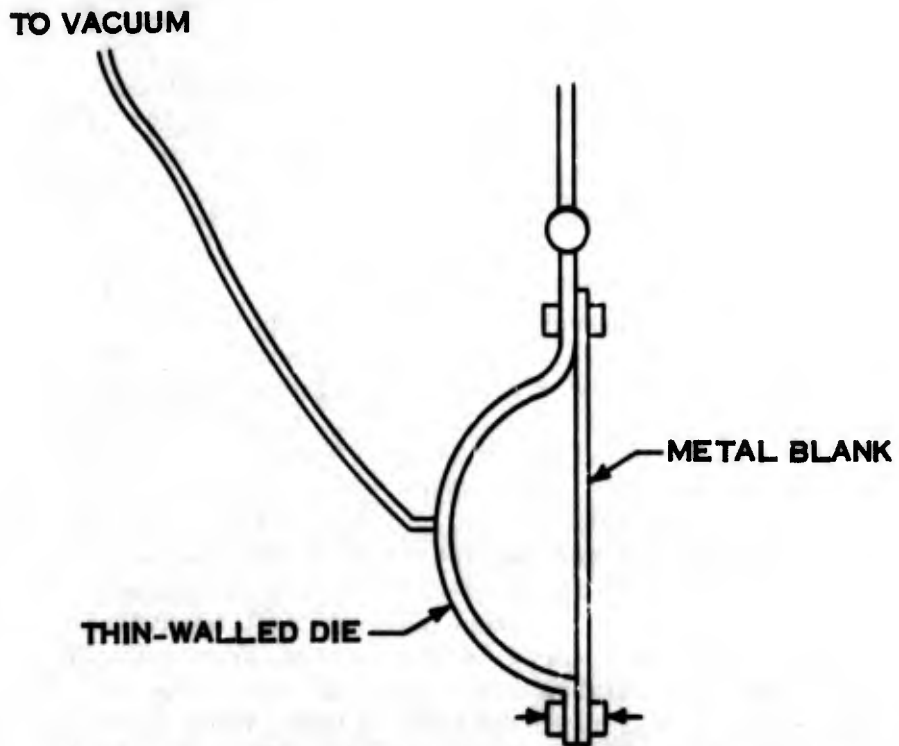


Figure 56. Swing Die Concept (Sheet Metal Parts)

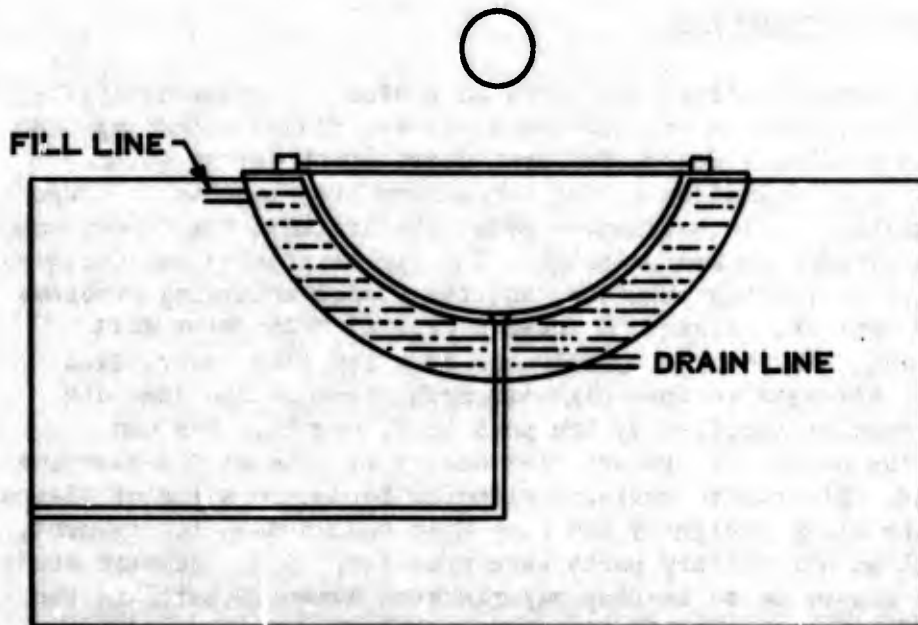


Figure 57. Interchangeable Die Cavity Concept Using Water for Die Support

similar shape fabricated by welding gore segments together. Although the fiberglass die shell was found to have limited life, the use of such shells to produce full-scale hardware to accurate tolerances was demonstrated. The results of the forming program (1) on Titan II components are presented in a Martin Marietta report.

Using the results of previous work cited above, further development of shell die concepts was accomplished under this program. Because the pendulum die concept had some inherent drawbacks for use in forming pools and because the fiberglass shell die was found to have limited applicability to metals of higher strength and toughness than aluminum, a modification of the die configuration resulted in the fabrication of a metal shell die supported by a steel cylindrical shell. Figure 58 is a schematic view of a six-inch-diameter die fabricated from 12% nickel maraging steel. To design dies to withstand the forces causing failure of the die, the modes of blank failure must be understood. Generally, there are three important considerations in the design of a suitable forming die: clamping stiffness to prevent flange wrinkling of high-strength alloys, blank failure that imposes severe loads on the die shell and sizing shots in which the explosive charge is within the cavity of the die with the part partially contacting the die shell. Each of the important design factors will be discussed in some detail to show the criteria developed for the design of a 156-inch shell die.

1. CLAMPING STIFFNESS

Considerable effort was spent in a study of clamping stiffness because, for the high-strength steels, flange wrinkling was a serious problem. Successful deep-drawn parts depend on the elimination of wrinkling during the deformation process. It was on an existing 24-inch-diameter Meehanite die that the importance of die stiffness became apparent. The die originally was designed for explosive forming aluminum, and few flange-wrinkling problems had ever existed. Figure 59 shows a typical deep-drawn part of aluminum. Notice the symmetrical draw and flat, unwrinkled flanges. Attempts to form high-strength steel in the same die yielded results typified by the part in Figure 60. One can observe the severe flange wrinkles caused by lack of die-clamping stiffness. Efforts to maximize clamping force, location of clamps around the blank periphery and ring mass resulted in improvement, but still unsatisfactory parts were produced. A systematic study was then conducted to develop experimental numbers useful in the design of a suitably stiff clamping system.

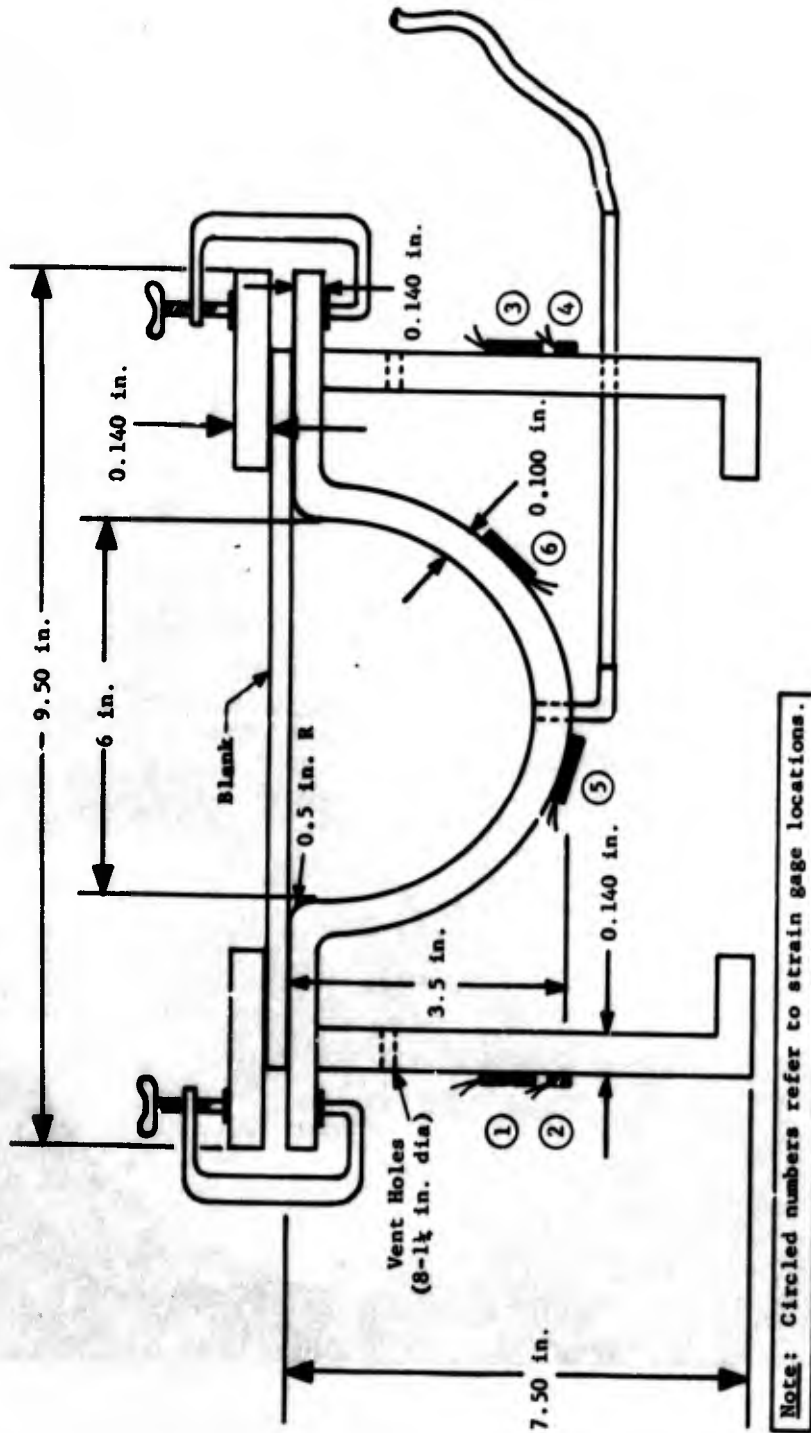


Figure 58 Shell Die Concept for Explosive Forming of High Strength Steels



Figure 59 24-Inch Diameter Hemisphere Formed From 0.150-Inch Thick 7039-O Aluminum



Figure 60 Flange Wrinkling of Explosively Formed D6AC Steel Sheet
Caused by Inadequate Clamping Force and Force Location

The flange wrinkling problem can be considered analogous to a beam column supported by an elastic foundation. This assumption can be made because the wavelength between buckles is relatively short, thus precluding any consideration of the fact that one edge is free and the other simply supported.

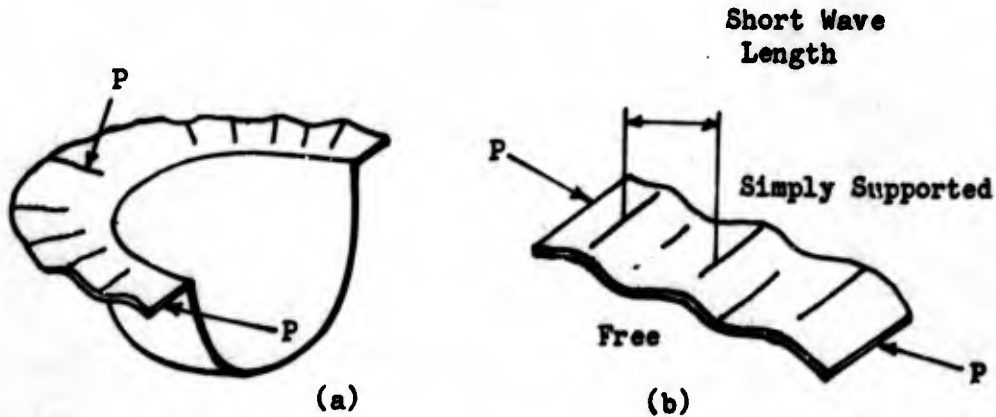


Figure 61. Schematic of Flange Wrinkling Problem

It can be shown that the critical buckling load in the case of Figure 61 is

$$P_{cr} = 2\sqrt{KEI} \quad (1)$$

where K is the elastic foundation modulus provided by the hold-down clamping system. We must observe the fact that as the load progresses up to the value P_{cr} , the sheet remains flat and clamping action between the hold-down plate and the draw ring reacts to the flange as an elastic foundation. If we consider a one-inch wide element of the flange we may say that

$$P_{cr} = \sigma_{cr} t \quad \text{and} \quad I = \frac{t^3}{12(1-\nu^2)}$$

Making this substitution into equation (1) we have:

$$\sigma_{cr} t = 2\sqrt{KE \frac{t^3}{12(1-\nu^2)}} \quad \text{or} \quad K = \frac{3 \sigma_{cr}^2 (1-\nu^2)}{t (E_t)}$$

The units of K are lb/in./in.² or (lb/in.³).

This relationship indicates that the stiffness required approaches infinity because E_t diminishes as ϵ_{cr} increases.

Experiments to determine required stiffness on the six-inch die and on the Titan II Improvement Program indicate that the stress level ϵ_{cr} should be an average between the yield and the proportional limit of the blank material.

$$\epsilon_{cr} = \frac{\epsilon_y + \epsilon_p}{2}$$

With respect to flange wrinkling, the position of the clamps or points of application of the clamping force was found to be very important. When the blank was clamped with hold-down force applied around the periphery of the blank, severe wrinkling of the flange resulted. The nature of the wrinkles is such that further drawing of the part (if sealing could be effected to permit cavity evacuation) would result in wrinkle progression into the die cavity. Subsequent "ironing" of the wrinkles is very difficult and challenges the integrity of the die. Peripheral clamping torque variations from 5 to 125 foot-pounds had little influence on wrinkle reduction. Using C clamps at any position from the centerline of the clamping ring to the die draw radius increases the clamping force significantly for a given applied load. This increase in clamping efficiency results in reduced tendency for blank wrinkling. Calculations show that when peripheral clamping is used, only 35% of the applied load is used for blank restraint, while clamps between the die draw radius and the clamping ring centerline result in clamping forces that are 83% of the applied load.

In an effort to establish the stiffness requirements to prevent flange wrinkling of the high-strength steel alloys, a number of experiments were conducted on a modified six-inch-diameter forming die. Figure 15 (shown in Section II 1. b) presents one of the arrangements used to study clamping stiffness. Several different combinations were evaluated in which clamping force, clamp location, hold-down ring thickness, number of clamps, and mass of clamps were varied. Table XXXIV lists the experimental results. In addition to stiffness experiments on the forged six-inch-diameter die, numerous tests were conducted on the six-inch shell die and the 24-inch Meehanite die shown earlier. The results of experiments with a multitude of arrangements using the three dies revealed the following die criteria for clamping:

TABLE XXXIV

Results of Stiffness Experiments to Evaluate Holddown Ring and Clamp Combinations

Specimen	Shot	Clamping device	Force/clamp or stud in.-lb.	Ring dimensions in.	Lubricated	W
D6-032-D4	1	8 Clamps	10	½ x 12	Yes	1.3
-D4	2	8 Clamps	10	½ x 12	Yes	2.0
D6-032-C1	1	12 Clamps	30	½ x 12	Yes	1.3
-C1	2	12 Clamps	30	½ x 12	Yes	2.08
D6-032-D5	1	12 Clamps	10	½ x 12	Yes	1.27
-D5	2	12 Clamps	10	½ x 12	Yes	2.01
D6-032-C2	1	12 Clamps	60	½ x 12	Yes	1.33
-C2	2	12 Clamps	60	½ x 12	Yes	2.13
D6-032-C3	1	12 Clamps	30	1 x 12	Yes	1.43
-C3	2	12 Clamps	30	1 x 12	Yes	2.19
D6-032-C4	1	12 Clamps	60	1 x 12	Yes	1.43
-C4	2	12 Clamps	60	1 x 12	Yes	2.27
D6-032-C5	1	6,1-in. Studs	35	1 x 16.5	Yes	1.4
-C5	2	6,1-in. Studs	35	1 x 16.5	Yes	2.2
D6-032-F1	1	6,1-in. Studs	35	1½ x 16.5	Yes	1.52
D6-032-C6	1	6,1-in. Studs	35	1½ x 16.5	No	1.41

Notes: Material - D6AC
Die - 6-in. hemispherical
B/D - 1.58
D/t - 175
L/D - .167
σ - 115 ksi
e - 30 grains TNT + 5 grains RDX
2 shots made on each blank

- 1) Clamp location is important in the prevention of wrinkling. The optimum location appears to be near the draw radius, although satisfactory results can be obtained when clamps are between the draw radius and the centerline of the clamping ring. Bolts can be used at the periphery of the blank if a suitable method for "beaming" the load forward can be devised;
- 2) Clamping stiffness (K) of at least 1,000,000lb/in. is required to prevent wrinkling of high-strength steels;
- 3) Clamping rings become prohibitively thick if conventional design is used; therefore, an integrally stiffened ring using channels radial to the ring circumference is a lightweight alternative that is significantly stiff;
- 4) Metal shims should be used around the periphery of the blank to prevent clamping-ring tipping during deformation, which will release clamping pressure on the blank and cause severe wrinkling.

2. EVALUATION OF DIE LOADS

To permit a more accurate design for a scaled die, the six-inch modified-shell die shown earlier was instrumented to establish strains developed in the die shell itself and the cylindrical support structure. Standard SR-4 strain gages were mounted on the under side of the cavity shell near the deepest section of the shell. Gages were also mounted on the cylindrical support, 180° apart, to measure both compressive and hoop strains resulting during explosive deformation. Table XXXVI presents some typical strain values recorded with calculated stress listed for reference.

TABLE XXXV

Evaluation of Die Loads

Shot No.	Charge grains	Strain						Draw depth
		1	2	3	4	5	6	
1	60 + RDX	- 0.0007	-	0.0012	0.008	0.004	2.49	
2	50 + RDX	- 0.0015	-	0.0015	0.0012	-	Blank fracture	

It should be noted that significant support is provided by the water under the die shell as evidenced by the rather large values of hoop stress calculated. The cylindrical support behaves as a pressure vessel where the hoop stresses are twice the stresses in the longitudinal direction. The pressure-relief ports at uniform intervals around the cylinder periphery allow water to fill the cylinder during die immersion and create the necessary water entrapment during explosive forming. If the holes are too large, less support is given the die shell as indicated by greater strains in the shell; however, if very small holes are used, the hoop stresses rise significantly in the support cylinder and create the need for thicker walls and thus add weight to the tool. On the six-inch die one-half-inch-diameter holes were found to give the proper balance between hoop stress in the support cylinder and support of the die shell.

Performance was good during repeated use of the die with explosive charges of increasing size. When blanks were formed in one operation to a given draw depth without filling the die, the hoop stresses and shell strains were quite low, i.e., on the order of 10 to 15,000 psi. However, if during the forming process multiple shots were used wherein the explosive charge was placed in the cavity of the die or if the blank fractured during deformation, the stresses in the die shell rose to 50,000 psi or about 50% of the static tensile yield strength for the shell material. Charges required to produce the higher strains were on the order of 200 grains, which when scaled would correspond to 502.2 pounds for a 156-inch-diameter tool. Thus, the design of the six-inch shell die appears adequate for fabrication of high-strength alloys.

One problem was uncovered during the small-scale die evaluation, i.e., weld cracks developed at the junction of the draw ring with the steel shell. The design of the 24-inch die for use in Phase III took this problem into account. Measurements of the small die to determine draw-ring distortion, shell growth, cylinder compression, or cylinder growth did not reveal any change in dimensions that would indicate plastic deformation.

Using the information obtained with the six-inch-diameter shell die and the 24-inch-diameter Meehanite tool, a 24-inch-diameter shell die was designed and fabricated. Figure 62, which is a repeat of Figure 18, illustrates the die. As previously stated, clamping stiffness is an extremely important variable when deep drawing of high-strength materials is required. The figure shows the method used to produce high clamping stiffness while die weight is kept minimal. Channel-type stiffener members were fusion

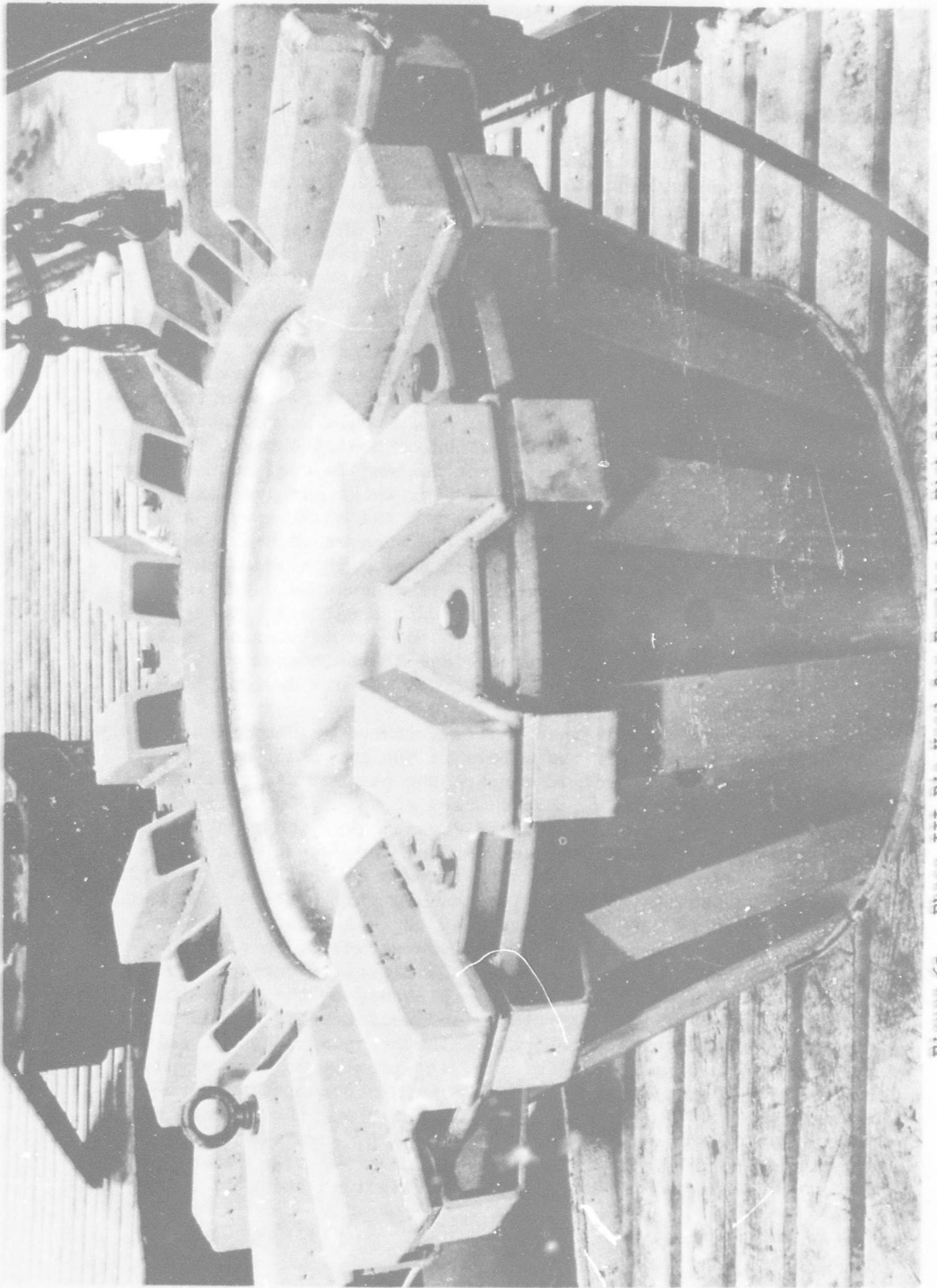


Figure 62. Phase III Die Used for Forming the High Strength Steels

welded radially around the clamping ring. Bolt holes between the stiffeners permitted application of force to the blank. Because it was discovered in earlier work that peripheral clamping does not eliminate flange wrinkling, some method had to be devised for the application of load at some point between the centerline of the clamping ring and the die draw radius. Shim pads outside the die proper were used on which metal shims between the pads and extensions of the radial stiffeners forced forward clamping of the blanks near the die draw radius. To aid cylindrical support stiffness of the die, gussets that extended to the shim pad areas were welded to the base. The die shell was fabricated from 4340 alloy steel. Because the shell, as delivered, was somewhat thicker than necessary, it was decided to use the alloy in the normalized condition. It was felt that design loads could be withstood by such a die. Additionally, elimination of heat treatment for the shell would make construction of the full-scale tool much simpler. The shell was designed with a girth ring welded around its periphery midway between the flange area and the shell apex. A stepped channel configuration permitted support of the die by a matching ring attached to the support base. This added support for the die was felt to be necessary to prevent weld tearing or bolt shearing in the region where the die shell was attached to the support base. More rigid support for the cylindrical base was provided by a circular plate welded to the bottom of the assembly. Figure 60 presents details of the die design.

The 24-inch die, designed and fabricated as described above, was used for forming all the alloys in the program. Charges of increasing size were used to compare the performance of the tool to initial forming shots. For charges up to 14,000 grains (two pounds) of pressed TNT no measured changes were observed in die shell dimensions, clamping ring flatness, or support structure dimensions. Repeated forming with charges in the 5,000- to 14,000-grain region caused problems with the clamping system. The channel stiffener members used for increasing the stiffness of the system were initially designed with rear closures welded in place but open frontal area. The blast from the explosion during forming caused a large increase in internal pressure of the channels, causing bulging of the rear plates and weld tearing around the plates. Addition of frontal plates to the channels and drilled holes in the rear panels eliminated the problem to some extent, but severe deformation of the frontal plate occurred with repeated forming. In addition, weld cracks along the channel members, caused when open frontal area existed, were extended during subsequent forming after repair. Weld cracking also occurred around the shim-pad attachments. The effect of the weld cracks

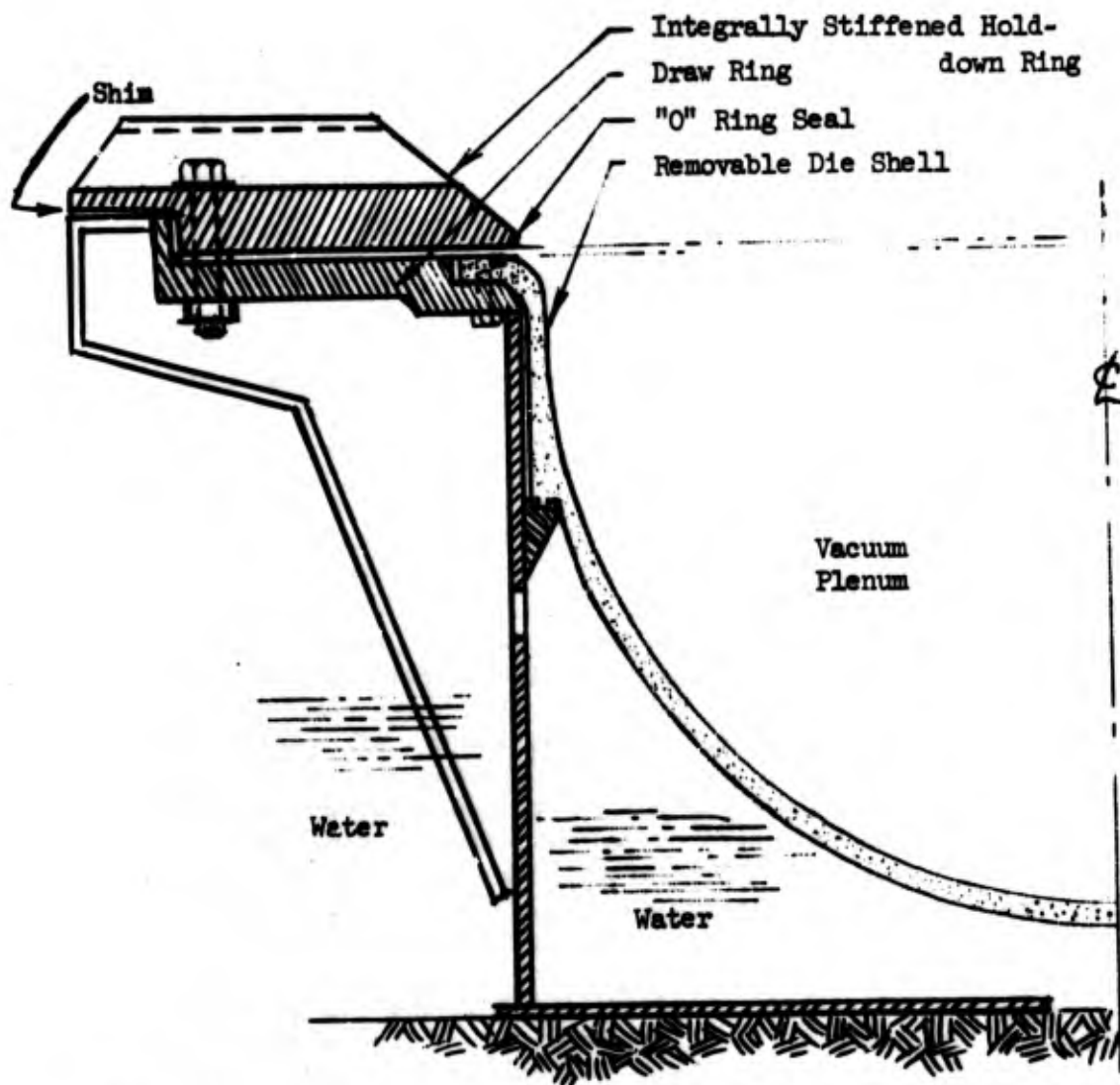


Figure 63 Die Design Details for 24-Inch Phase III Forming Tool

was to seriously impair the stiffness of the clamping system. This was evidenced by the flange wrinkling, which was virtually nonexistent during early forming experiments but became more severe in later tests. Die modifications are necessary to reduce the frontal area of the channel members and to effect more positive attachment of necessary stiffening components. The relocation of bolt holes also appears wise to aid in the proper application of clamping force.

To evaluate more stringent conditions created by blank breakage or sizing operations, numerous shots were made in which the blank was caused to fail or severe stresses were placed on the die shell as a result of sizing charges. In cases where blank breakage occurred, no apparent effects on the die shell or associated members resulted. Forming operations that combined blank breakage with sizing (i.e., the charge was within the shell cavity when the blank failed) did not cause any effects on the die at charges to 3500 grains (one-half pound). Even when sizing was accomplished and no breakage resulted, no die effects were noted for similar charges. However, when sizing charges up to 7000 grains (one pound) were used, plastic die-shell growth occurred. Figure 64 shows the extent of plastic die deformation after sizing. Because it is not possible to cold form the high-strength alloys in one operation to hemispherical shape, the use of one-half to three-quarters of a pound for sizing should result in a forming sequence of five operations or less. The use of several multiple shots instead of two or three has an advantage in that less total apex strain in the part results with lower attendant thinout. If requirements existed for larger charges, then the die shell could be fully heat treated to prevent plastic flow at the loads desired.

The method of attachment of the shell to the support structure was another weak point of the shell die system uncovered when one-pound sizing shots were used. Several high-strength bolts were sheared as a result of the outward growth of the die shell, and most of the remaining bolts were loosened. This problem can be eliminated by increasing the shear area of the bolts and by allowing space around the bolts for growth to occur (elastically) during the forming operations.

As a result of the six-inch- and 24-inch-diameter die experiments several important conclusions were reached regarding die design:

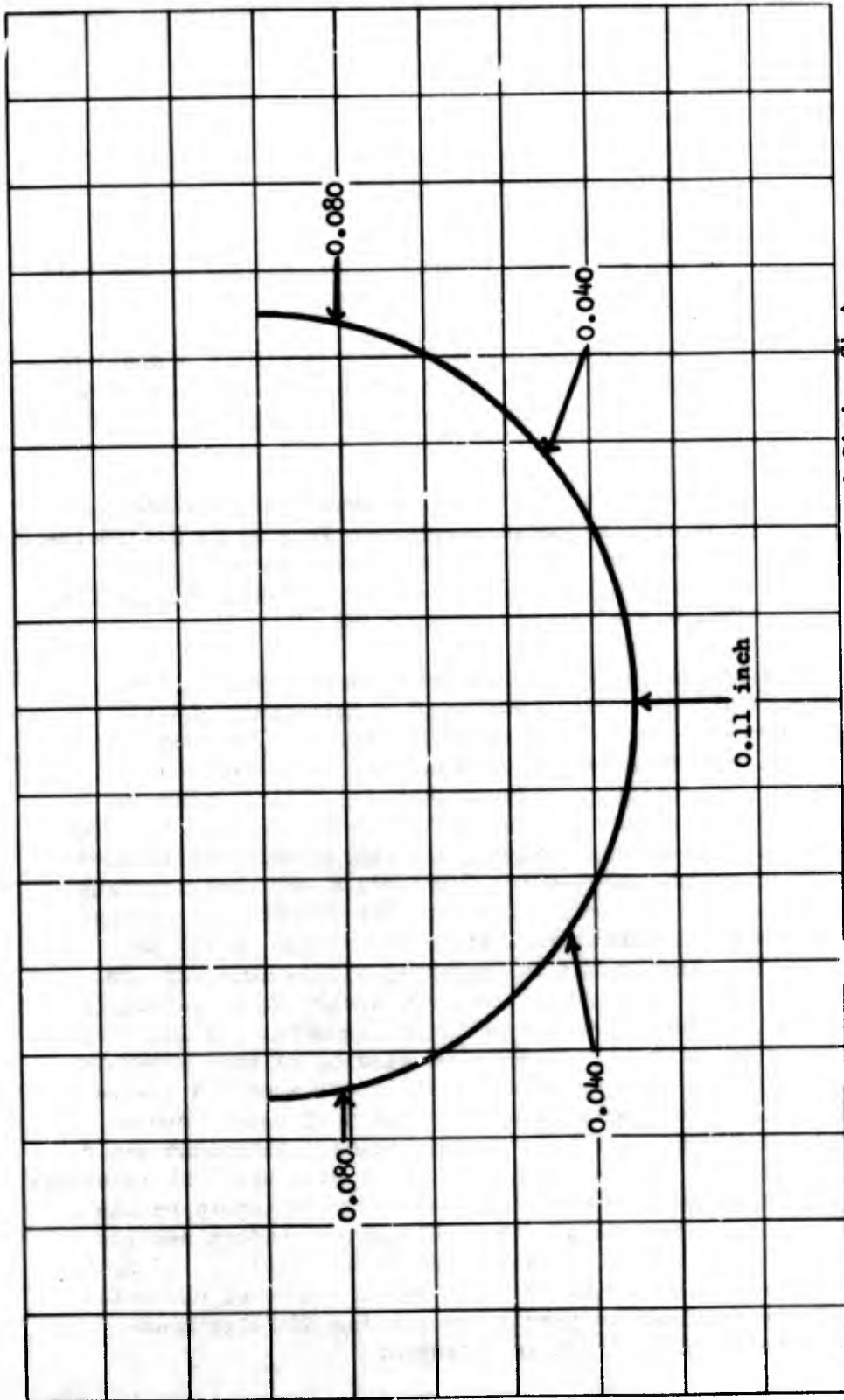


Figure 64 Die Growth Caused by One Pound Sizing Shots

- 1) Lightweight clamping systems of great stiffness can be made that perform well if attachment points remain intact;
- 2) Lightweight support structure using gusset-stiffened steel cylinders perform well under the most stringent conditions;
- 3) Unheat-treated 4340 steel can be used effectively for the die shell provided sizing shots of one-half pound are not exceeded;
- 4) Close-tolerance holes for bolting the die shell to the base structure are unacceptable because of high shear loads imposed by elastic/plastic growth of the shell;
- 5) The use of shim pads for prevention of clamping-ring tipping during explosive forming is not recommended, but metal inserts around the periphery of the blank between the clamping ring and the die flange surface are recommended.

Based on the criteria established on subscale dies, the recommended details for construction of a full-scale die (156 inches diameter) are presented in Table XXXVI. The most serious considerations for fabrication of full-scale dies are the die shell and support structure. Techniques for roll forming and welding cylindrical structures up to 156 inches in diameter from alloy steel or high-strength steels are rather well established as a result of solid-rocket-motor fabrication and tank construction for ground storage, etc. However, the fabrication of the 156-inch-diameter die shell with attaching flange is not as straightforward. Due to the rolling-mill limitations for the production of sheet much larger than 200 inches in diameter, it is necessary to produce the die shell in segments. At least two possibilities exist, i.e., forming and welding of gore segments or forming a large dome cap to which shallower segments can be attached. The latter approach appears the most sound from a structural standpoint although the gore segment technique would probably be cheaper because only one set of dies would be required. If annealed or normalized material could be used (based on the guidelines stated previously), then welding of uniform section pieces could be accomplished without undue difficulty. If heat-treated properties are required, then heavier area at the weldments would be required to permit the joining of fully heat-treated segments without loss in strength.

TABLE XXXVI

Design Criteria For Full-Scale Explosive Forming Dies
(156 inches diameter)

Details	24-inch die	156-inch die
Die Shell		
Thickness, inches	0.7	4.55
Depth (from draw ring surface), inches	13.0	84.50
Material	4340	4340
Support structure		
Diameter, inches	26.5	172.25
Height, inches	16.0	104.0
Thickness, inches	0.42	2.75
Relief ports	1.0	6.5
Clamping Ring		
Diameter, O.D.	40.0	260.0
Diameter, I.D.	26.5	172.25
Thickness, inches	1.3	8.45
Channel Stiffeners		
Foot length, inches	9.25	60.00
height, inches	2.00	13.00
width, inches	3.00	19.5
thickness, inch	0.375	2.44
Gusset supports		
Vertical length, inches	15.00	97.5
Width at draw ring, inches	2.50	16.25
Rear height, inches	2.50	16.25
Thickness, inches	0.25	1.65
Draw radius, inches	1.0	6.5

In the case where a dome cap and shallow gore segments are used, it is possible to use a heat-treated cap and heat-treated segments, which can be welded in uniform section without impairment of die performance. The highest die loads are sustained by the dome cap-section as evidenced by die-growth measurements. Therefore, lower properties in the region just below the die draw radius can be tolerated. The cap could be free-formed to rough tolerance and subsequently machined to final contour to reduce costs. The shallow gores can be mechanically or explosively formed to contour without serious problems.

In conclusion, the data and analyses suggest that a light-weight die of sufficient stiffness can be fabricated for the explosive forming of high-strength steels. Economics are not clear at this point. However, even at the same cost, a shell die arrangement would alleviate many logistics problems. In addition, shells of different types can be used interchangeably for different jobs with a minimum turn-around time.

SECTION V

CONCLUSIONS AND RECOMMENDATIONS

The technical results of this program have revealed several important conclusions regarding the effects of explosive deformation on mechanical behavior of high-strength alloys, formability limits, charge prediction, and die criteria:

- 1) Explosive deformation does not affect the fracture-toughness behavior of any of the alloys;
- 2) The high-strength steels HP 9-4-25, 12Ni-5Cr-3Mo, and vacuum-melted 18% nickel maraging steel are resistant to stress corrosion after explosive forming;
- 3) The air-melted 18% nickel maraging steel is unsatisfactory for use under stress in a corrosive environment;
- 4) Explosive deformation influences the response of high-strength alloys to heat treatment. Alloys gaining their strength from precipitation hardening appear to be more affected by explosive forming than are quench- and temper-conditioned alloys;
- 5) The greatest formability was exhibited by the HP 9-4-25 alloy, followed rather closely by the D6AC alloy steel;
- 6) Only the 7039-0 aluminum alloy could be explosively formed into hemispherical shape in one forming operation;
- 7) The data show that the relationship between explosive charge and draw depth scales with the volume of the blank. It also depends on material properties. It is plotted in nondimensional form against yield stress; however, this does not scale between different materials. Other parameters, such as strain-hardening exponents and elastic moduli that give a measure of toughness, should be included before scaling for charge requirements will be accurate between materials;

- 8) The use of computer predictions for metal draw depth and radial strain are quite accurate as long as blank pull-in is known. Predictions based on empirical relations predicting initial blank momentum for specific impulse for the explosive tend to overestimate draw depth;
- 9) Lightweight dies of great stiffness can be effectively used if rigid stiffener attachment is maintained and die shell attachments are suitably designed;
- 10) Initial forming shots up to two pounds on the 24-inch scale die can be used with no detrimental effects on the die (assuming proper stiffener design and attachment);
- 11) Sizing shots that cause blank failure or part seating, using charges up to 3500 grains, have no detrimental effects on the die;
- 12) Sizing shots of one pound, whether the blank breaks or not, cause the die shell to grow plastically.

The scope of work of the present contract was broad. Work progressed in several areas simultaneously. Some problems were solved, some were not, and new problems were identified. It seems worthwhile to review the present status of explosive forming of large domes. Results from the present contract, the Titan II Improvement Program, and the ARPA contract to establish a Center for High Energy Forming Processes (CHERP), have all contributed to this technology.

The manufacturing process for domes, as well as other applications, can be broken down into four major engineering requirements: adequate energy transfer from source to blank, suitable material properties during forming and in service, determining the mechanics of blank deformation, and design of dies that can produce the required blank deformations.

It is not necessary that all phases of the manufacturing be completely understood, but they must all be controlled within certain limits for successful production. The energy transfer mechanism for explosive forming is an example. The energy from charges is reproducible. Although the interaction between the shock-wave pressure and gas-bubble pressure and the blank deformation is not well known, it is predictable from subscale tests.

The material properties of stress-corrosion resistance and fracture toughness of explosively formed parts were studied as part of this contract. None of the materials tested would be excluded as unsuitable for explosive forming because of degradation of these properties except air-melted 18% nickel steel, as noted in the conclusions. A related question that arose during this and earlier contracts is what is the optimum heat treatment response of explosively formed metals. Denver University will examine this question during the next year as part of the ARPA contract. Metals of interest will include the 2014, 2219, and 7039 aluminum alloys; the 6Al-4V and 8Al-1Mo-1V titanium alloys; 301 stainless steel; and the maraging steels of 18%, 12% and 9% nickel content.

The properties of weld joints after explosive forming have not been studied extensively. Welded blanks are required when the blank dimensions exceed the capacity of the largest rolling mills. A subscale testing program should be carried out before using welded blanks in a full-scale program.

Formability limits have been established for the five alloys used in the present program. The draw depths achieved are adequate for most dome shapes without resorting to intermediate annealing. The formability limits for failure by tearing or shearing are a property of the materials. The limits for failure due to wrinkling or to uneven draw are also a function of die stiffness and can change under different applications.

Uneven draw of blanks with low R/D ratios was a recurring mechanics problem during the contract, and appeared during the Titan II Improvement Program. After encountering this basic problem in the Titan program, we made its solution one of the aims of the CHERF program.

Rather than rely on friction, which is inherently difficult to scale from model to prototype, a search was made for a positive means of supplementing the stiffness against radial pull-in of the material in the flange of the blank. An effective method has been to provide a rim on the blank and a ring to engage the rim, preventing further radial pull-in. The ring is cut in a chevron pattern and extended over the blank surface to prevent flange wrinkling due to pull-in during forming. This device for making edge pull-in an independent variable in the forming process rather than a dependent one is described in the Sixth Quarterly Technical Progress Report of the ARPA contract.

Theoretical work to provide better estimates of strain distribution in deformed blanks is also proceeding steadily. This information will allow better control of thinout, springback, and charge requirements.

Progress in the other major problem area, die design, has been made during the present contract and during the Titan II Improvement Program. Die contours have been supplied successfully with thin shell dies. Supporting the die on a cylinder filled with water has proved feasible. Designing the hold-down system to prevent flange wrinkling of the high-strength alloys has not been entirely successful, even with the increased stiffness of the Phase III die.

Figure 65 shows a possible die design that could be assembled for forming large domes. The shell contour lies on the inside of a fiberglass shell similar to the 120-inch-diameter die used on the Titan program. Fiberglass is inexpensive and easy to lay up. Its only bad feature is that it will not hold a vacuum after several shots because of fine cracks in the epoxy matrix surrounding the glass fibers. This feature can be circumvented by first free forming a metal shell to use as part of the vacuum system. The fiberglass shell would be laid up in this shell.

Supporting the die shell with sand instead of water would reduce the lateral loads on the support cylinder. Martin Marietta has not used sand in past work; but it has been used by other companies in other configuration to support dies. The Russians support platforms for crushing scrap iron with sand, and its use to protect buried structures from blast loads is well known.

Flange wrinkling must be controlled by a stiff hold-down system. The integral ring shown in Figure 65 would be built up of plates and gussets to combine a large section modulus with light weight. To clamp around the edge of the blank, the ring must be hinged like a Marsan clamp.

The complete die would be too heavy to swing in the air. It could be assembled at the explosive forming site. The cylinder would be placed on a carriage, then partially filled with sand. The fiberglass shell, metal shell, blank, and hold-down ring could be assembled separately and placed on the cylinder. The complete assembly would then be lowered into the pool on the carriage.

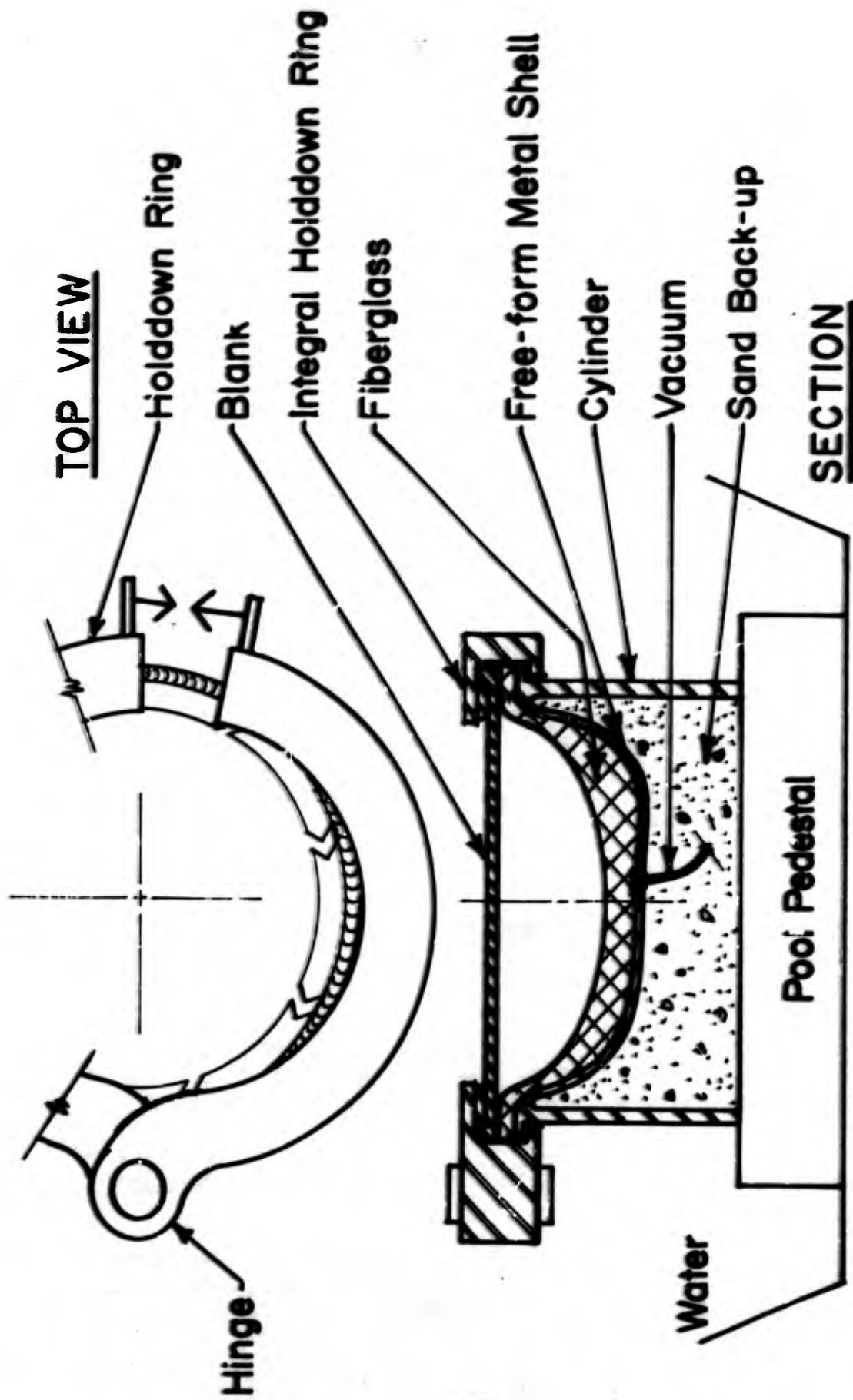


Figure 65. Possible Light Weight Die Design

VI

REFERENCES

1. Martin Report CR 66-61 "Explosively Formed One Piece Domes". Final Report Air Force Contract AFO4(694)-681. 25 December 1966.
2. Wallen, H. F. and Hawkins, K. D. "NASA S-1C 2219-T37 Gore Section Explosive Forming Development Program". NASA contract NAS 8-5129. June 5, 1964.
3. Hasemeyer, E. A. "Explosive Forming of Seventeen-Inch Diameter Elbows". National Aeronautics and Space Administration Report (MSFC) MTP-ME-63-1. May 22, 1963.
4. Savitt, J. and Conover, R. E. Final Report on Direct Contact Detonation Explosives Metalforming. AFML-TR-65-422. Air Force Materials Laboratory, Wright-Patterson Air Force Base, Ohio. Air Force Contract AF33(615)-1722. December 1965.
5. Hall, A. W. and Lieberman, I. "Explosive Forming of Closures for Large Solid Propellant Motor Cases". Air Force Contract AFO4(611)-8395. Aerojet General Corporation. May 1963.
6. Wood, W. W., et. al. "Sheet Metal Forming Technology". Air Force Materials Laboratory, Wright-Patterson Air Force Base, Ohio. Air Force Contract AF33(657)-7314. Final Report. July 1963.
7. Wood, W. W. et al. Final Report on Advanced Theoretical Formability. AFML Report TR-64-411, Air Force Materials Laboratory, Wright-Patterson Air Force Base, Ohio. Contract AF33(657)-10823. January 1965.
8. Pipher, F. C., Rardin, G. N. and Richter, W. L. "High Energy Rate Forming". Final Technical Engineering Report Air Force Contract AF33(600)-35543. Lockheed Aircraft Corp. October, 1960.
9. Hasemeyer, E. A. "Explosion Forms Saturn Manifolds". Missiles and Rockets, p 31, August 29, 1960.
10. Sheffield, I. K. and Agricola, K. R. "Development of Explosive Forming Techniques for Saturn V Components". Final Report NASA Contract NAS 8-11616. January 1966.

11. Snyder, J. T. and Agricola, K. R. "Explosive Forming of 2219 Aluminum". Final Report NASA Contract NAS 8-11794. June 1965.
12. Ezra, A., Ida, N., Agricola, K. and Burningham, N. "Explosive Forming and Welding of Honeycomb Sandwich Material". Final Contract Report NAS 8-5963. October 1964.
13. Hayes, G. A. and Pearson, J. "Engineering Properties of Explosively Work-Hardened Steels". NAVWEPS Report 7953, NOTS TP 2994. September 1962.
14. Chromalloy Corporation, Propellex Chemical Division. "A Study of Explosive Forming Selected Refractory Metals". Navy Contract NOW 61-0832-c. Final Report. April 1962.
15. Johnson, P. C., Stein, B. A. and Davis, R. S. "Basic Parameters of Metal Behavior Under High Rate Forming". Report No. WAL TR 111 2/2c-1. Contract DA-19-020-ORD-5239. Arthur D. Little, Inc. June 1962.
16. Adams, D. S., Harrison, V. S. and Orr, J. P. "High Energy Forming of Metallic Sheet Materials". Ryan Report 61B272. Army Contract DA-04-495-JRD-1921. Final Report. February 1961.
17. Gagne, R. A. "Physical and Mechanical Properties of Ti-6Al-4V Alloy Subsequent to High Velocity Deformation". Technical Report AMRA-TR 65-29. November 1965.
18. Center for High Energy Rate Forming. First Annual Report AMRA CR-66-05/5. Contract DA19-066-AMC-266(X) August 1966.
19. Ezra, A. A. "Similitude Requirements for Scale Model Determination of Shell Buckling Under Impulsive Loads". NASA Technical Note D-1510. 1962.
20. Ezra, A. A. and Penning, F. A. "Development of Scaling Laws for Explosive Forming". Experimental Mechanics pp 234 - 239. August 1962.
21. Verbraak, C. A. "Explosive Forming Can Cause Problems". Metals Progress. January 1963.
22. Duncan, A. J. Quality Control and Industrial Statistics. Richard D. Irwin, Inc., Illinois. February 1959.

23. Agricola, K. R. and Tate, F. G. "A Preliminary Investigation of the Feasibility of Explosive Cold Forming Air Melted 18% Nickel Maraging Steel". Paper SP 66-50 ASTME, January 1960.
24. Lieberman, I. and Zernow, L. "Practical Aspects of Explosive Metal Forming". Technical Problems of Explosive Forming - Proceedings MAK Maschinenbau Kiel GmbH. Kiel, Germany, October 1965.
25. Beyer, W. K. "The Tool is the Pool". Paper No. SP 64-124, Creative Manufacturing Seminar, American Society for Tool and Manufacturing Engineers, May 1964.

Unclassified

Security Classification

DOCUMENT CONTROL DATA - R&D

(Security classification of title, body of abstract and indexing annotation must be entered when the overall report is classified)

1. ORIGINATING ACTIVITY (Corporate author) Martin Marietta Corporation Denver, Colorado		2a. REPORT SECURITY CLASSIFICATION Unclassified	
		2b. GROUP	
3. REPORT TITLE Final Report on Advanced Explosive Forming Processes (HERF)			
4. DESCRIPTIVE NOTES (Type of report and inclusive dates) Final Report, June 1965 to February 1967			
5. AUTHOR(S) (Last name, first name, initial) Agricola, Richard K.; Snyder, Jack T.; Patton, James B.; Mallon, Jerome A. and Keys, Robert D.			
6. REPORT DATE May 1967		7a. TOTAL NO. OF PAGES 163	7b. NO. OF REFS 24
8a. CONTRACT OR GRANT NO. AF 33(615)-3167		8a. ORIGINATOR'S REPORT NUMBER(S)	
A. PROJECT NO. 8-358		8b. OTHER REPORT NO(S) (Any other numbers that may be assigned this report) AFML-TR-67-70	
10. AVAILABILITY/LIMITATION NOTICES Qualified requesters may obtain copies from DDC. This document is subject to special export controls and each transmittal to foreign governments or foreign nationals may be made only with prior approval of the Manufacturing Technology Division (MATF), Wright-Patterson AFB, Ohio 45433			
11. SUPPLEMENTARY NOTES		12. SPONSORING MILITARY ACTIVITY Manufacturing Technology Division Air Force Materials Laboratory Wright-Patterson Air Force Base, Ohio	
13. ABSTRACT Several high strength steels, namely HP 9-4-25, D6AC, 12% nickel and 18% nickel maraging steels and a high strength aluminum alloy 7039 were investigated with respect to explosive forming and subsequent effects of forming on mechanical behavior. In addition criteria necessary for full scale die design was developed. The stress-corrosion behavior of each alloy was evaluated using a standard 3% NaCl alternate immersion test. Three of the alloys, i.e., HP 9-4-25, 12Ni-5-Cr-3Mo and vacuum melted 18% nickel maraging steel were found to be only slightly affected by stress-corrosion. Explosive deformation did not alter the resistance of the alloys. The D6AC steel and 18% nickel maraging steel had fair resistance to stress-corrosion while 7039 aluminum was unsuitable for structural use in corrosive environment. Using plane strain, center notch fracture toughness specimens, none of the alloys were found to be affected by explosive deformation. Both HP 9-4-25 and D6AC steels were highly formable in the annealed condition. The other alloys were formable but to a lesser degree. Formability limit curves were developed for each alloy using a blank diameter to die opening diameter ratio of 1.58. Explosive charge requirements to achieve specified draw depths were also established with pressed TNT explosive charges. None of the steels could be formed to hemispherical shape in one forming operation; however, hemispheres could be formed from all of the alloys in two or more operations. The 7039-O aluminum was			

Security Classification

14. KEY WORDS	LINK A		LINK B		LINK C	
	ROLE	WT	ROLE	WT	ROLE	WT
High Energy Rate Forming High Energy Effects on Properties Metal Formability (Explosive Forming) Explosive Forming Die Design						

INSTRUCTIONS

1. **ORIGINATING ACTIVITY:** Enter the name and address of the contractor, subcontractor, grantee, Department of Defense activity or other organization (corporate author) issuing the report.
- 2a. **REPORT SECURITY CLASSIFICATION:** Enter the overall security classification of the report. Indicate whether "Restricted Data" is included. Marking is to be in accordance with appropriate security regulations.
- 2b. **GROUP:** Automatic downgrading is specified in DoD Directive 5200.10 and Armed Forces Industrial Manual. Enter the group number. Also, when applicable, show that optional markings have been used for Group 3 and Group 4 as authorized.
3. **REPORT TITLE:** Enter the complete report title in all capital letters. Titles in all cases should be unclassified. If a meaningful title cannot be selected without classification, show title classification in all capitals in parentheses immediately following the title.
4. **DESCRIPTIVE NOTE:** If appropriate, enter the type of report, e.g., interim, progress, summary, annual, or final. Give the inclusive dates when a specific reporting period is covered.
5. **AUTHOR(S):** Enter the name(s) of author(s) as shown on or in the report. Enter last name, first name, middle initial. If military, show rank and branch of service. The name of the principal author is an absolute minimum requirement.
6. **REPORT DATE:** Enter the date of the report as day, month, year; or month, year. If more than one date appears on the report, use date of publication.
- 7a. **TOTAL NUMBER OF PAGES:** The total page count should follow normal pagination procedures, i.e., enter the number of pages containing information.
- 7b. **NUMBER OF REFERENCES:** Enter the total number of references cited in the report.
- 8a. **CONTRACT OR GRANT NUMBER:** If appropriate, enter the applicable number of the contract or grant under which the report was written.
- 8b, 8c, & 8d. **PROJECT NUMBER:** Enter the appropriate military department identification, such as project number, subproject number, system numbers, task number, etc.
- 9a. **ORIGINATOR'S REPORT NUMBER(S):** Enter the official report number by which the document will be identified and controlled by the originating activity. This number must be unique to this report.
- 9b. **OTHER REPORT NUMBER(S):** If the report has been assigned any other report numbers (either by the originator or by the sponsor), also enter this number(s).
10. **AVAILABILITY/LIMITATION NOTICES:** Enter any limitations on further dissemination of the report, other than those

imposed by security classification, using standard statements such as:

- (1) "Qualified requesters may obtain copies of this report from DDC."
- (2) "Foreign announcement and dissemination of this report by DDC is not authorized."
- (3) "U. S. Government agencies may obtain copies of this report directly from DDC. Other qualified DDC users shall request through _____."
- (4) "U. S. military agencies may obtain copies of this report directly from DDC. Other qualified users shall request through _____."
- (5) "All distribution of this report is controlled. Qualified DDC users shall request through _____."

If the report has been furnished to the Office of Technical Services, Department of Commerce, for sale to the public, indicate this fact and enter the price, if known.

11. **SUPPLEMENTARY NOTES:** Use for additional explanatory notes.
12. **SPONSORING MILITARY ACTIVITY:** Enter the name of the departmental project office or laboratory sponsoring (paying for) the research and development. Include address.
13. **ABSTRACT:** Enter an abstract giving a brief and factual summary of the document indicative of the report, even though it may also appear elsewhere in the body of the technical report. If additional space is required, a continuation sheet shall be attached.

It is highly desirable that the abstract of classified reports be unclassified. Each paragraph of the abstract shall end with an indication of the military security classification of the information in the paragraph, represented as (TS), (S), (C), or (U).

There is no limitation on the length of the abstract. However, the suggested length is from 150 to 225 words.

14. **KEY WORDS:** Key words are technically meaningful terms or short phrases that characterize a report and may be used as index entries for cataloging the report. Key words must be selected so that no security classification is required. Identifiers, such as equipment model designation, trade name, military project code name, geographic location, may be used as key words but will be followed by an indication of technical content. The assignment of links, roles, and weights is optional.

DOCUMENT CONTROL DATA - R&D

Abstract - continued

formed to full contour in one operation.

Verification of scaling was demonstrated by forming the steels on both six-inch and twenty-four inch diameter dies.

Computer predictions used in conjunction with experiments did not agree well with experiment when metal draw depth or blank pull-in were unknown. When blank pull-in was known the computer program could rather accurately predict radial strains and draw depth. Program accuracy was greater for the shallower draw depths and in general overprediction resulted since accurate data on explosive energy transfer and energy release are not available.

Criteria developed on six-inch and twenty-four inch diameter shell dies showed the practicality of the concept. Clamping stiffness was found to be the most critical design parameter.